UNIVERSITAT POLITÈCNICA DE CATALUNYA
BARCELONATECH
Escola Superior d'Enginyeries Industrial,
Aeroespacial i Audiovisual de Terrassa

Polytechnical University of Catalonia

Aerospace Engineering

REPORT:
Design of an azimuth/elevation mount for Sun-tracking of a solar panel

Iker Blanco Bravo

Supervised by

Prof. Beatriz amante
Projects and Construction Engineering Department

Prof. David de la torre
Physics Department

June 2020

Abstract

Despite the fact that renewable energies are progressing, the present reality shows us that conventional methods of energy generation are more efficient just as contaminating. It leads to find not only new greener methods, but systems capable of improving the efficiency of the renewable energies. This is just what Sun-tracking solar panels try to do. In this project, an azimuth/elevation mount for Sun-tracking in Burkina Faso with specific space, transport and power requirements is designed. The document includes an initial study of solar geometry, the state-of-the-art of the solar technology, the design decision from several options and the structural analysis. The final result is a preliminary design of a Sun-tracking solar panel.

Keywords: solar energy, Sun-tracking, photovoltaics, solar geometry, design, structural analysis, requirements.

Contents

List of Figures

List of Tables

1 Introduction

1.1 Aim

The main objective of this project is to design an azimuth/elevation mount for Sun-tracking of a solar panel accomplishing space, transport and power requirements presented in section 1.3.

1.2 Scope

As a part of a global project, the design is focused on the design of a Sun-tracking system that fulfill the requirements.

The scope of this project will be presented defining different steps:

- Firstly, solar geometry and photovoltaic cell technology are presented in a theoretical point of view to introduce the topic.
- A study of radiation for different Sun-tracking systems is conducted to justify the dual-axis tracking PV.
- Different designs and solar panel configuration are contemplated.
- After studying the different designs, one conceptual design, which accomplishes the requirements, is chosen.
- The design is sketched and preliminary structural analysis are performed in order to guarantee it works under bending and shear stresses.
- Preliminary CAD design.
- Economical and environmental viability.
- Future work to improve and complete the project.
- Final budget.

Actuator, pins and bolts used to develop the preliminary CAD design are off-the-shelf products.

The code presented to track the Sun (Section 5.11) is not developed in this project. Also, the internal design of the shipping container (water treatment equipment) is out of the scope of this project.

The final CAD design shall finish in a mount capable of performing an azimuth and elevation tracking of the Sun.

1.3 Requirements

The requirements have been divided in operational and design requirements.

1.3.1 Operational requirements

- The mount shall track the sun in order to capture the rays as perpendicular as possible.
- The unique input shall be the latitude (ϕ) of the user.
- The solar panels shall be deposited over the Sun-tracking mount.
- At nighttime, the mount shall re-align facing the next day sunrise position.
- The system shall unfold manually once the container roof is taken off.

1.3.2 Design requirements

Power

- The system shall provide the shipping container with energy between 1-11 kWh.
- Remaining power shall be used as current for the population.

Solar cells

- Solar modules shall be chosen using efficiency, lifetime, energy payback time and proximity criteria.
  - Efficiency shall be over 15%
  - Lifetime shall be over 15 years.
  - Energy payback time can't exceed 2 years.
  - Manufacturing and distribution proximity shall be taken into account.

- Evidences of work temperature compliance shall be provided before choosing cells.

Size and space

- The entire design shall fit in a standard ISO shipping container: 2,43 m wide, 2.59 m high and 6.06 m long.
- The design shall leave two thirds of the shipping container space for the water treatment equipment.
- Only left margins can be used to locate the design.

Transport

- Solar cells shall be protected during transport. Safety considerations shall be done when designing the mount.
- Safety solutions can be transformed into available sunlight area after transport issues.

Structure

- Evidences of structural support shall be provided in form of structural analysis.

1.4 Background

The usage of technology in remote rural African places is highly conditioned by the lack of electricity. It leads to find self-efficient and alternative energy production methods such as wind or solar energies to provide current on site.[51] In addition, they are greener than conventional methods and, above all, inexhaustible.

Water treatment equipment will be sent to Burkina Faso rural towns to provide potable water to the citizens. Considering that Africa is the country which receives more radiation per year (see Figure 1), the power supply chosen to run the water treatment system is a Sun-tracking solar panel.

As the azimuth/elevation Sun-tracking panel will operate in resourceless rural areas, the remaining electricity will be used to provide current to the population. This is the reason for which the design has been developed to capture the maximum possible Sun radiation.

Regarding the water treatment in Africa, there are numerous companies that provide potable water using solar energy. *OffGrid Box*, *Elemental water Makers*, *Sustain Power* or *ERM Energies*, for example. However, they use static solar panels and the deployment requires labour. Semi-automatic or automatic unfolding solar panels are not provided.

There are more companies that work on providing electricity to small businesses using solar panels. *SolarTurtle* and *Africa GreenTec* provide a wide variety of models to run small kiosks or improve life in Africa. As the mentioned before, they can't track the Sun and their designs need to be manually unfolded.

Existing patents present mounts for Sun-tracking solar panels: US 8,273,978 B2,[52] US 2010/0051083A1,[53] US 8,487,180 B1,[54] US 8,492,645 B1.[55] Although solar panels are designed to rotate over a structure, they can only track 1-axis, the assembly requires labour or they use a central pedestal.

Keeping in mind that the water treatment equipment and the solar panel system are transported inside a shipping container, the Sun-tracking system has been designed to resist the hits of the transportation process. Once in place, the design will be capable of unfolding itself with low labour. The easy use is key when technology is handled in rural African zones. As an unstable areas, quick folding and unfolding is vital in case of violent crisis too.[31]

There is a need of improved Sun tracking in the context of dual rotation and automatic unfolding with low labour after shipping container transportation.

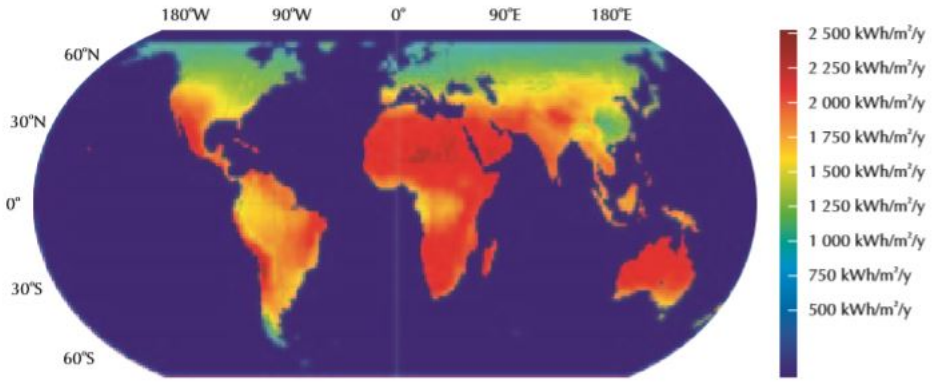

Figure 1: The global solar flux at the Earth's surface over the year

Adapted from: Adapted from: Solar Energy Perspectives, p38[1]

1.5 Planning

This section presents a brief task description, the interdependence among tasks and a Gantt diagram.

1.5.1 Work Breakdown Structure

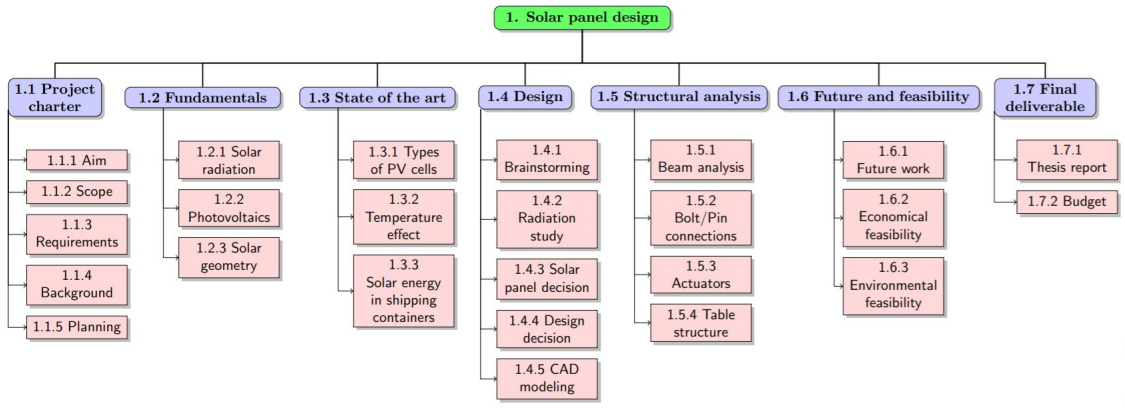

1.5.2 Brief task description

1.1.1 Aim: description of the main objective of the project.

1.1.2 Scope: list of tasks, activities and documents to deliver to accomplish the aim.

1.1.3 Requirements: technical specifications to satisfy the final design.

1.1.4 Background: justification of the project, advantages and disadvantages of the design, utility and critical points.

1.1.5 Planning: description of the tasks, interdependence among them, estimated duration and a Gantt diagram.

1.2.1 Solar radiation: brief approach to solar energy, solar radiation and its components.

1.2.2 Photovoltaics: introduction to semiconductor materials, PN junctions and electricity generation from photovoltaics.

1.2.3 Solar geometry: specify the position of the sun from a particular point of the Earth's surface and from a photovoltaic panel with different tilt angles.

1.3.1 Types of PV cells: state-of-the-art of different cell technology in the current market.

1.3.2 Temperature effect: state-of-the-art of the effect of the temperature in a photovoltaic panel. Definition of the work temperature cell.

1.3.3 Solar energy in shipping containers: state-of-the-art of the solar technology applied and combined with shipping containers.

1.4.1 Brainstorming: brainstorming of design ideas.

1.4.2 Radiation study: study of the radiation in a photovoltaic panel in Burkina Faso. The radiation is studied for different Sun-tracking systems: static, azimuth 1-axis, horizontal 1-axis and 2-axis.

1.4.3 Solar panel decision: analysis of the most suitable cell material, installation calculations to satisfy energy requirements, description of the different solar module options. Selection of a solar panel from the criteria presented in the requirements.

1.4.4 Design decision: selection of one design which satisfy the requirements.

1.4.5 CAD modeling: computer modeling of the design selected.

1.5.1 Beam analysis: structural analysis to size the vertical and horizontal beams that support the solar panels. Shear stresses, bending stresses and deflection are calculated. Structural requirements are imposed.

1.5.2 Bolt/Pin connections: structural analysis of bolts and cotter pins used in the design. Shear stresses, bending stresses and deflection are calculated to verify the structural requirements.

1.5.3 Actuators: sizing of the actuators to track the azimuth and zenith angles. The minimum force to lift the system is calculated. Wind loads are considered.

1.5.4 Table structure: structural analysis of the four legs and the horizontal board, which is calculated as a rectangular plate supported on the corners.

1.6.1 Future work: new developing lines to improve and complete the actual design.

1.6.2 Economical feasibility: brief analysis of the viability from an economical point of view.

1.6.3 Environmental feasibility: brief analysis of the viability from an environmental point of view.

1.7.1 Thesis report: document that gathers all the steps followed during the project.

1.7.2 Budget: cost of the study.

1.5.3 Interdependence among tasks

Code of task	**Task identification**	**Preceding task(s)**
1.1.1	Aim	-
1.1.2	Scope	-
1.1.3	Requirements	-
1.1.4	Background	-
1.1.5	Planning	1.1.2 & 1.1.4
1.2.1	Solar radiation	1.1.5
1.2.2	Photovoltaics	1.2.1
1.2.3	Solar geometry	1.2.1
1.3.1	Types of cells	1.2.2
1.3.2	Temperature effect	1.3.1
1.3.3	Solar energy in shipping containers	1.3.1
1.4.1	Brainstorming	1.3.3
1.4.2	Radiation study	1.2.3
1.4.3	Cell material decision	1.3.1 & 1.3.2
1.4.4	Design decision	1.4.1 & 1.4.2
1.4.5	CAD modeling	1.5.4
1.5.1	Beam analysis	1.4.4
1.5.2	Bolt/Pin connections	1.5.1
1.5.3	Actuators	1.5.2
1.5.4	Table structure	1.5.3
1.6.1	Future works	1.4.5
1.6.2	Economical viability	1.4.5
1.6.3	Environmental viability	1.4.5
1.7.1	Thesis report	-

Code of task	Task identification	Preceding task(s)
1.7.2	Budget	1.7.1

Table 1: Interdependency relationship among tasks

1.5.4 Gantt chart

Through Gantt chart is possible to show the preliminary calendar proposed for the project and the level of effort (in weeks) of each task. Week 1 starts on the 20th January and Week 23 starts on 22nd July.

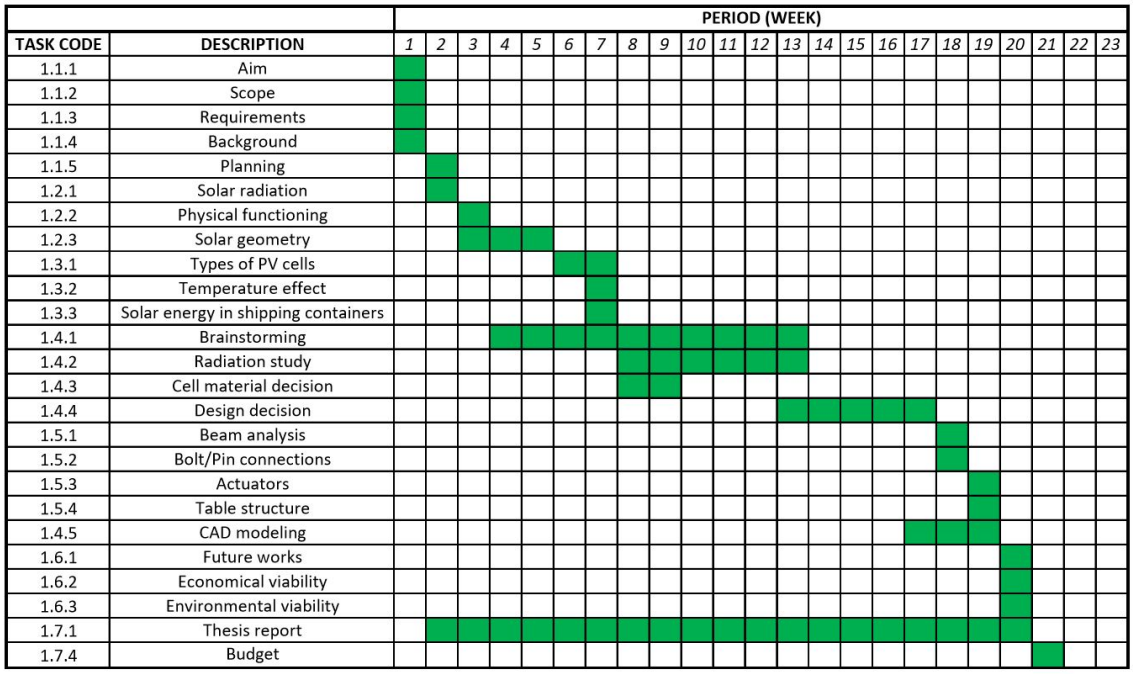

Figure 2: Gantt chart

2 Fundamentals

This sections presents theoretical points, necessaries to understand the entire document. Solar radiation and the functioning of photovoltaic cells are presented to have a general idea of how a solar panel works. In addition, solar geometry fundamentals are necessary to perform the radiation study in Burkina Faso.

2.1 Solar radiation

The solar energy is obtained due to the electromagnetic radiation coming from the Sun. It means it is produced by the light and heat of our star.

The solar irradiance is the amount of energy per unit time (power) that the Sun generates per unit area. It is calculated as Equation 1 states.

$$K = \sigma T_{eff}^4 \left(\frac{r_s}{a_0}\right)^2 \tag{1}$$

Where T_{eff} is the effective Sun temperature, r_s is the Sun radius and a_0 is the radius of the sphere whose center is the Sun and its limit is the body measured.[2]

For the Earth: $K = 1.368\ \frac{W}{m^2}$

However, the power that arrives to the surface is attenuated by the effect of the atmosphere, so $1.000\ \frac{W}{m^2}$ arrives in normal conditions when the sun is near the zenith.[1]

The entering radiation has two components: the direct and the diffuse irradiance. The direct radiation arrives directly, as his name indicates, from the solar disc. The diffuse radiation reach the surface after going through some reflection and refraction procedures with the atmosphere.

A third component appears when the radiation reaches the surface and it is reflected. This component is called albedo.

The global radiation, which arrives to the solar panel, is the sum of the three components (see Figure 3).

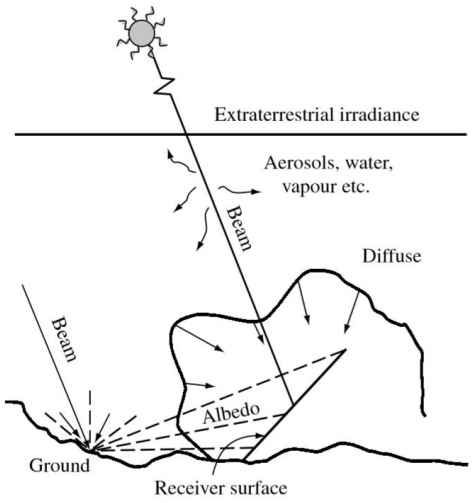

Figure 3: Radiation components

Adapted from: Handbook of photovoltaics Science and Engineering, p913[2]

As has been said, only a few energy will arrive to the solar panel. Thus, taking advantage of the radiation using Sun-tracking systems becomes relevant. In addition, the radiation does not arrive everyday with the same value in the whole Earth's surface. As can be seen in Figure 4, it depends on the latitude[1] and the day of the year.

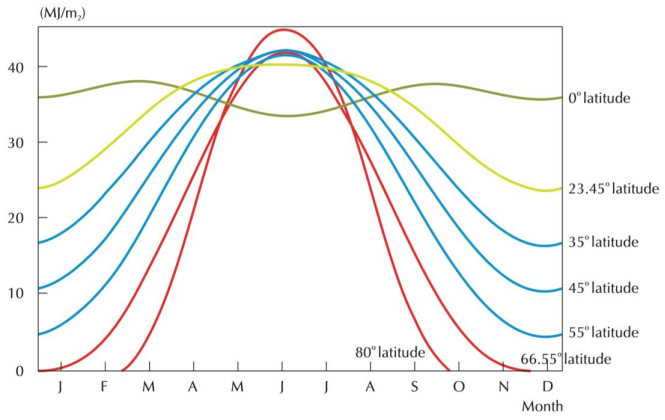

Figure 4: Total daily irradiance on a plane horizontal to the earth surface

Adapted from: Solar Energy Perspectives[1]

[1] Angular distance of a place, north or south from the earth's equator

2.2 Functioning of the photovoltaic cell

The main benefit from the Sun is the light it provide us. However, the solar energy have multiple and useful usages for our day-to-day. One of them is the generation of electricity with photovoltaic panels.

Solar radiation can be used as a flow of photons. Photovoltaic panels are able to transform this solar energy in direct current (electricity) when semiconductor material is lighted up.

This section presents the physical functioning of a silicon conventional cell. Although every type of cell has its own operation principles it is a base to understand how the current is produced.

Semiconductor materials

Photovoltaic cells are made of semiconductor materials, which behave as conductors or insulating depending on the external conditions. Semiconductor elements are silicon, phosphorus, boron, germanium, aluminium, gallium and cadmium among others.

As is well-known, atoms have neutral charges and they are compounded by nucleus and electrons orbiting around it. When electrons are moved from an atom to another they produce current. When movement is not possible, they behave as insulating materials.

Every orbital or layer in which electrons are orbiting is called energy band. All the electrons in the same band have the same energy. To jump from an orbit to a higher one is necessary more energy. The higher the orbital, the higher the energy of the band, so the last orbital contains the most energetic electrons. Nevertheless, they are more favorable to leave the atom due to its distance to the nucleus.

The electrons of the last orbital are called valence electrons. When they receive an specific energy level (band gap) they become free and reach a new band known as conduction band, where they are able to produce electricity.[5]

Dopants

Typical solar cells are made of silicon, which have four valence electrons available for chemical bonding. The silicon is not 100% pure and present impurities. In a process called doping, the silicon impurities are substituted

by other semiconductor atoms with three and five valence electrons (usually boron and phosphorus, respectively).

- Silicon + Element with 3 valence electrons = P-type semiconductor
- Silicon + Element with 5 valence electrons = N-type semiconductor

The four silicon valence electrons interacts with the dopants. In the case of a N-type semiconductor, only four covalent bond can be formed. The fifth electron is weakly attached to the dopant atom. The thermal energy of the ambient temperature is sufficient to free the electron. In the case of a P-type semiconductor, only three covalent bonds are formed. At this point appears a vacancy (*a hole*) that can be filled by a free electron.

PN junction

A PN junction is a piece of silicon doped in a special way. On one side of the piece, the silicon is doped with a P-type dopant. On the other side, a N-type dopant is used. Firstly, the two sides are considered separately (see Figure 5).

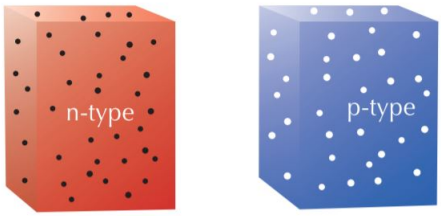

Figure 5: Doped silicon

Adapted from: Understanding the p-n junction[4]

The N-type semiconductor has free electrons with negative charge that can move wherever. In a similar way, the P-type semiconductor has free holes with positive charge that can move through the material. Both free electrons and holes are exactly balanced. Electrons compensate the cations of the N-type side and holes compensate the anions of the P-type side.

When the P side and the N side are joined, a process called diffusion starts and the free electrons from the N-type side diffuse into the P-type side. Similarly, the holes from the P-type side diffuse into the N-type side. With

this movements, it appears an intermediate region polarized as a result of the jumping out of the electrons and the holes (see Figure 6).

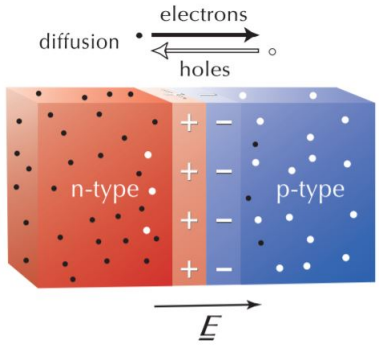

Figure 6: Diffusion effect

The electric field (E) that appears influences the holes and the electrons. The electrons are moved to the positive zone and the holes to the negative zone (opposite poles attract each other). Thus, the electric field causes that some of the electrons and holes flow in the opposite direction to the one caused by the diffusion.

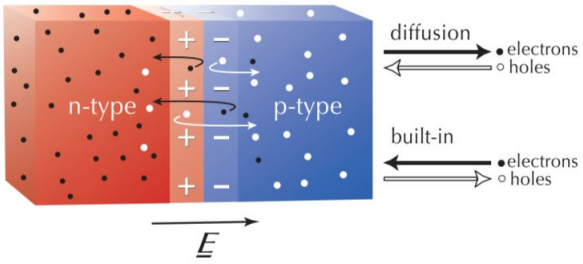

Figure 7: Motion of the electrons and holes due to the electric field

Adapted from: Understanding the p-n junction[4]

The opposite flows arrive to a stable equilibrium. The diffusion flow is the same as the electric field flow. At this point, the electrons and the holes reduce the rate of motion. This new intermediate zone is called depletion zone[2].

[2]Depleted means exhausted

Power

The depletion zone is highly resistant and it behaves as an insulator due to the reduction of motion. This feature can be modified by using an external electric field. If the added electric field is applied in the same direction, the resistance becomes greater. If it is opposite to the PN junction electric field, the depletion zone becomes less resistant.

When a positive voltage is applied to the P-type side and a negative voltage to the N-type side there is current. The configuration shown in Figure 8 is named *Forward Bias* and it is capable of reduce the resistance of the depletion region.

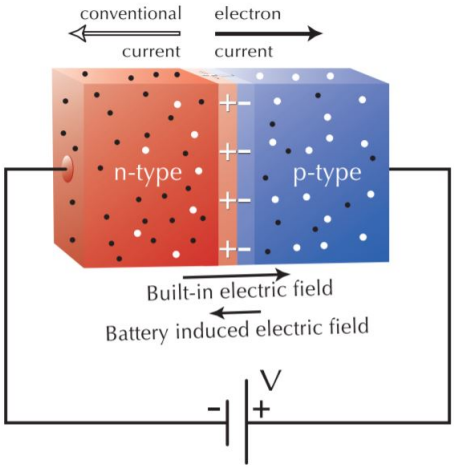

Figure 8: Forward bias of the PN junction

Adapted from: Understanding the p-n junction[4]

At a certain applied voltage, the external electric field can make the depletion region's resistance negligible. From 0 to 0.6V, the resistance at the depletion zone is still considerable. Above 0.6V, the resistance of the depletion region current can flow without impediment.

Now it is possible to understand what happens in a solar cell. Solar cell are made of PN junctions. When the sun shines the panel, the light has enough energy to break the bonds of the doped silicon. The excited electrons and the holes are free to move through the material and create an electric field. The electrons are attracted to the positive charges of the N-type side and

the holes are attracted to the negative charges of the P-type side due to this *built-in* electric field. The polarisation of the charges causes a current flow. The direction of the current is taken as positive in the same direction as holes motion. Thus, it goes from N side to the P side. Now, if a low resistant wire is connected externally between the P side and the N side, the current will flow through the wire.

However, not all the electric energy is transformed in current. Both electron and holes are excited only for a short period of time. In a process called recombination, electrons find a new hole and end again in bonded positions. This process transforms the electrical energy in lost heat.

In order to achieve power from the solar panel it is necessary to have current and voltage. With a wire, current flow through it but there is no voltage. If the wire is cut, there is no current and appears a voltage. This voltage is generated because there is no external circuit for the charges. To maintain both voltage and current at the same time, it has to be used an appropriate resistance to generate the optimal voltage and the optimal current.[4]

2.3 Solar geometry

The aim of this section is to specify the position of the sun from a particular point on the Earth's surface.

The Earth spins around the polar axis[3] once a day. At the same time, the polar axis orbits around the sun maintaining a constant angle of 23,45 degrees with the ecliptic plane[4]. This inclination is what makes longer days of light in summer and shorter in winter. It also causes the sun to be higher in the sky in summer than in winter.

The angle between a straight from the center of Earth to the center of Sun and the equatorial plane[5] is known as solar declination (δ) and it doesn't remain constant during the year. Equation 2[28] shows how declination varies with time. Declination is given in radians. From a physical point of view its range varies from -23.45º (minus Earth's obliquity angle) to 23.45º (Earth's obliquity angle).

[3] Axis around the Earth spins
[4] Imaginary plane containing the Earth's orbit around the sun
[5] Perpendicular plane to the rotating axis of the Earth

$$\begin{aligned}\delta = 0.06918 - 0.399912 \cdot \cos(X) + 0.070257 \cdot \sin(X) \\ -0.006758 \cdot \cos(2X) + 0.000907 \cdot \sin(2X) \\ -0.002697 \cdot \cos(3X) + 0.001480 \cdot \sin(3X)\end{aligned} \tag{2}$$

Where X is calculated as Equation 3 states and d_n is the day of the year, from 1 (1st January) to 365 (31st December). The equation is given in radians.

$$X = 2\pi \cdot \frac{d_n - 1}{365} \tag{3}$$

Declination takes characteristic values that define the stations and its transition dates. Declination is zero at equinox; the sun sunrises and sundowns exactly at the East and West, respectively. In the summer solstice (21-22 June) declination takes the value $\delta = 23.45^{\circ}$. At the northern hemisphere it is called summer and represents the longest day of the year. In the winter solstice (21-22 December) declination takes the value $\delta = -23.45^{\circ}$. At northern hemisphere it is called winter and represents the shortest day of the year. At the southern hemisphere, the winter solstice occurs in June and the summer solstice occurs in December.

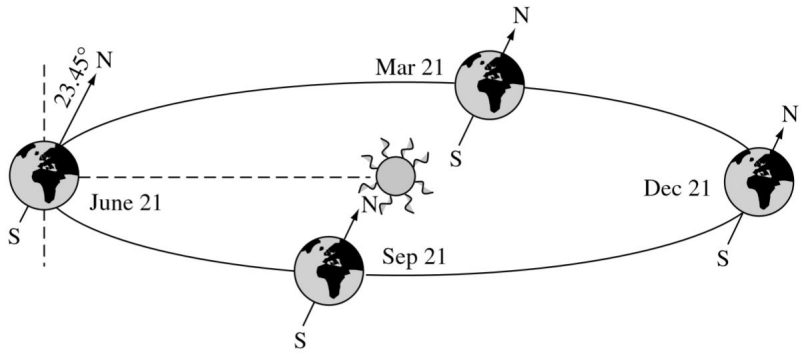

Figure 9: Declination angle of the Earth

Adapted from: Handbook of photovoltaics Science and Engineering, p908[2]

The greatest error in one-year algorithms for solar declination occurs at the equinoxes in leap years. Declination varies by 0.3 degrees from year to year during the leap year cycle on a given day near the equinox and by 0.15

degrees in midsummer and midwinter. Precise values of declination can be obtained from *A note on solar declination and the equation of time*,[29] where a comparison between several algorithms is performed and also it lists a four-year algorithm. The article confirm that Equation 2 is correct within 0.04 degrees, except near the equinoxes in leap years, when the error is 0.08 degrees.

To describe the movement of the Sun from the Earth, two reference systems can be used:: terrestrial axis and local axis. Firstly, it is necessary to place an observation point at the Earth surface through a meridian (longitude) and the angular distance from the equatorial plane (latitude).

Besides, the intersection of the parallel planes of the equator with the terrestrial surface defines the latitude circles. Latitude is positive for places to the north of the equator and negative for places at southern hemisphere.

The reference system based on terrestrial axis has the following vectors:

- $\vec{\mu_p}$: polar vector, with direction of the polar axis and sense south to north.
- $\vec{\mu_{ec}}$: equatorial vector, contained in the equatorial plane and pointing to the intersection between the plane and the meridian (indicates the direction of the solar noon).
- $\vec{\mu_\perp}$: cross product of $\vec{\mu_p} \times \vec{\mu_{ec}}$ pointing to East.

Solar vector $\vec{\mu_s}$ referred to terrestrial axis depends on the declination (δ) and the solar time angle (ω). The solar time angle measure the difference between an instant and the solar noon. The solar time is zero at noon, negative in the mornings and positive in the afternoons.

Projecting terrestrial axis with declination and solar time angles (see Figure 12), Equation 4[28] is obtained.

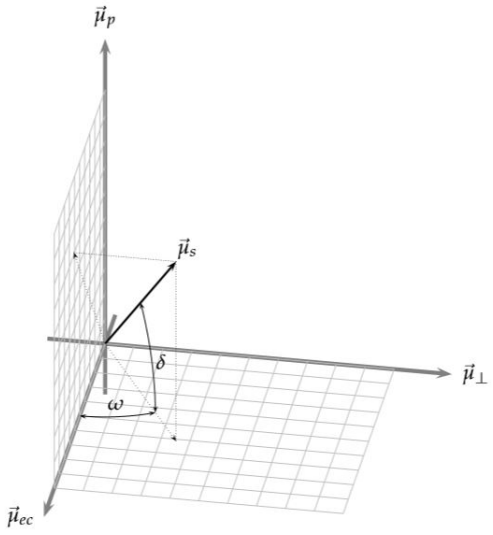

Figure 10: Coordinates system based on terrestrial axis

Energía solar fotovoltaica, p10[28]

$$\vec{\mu_s} = [cos(\delta)\ cos(\omega)] \cdot \vec{\mu_{ec}} - [cos(\delta)\ sin(\omega)] \cdot \vec{\mu_\perp} + sin(\delta) \cdot \vec{\mu_p} \qquad (4)$$

The $\vec{\mu_\perp}$ term has a negative sign the solar time angle is negative on the first quadrant and the solar vector must remain positive on the first quadrant.

The reference system based on local axis is referred to a meridian and a point of it with latitude ϕ.

- $\vec{\mu_c}$: zenith vector, perpendicular to the Earth's surface.
- $\vec{\mu_h}$: vector tangent to the meridian, pointing the equator. Thus, it is pointing to the south horizon (northern hemisphere) or pointing to the north horizon (southern hemisphere).
- $\vec{\mu_\perp}$: cross product of $\vec{\mu_c} \times \vec{\mu_h}$ (northern hemisphere) or $\vec{\mu_h} \times \vec{\mu_c}$ (southern hemisphere) in order to point always the East.

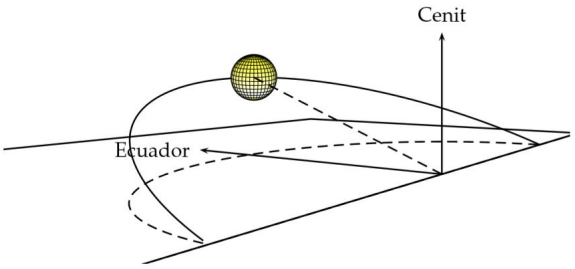

Figure 11: Movement of the Sun from a point of the Earth

Energía solar fotovoltaica, p10[28]

The solar vector $\vec{\mu_s}$ referred to local axis depends on the solar azimuth angle (ψ_s) and the solar zenith angle (θ_s). The solar azimuth angle is the angle between the solar meridian and the meridian of the reference point. The sign criteria is the same as used in terrestrial axis. Negative in the mornings and positive in the afternoons. The solar zenith angle is the angle between the solar vector and the vertical vector of the reference point. Its complementary is the solar elevation angle.

Projecting local axis with azimuth and zenith solar angles (see Figure 12), Equation 5[28] is obtained.

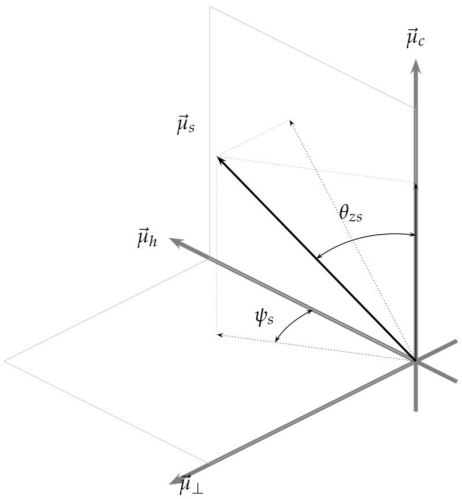

Figure 12: Coordinates system based on local axis

Energía solar fotovoltaica, p11[28]

$$\vec{\mu_s} = [cos(\psi_s)\ sin(\theta_{zs})] \cdot \vec{\mu_h} - [sin(\psi_s)\ sin(\theta_{zs})] \cdot \vec{\mu_\perp} + cos(\theta_{zs}) \cdot \vec{\mu_c} \qquad (5)$$

The change of terrestrial axis to local axis can be made using the latitude of the local point (see Figure 13). Equation 6[28] presents the rotation matrix.

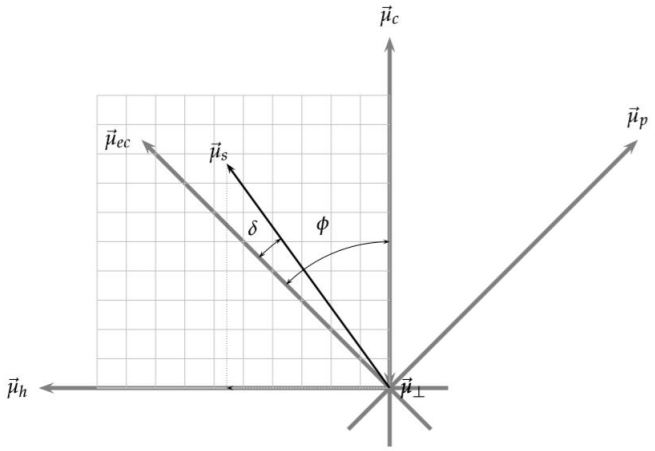

Figure 13: Relation between terrestrial coordinates and local coordinates

Energía solar fotovoltaica, p12[28]

$$\begin{bmatrix} \vec{\mu_{ec}} \\ \vec{\mu_\perp} \\ \vec{\mu_p} \end{bmatrix} = \begin{bmatrix} sign(\phi) \cdot sin(\phi) & 0 & cos(\phi) \\ 0 & 1 & 0 \\ -sign(\phi) \cdot cos(\phi) & 0 & sin(\phi) \end{bmatrix} \begin{bmatrix} \vec{\mu_h} \\ \vec{\mu_\perp} \\ \vec{\mu_c} \end{bmatrix} \qquad (6)$$

The solar movement from a photovoltaic panel is defined using local axis by convenience. Using the rotation matrix, the solar vector from Equation 4 (terrestrial axis) now depends on the latitude, the declination angle and the solar time. It is now referred in local axis.

$$\begin{aligned} \vec{\mu_s} = sign(\phi) \cdot [cos(\delta)\ cos(\omega)\ sin(\omega) - cos(\phi)\ sin(\delta)] \cdot \vec{\mu_h} \\ -[cos(\delta)\ sin(\omega)] \cdot \vec{\mu_\perp} \\ +[cos(\delta)\ cos(\omega) \cos(\phi) + sin(\delta)\ sin(\phi)] \cdot \vec{\mu_c} \end{aligned} \qquad (7)$$

By comparison between Equation 5 and Equation 7, both in local axis, zenith and azimuth angles are obtained.[28]

$$cos(\theta_{zs}) = cos(\delta)\ cos(\omega)\ cos(\phi) + sin(\delta)\ sin(\phi) = sin(\gamma_s) \tag{8}$$

$$cos(\psi_s) = sign(\phi) \cdot \frac{cos(\delta)\ cos(\omega)\ sin(\phi) - cos(\phi)\ sin(\delta)}{sin(\theta_{zs})} \tag{9}$$

$$sin(\psi_s) = \frac{cos(\delta)\ sin(\omega)}{sin(\theta_{zs})} = \frac{cos(\delta)\ sin(\omega)}{sin(\gamma_s)} \tag{10}$$

Zenith and azimuth angles depend on the declination angle, the solar time angle and the latitude. Angle γ_s is defined as the sun elevation angle, which is complementary to the zenith angle.[28]

To obtain the value of the azimuth angle, the projection of the sun must be located within the right quadrant. Arc cosine function allows to decide between the first[6] and the second[7] quadrant, or between the third[8] and the fourth[9] one. However, it is not capable of distinguish between the first and the fourth quadrant, or between the second quadrant and the third one. This difference can be solved having in mind if the sun has crossed the noon (first quadrant for S-hemisphere and second quadrant for N-hemisphere) or not yet (third quadrant for S-hemisphere and fourth quadrant for N-hemisphere).

Figure 14 shows the elevation angle during the year at the noon for northern and southern hemisphere.

[6] between S-W
[7] between W-N
[8] between N-E
[9] between S-E

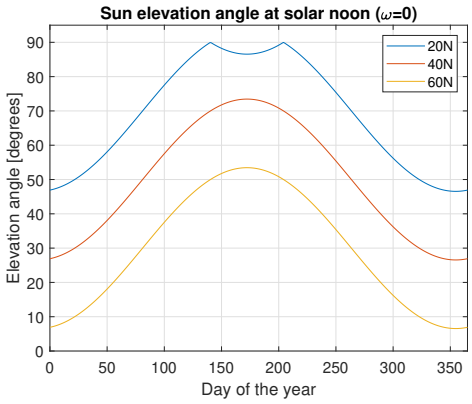

(a) Solar elevation northern hemisphere

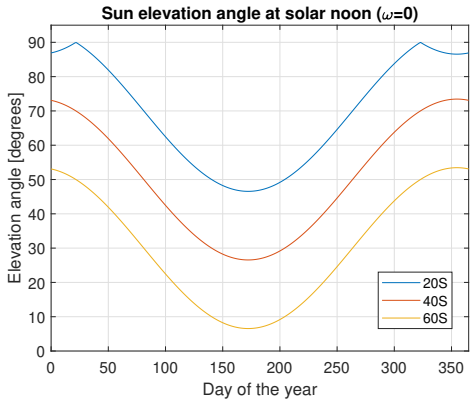

(b) Solar elevation southern hemisphere

Figure 14: Elevation angle at the noon during the year

The sunrise and the sundown solar occurs when the elevation angle of the sun is zero. Both situations can be calculated imposing $\theta_{zs} = 90^{o}$ at Equation 8.[28]

$$\omega_s = -arc\ cos(-tan\ \delta\ tan\ \phi) \tag{11}$$

The duration of a light day is $2 \cdot |\omega_s|$

2.3.1 Official time and solar time

The official time in a place is the time measurement associated to a meridian (time zone) which works as reference in a specific zone. All the time zones are counted from Greenwich (GMT). Time zones situated at East from Greenwich are considered positive. There is a formula (see Equation 12[28]) that measures the difference between the local longitude of a place (λ_L) and the time zone longitude (λ_H).

$$\Delta\lambda = \lambda_L - \lambda_H \tag{12}$$

It must be taken into account that some countries use a summer time for daylight time saving reasons. In this cases, the official time is advanced 60 minutes.

It exists a relation between the mean solar time and the real time expressed in the equation of time (EoT). This equation expressed in minutes (see Equation 13[28]) keeps in mind the ecliptic orbit around the Sun and the inclining polar axis of the Earth.

$$EoT = 229.18 \cdot (-0.0334 \cdot sin(M) + 0.04184 \cdot sin(2 \cdot M + 3.5884)) \quad (13)$$

Where M, in radians, is related to the day of the year (see Equation 14).

$$M = \frac{2\pi}{365.24} \cdot d_n \quad (14)$$

All the necessary corrections to translate the official time (TO) and obtain the solar time ω are presented in Equation 15.

$$\omega = 15 \cdot (TO - AO - 12) + \Delta\lambda + \frac{EoT}{4} \quad (15)$$

Where AO is the official summer advance. TO and AO are in hours, $\Delta\lambda$ in degrees and EoT in minutes.[28] Solar time (ω) is expressed in degrees.

2.3.2 Photovoltaic panels geometry

Sun-tracking solar panels track the Sun in order to capture perpendicularly the direct solar radiation.

The direction vector of the photovoltaic panel plane referred to local axis is:

$$\vec{\mu_\beta} = [sin(\beta)\ cos(\alpha)] \cdot \vec{\mu_h} - [sin(\beta)\ sin(\alpha)] \cdot \vec{\mu_\perp} + cos(\beta) \cdot \vec{\mu_c} \quad (16)$$

The angle (θ_s) between the direction vector of the PV and the solar vector is schematised in Figure 15. Equation 17[28] calculates the angle θ_s.

$$\begin{aligned} cos(\theta_s) = sign(\phi) \cdot [&sin(\beta)\ cos(\alpha)\ cos(delta)\ cos(\omega)\ sin(\phi) \\ &-sin(\beta)\ cos(\alpha)\ cos(\phi)\ sin(\delta)] \\ &+sin(\beta)\ sin(\alpha)\ cos(\delta)\ sin(\omega) \\ &+cos(\beta)\ cos(\delta)\ cos(\omega)\ cos(\phi) \\ &+cos(\beta)\ sin(\delta)\ sin(\phi) \end{aligned} \quad (17)$$

It can be simplified as:

$$cos(\theta_s) = cos(\theta_{zs})\ cos(\beta) + sin(\theta_{zs})\ sin(\beta)\ cos(\psi_s - \alpha) \tag{18}$$

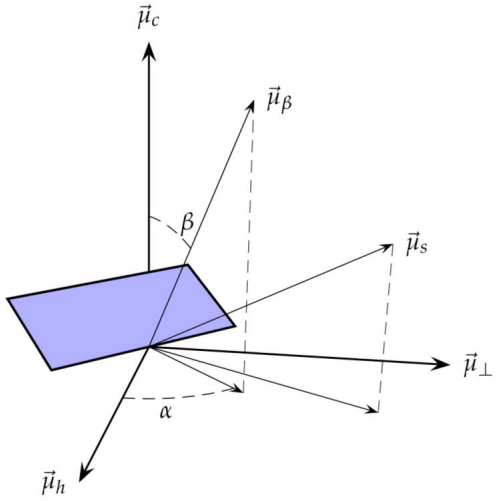

Figure 15: Angles and vectors in a PV system

Adapted from: Energía solar fotovoltaica, p16[28]

A two-axis Sun-tracking solar panel maintains its orientation equal to the azimuth solar angle and the panel elevation (β) equal to the zenith angle. Thus, the angle θ_s between the PV director vector and the sun vector is zero.[28]

$$\beta = \theta_{zs} \tag{19}$$

$$\alpha = \psi_s \tag{20}$$

$$cos(\theta_s) = 1 \tag{21}$$

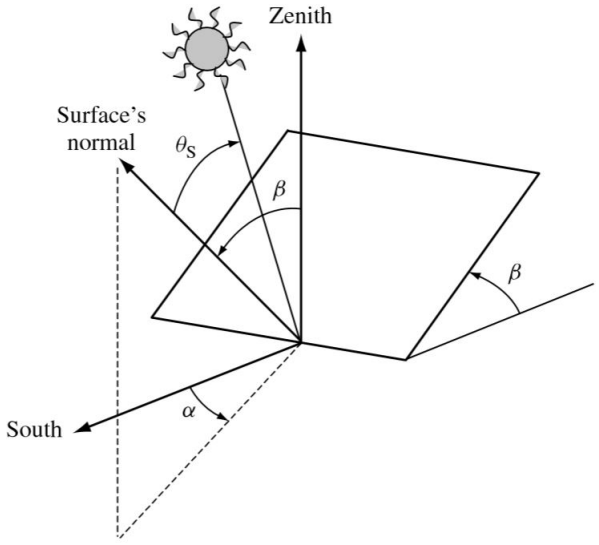

Figure 16: Angle θ_s visualization

Adapted from: Handbook of photovoltaics Science and Engineering, p912[2]

3 State of the art

This section presents the state of the art regarding to the different types of photovoltaic cells and the solar panels integrated in shipping containers.

3.1 Types of photovoltaic cells

Silicon crystalline form (c-Si) is the most used material in photovoltaic applications. However, other semiconductors are better to absorb solar energy. This new materials are being developed or have been launched recently. Amorphous silicon (a-Si), copper indium gallium diselenide (CIGS) and cadmium teluride (CdTe) cells are the most advanced to date in sunlight absorption and its commercialization is now a reality.

The research of new materials responds to the demand of improving the efficiency. In this context, mechanisms like concentrator panels and tracking panels must be outlined too.

3.1.1 Crystalline silicon solar cells

Crystalline silicon cells represent the 85% of the market and they average lifetime is around 25 years. The cells are made from ingots or by casting of pure silicon. To take advantage of the maximum solar energy, a layer of unreflecting material is added. Also, metallic contacts are used to conduct the electricity. To build the panel, cells are joined between them with a frontal piece of glass and an aluminium frame.[1]

Although c-Si cells are the most mature PV technology, there is still margin for improvement. Important progress have to be made in thickness issues in order to reduce the costly purified silicon under 5 gr/W. Cheaper purified silicon would reduce the energy and the labour costs of the manufacturing process.

As a benefit, silicon is the second most abundant element in Earth (after oxygen). Thus, the use of silicon does not inflate excessively the final manufacture cost.

Mono-crystalline (s-Si)

Mono-crystalline cells are the most used because of its high efficiency. However, the cost is higher than the poly-crystalline option. The main reason is

that s-Si cells require more purity. During the manufacturing, the solidification is made over a single silicon crystall to obtain ordered structure with the same orientation. In standard conditions, s-Si cells show efficiencies[10] around 14% and 22%.

Poly-crystalline (m-Si)

Poly-crystalline cells are manufactured from the silicon without the need to control neither the temperature nor the growing of the crystalline structure. Its solidification is made in several crystalls. The efficiency of poly-crystalline cells is from 12% to 19% and the simple manufacturing process makes them cheaper.[7]

Heterojunction cells (HJT)

HJT combines crystalline silicon with amorphous silicon thin-film (see Section 3.1.2) to produce a high-power hybrid cell.

PERC

PERC (Passivated Emitter and Rear Cell) is a solar technology that defines a different cell architecture and differs from the standard cell architecture. PERC improves the light capture near the rear surface and optimise the electrons capture. It is considered a high efficiency cell.[45] Marketable PERC modules can reach 22% of efficiency.[46]

3.1.2 Thin film solar cells

Thin-film solar cells are made by placing thin layers of photovoltaic materials on a substrate (glass, plastic or metal). The film manufacture is automated with roll-to-roll printing machines (lamination), which reduce the costs.

The thickness of this technology goes from a few nanometers (nm) to tens of micrometers (μm). They contrast with the conventional c-Si cells, which use silicon wafers of up to 200 μm.[6]

Thin-film solar cells are flexible and lower in weight. They are cheaper and work better under high temperature levels than conventional s-Si cells. Despite the fact that they have lots of advantages, they are less efficient. At the

[10] Ratio of electric output over the incoming solar energy

moment, the most efficient thin-film solar cell barely reach the 14%. However, some researchers believes that this percentage could be increased until 16% during the following years. The market-share of thin-film solar cells has never reached more than 20 percent in the last two decades and its actual production is around 7-13%.

The usage of this technology starts in the 80s, when it was used as small strips in student calculators and watches. At the early 21st century they were used in curved surface and windows for building-integrated photovoltaics. Future application could be on cars or even on clothing to charge devices.

There are four main technologies that use the principles of thin-film cells: amorphous silicon, multi-junction, cadmium-telluride (CdTe) and cooper indium gallium diselenide (CIGS).

Amorphous silicon (a-Si)

With usual efficiencies from 4% to 8%, a-Si represents the non-crystalline form of silicon.[1] The a-Si panels are formed by vapor-depositing [11], producing about 1 μm triple thick layer over a substrate material (glass, metal or even plastic). It is remarkable to say that a-Si solar cell layers are 1/300th the size of mono-crystalline silicon solar cell.[6]

Amorphous silicon solar cell have three layers with a p-i-n or a n-i-p sequence. The usage of more than one layer finds an explanation in the Staebler-Wronski effect[12]. As illustrated in Figure 17, excess electrons are moved from the n-type layer to the p-type layer, trespassing the undoped intrinsic layer (i) and creating a built-in electric field.

[11] Process in which films of materials are deposited from the vapor phase on the surface of a substrate by the decomposition of chemicals

[12] Process in which the cell experiments photoconductivity changes and the efficiency of the conversion of sunlight into electricity decreases.

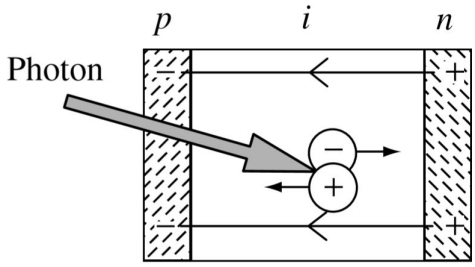

Figure 17: Pin photodiode operation

Adapted from: Handbook of photovoltaics Science and Engineering, p509[2]

Amorphous silicon is usually used on small devices such as calculators, travel lights and camping equipment.

Comparing the a-Si cells with other higher efficiency types of thin-film technologies (CdTe and CIGS), a-Si photovoltaics looks attractive because the production process is more mature and proven due to it has been developed during 20 years. In addition, the product does not contain any hazardous material as cadmium (CdTe) or a large amount of expensive metal as indium (CIGS).[2] The materials needed to produce a-Si cells are abundant on Earth and this could be a benefit for future developments.

Cadmium-telluride (CdTe) cells

CdTe solar panel is the second most common used photovoltaic technology (it represents the 5% of the whole market). Reaching average efficiency levels between 9-11%, some CdTe models can compete with less effective crystalline silicon models in terms of cost-effectiveness.[12]

CdTe cells present a high absorption due to the ability of absorbing ideal wavelengths. It means that panels can absorb shorter wavelengths than conventional silicon panels, which fits the solar spectrum of the sunlight.[8]

As an inconvenience, the toxicity of cadmium presents environmental concerns within the usage of this technology. However, recycling of CdTe thin films is possible and allows recovery of 95% of cadmium and tellurium.[6]

CdTe thin film panels are used for terrestrial power conversion, infrared detection, thermal imaging and gamma ray detectors for tomographic applications.[2]

Cooper indium gallium diselenide (CIGS) cells

Copper indium diselenide ($CuInSe_2$) was developed in the early 1970s. Years later it was found that substituting partially the indium (In) with gallium (Ga) the overall efficiency is increased. The increase is possible due to a more optimal band gap.

Although CIGS solar panels have reached laboratory efficiencies of 20%, commercial modules have efficiencies between 12% and 14%.[8]

$Cu(InGa)Se_2$ solar cells have excellent long-term stability in outdoor testing and large-area terrestrial applications. In addition, its high radiation resistance, its flexibility and lightweight features makes them a promising alternative for space applications.[2]

CIGS solar panels allows tandem designs (see Figure 18), which consist on either individual cells or connected in series with different band gaps. This tandem designs increase the solar spectrum absorbed and improves the efficiency.

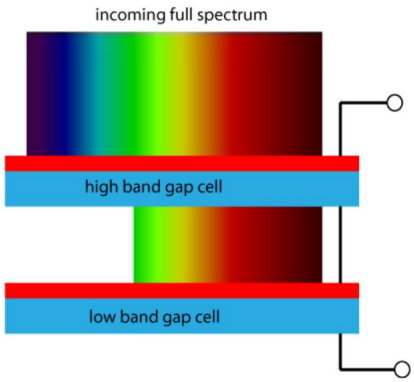

Figure 18: Series connected tandem solar cell

Adapted from: PVEducation.org

After depositing into the substrate the elements which formed $Cu(InGa)Se_2$, the final panel junction is formed by a chemical-bath deposition of the n-type layer (CdS). To finish the solar cell, a high-resistance zinc oxide (ZnO) layer is deposited.[8]

Despite the fact that CIGS cells present lots of advantages such as its flexibility and a good performance after the high-temperature deposition techniques, they must improve its laboratory scale correlation and the manufacturing costs.

3.1.3 Dye-sensitized solar cell (DSSC)

Dye-sensitized solar cells consist on a photoelectrode, a redox electrolyte and a counter electrode (see Figure 19). Oxide semiconductor materials (such as TiO_2) have a good stability under radiation. However, they can't absorb visible light because they have wide band gaps. In order to revert this situation, oxide semiconductors are sensitised with photosensitizers (organic dyes[13]).

Organic dyes can absorb visible light, so they are attached to the pores of the TiO_2. After absorbing the sunlight, the photosensitizers are excited ($S \longrightarrow S^*$). The excited electrons are injected into the conduction band of the TiO_2 electrode.

$$S^* \longrightarrow S^+ + e^-(TiO_2)$$

The electrons of the conduction band of the TiO_2 are transported until the contact, reaching the external load and traversing the wiring. The oxidized photosensitizer (S^+) accepts electrons from the I^- ion redox, regenerating the initial state (S). At the same time, I^- is oxidized due to the redox reaction with the electrons which came from the external load.[13]

$$I_3^- + 2e^- \longrightarrow 3I^-$$

[13]A natural or synthetic substance used to add a colour to or change the colour of something

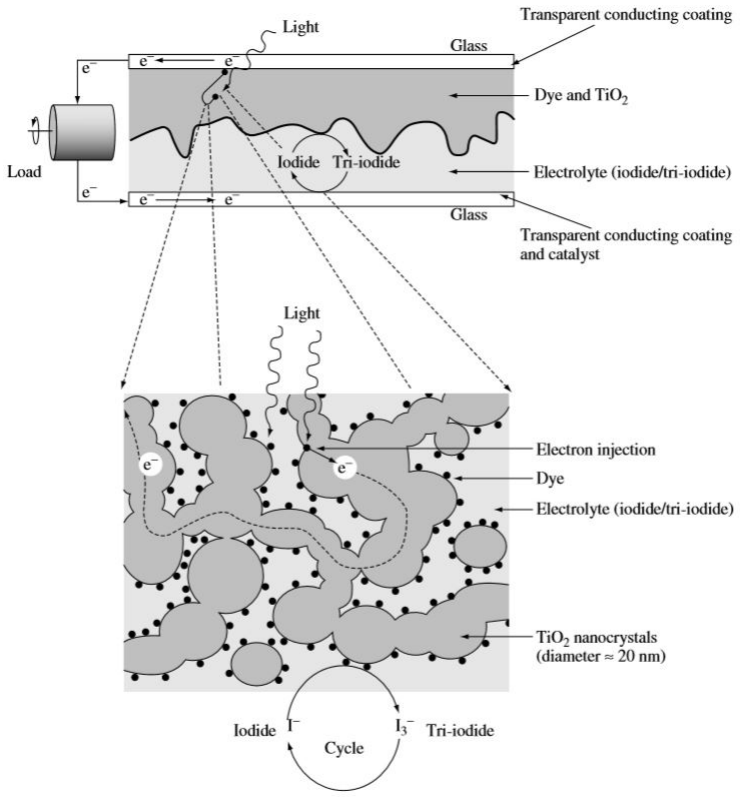

Figure 19: Schematic structure of the dye-sensitized solar cell

Adapted from: Handbook of photovoltaics Science and Engineering, p665 [2]

The DSSC can reach efficiencies of 7-10%. It presents low-cost fabrication processes using conventional roll-printing techniques. Its semi-flexible and semitransparent features facilitate the usage in windowpanes. In addition, dye-sensitized solar cells have a good recyclability.

On the other hand, the usage of liquid redox electrolyte (iodide/tri-ioide cycle) presents a serious challenge to use the cell in all weather.[6]

3.1.4 Perovskite solar cells

Perovskite cell is an hybrid material composed by lead (Pb), an organic molecule and a halogen anion (Cl^-, Br^- or I^-). The most common perovskite solar cells have the molecular formula $CH_3NH_3PbX_3$, where X is

usually taken up by iodine.[25]

Its photovoltaic properties were found out in 2012. Since then, perovskite cells have reached a power conversion efficiency of 25% for small areas and 16% for large areas (over 800 cm^2). It is the most promising photovoltaic technology for the moment.[26]

The materials used and the manufacture process are simple and economic. In contrast to conventional cells, multistep high temperature processes (upwards of 1000 °C) or vacuum in special clean rooms are not required.[6] However, it presents some inconveniences. Firstly, they contain lead, which is very toxic, and perovskite cells are water soluble. It is a huge environmental problem.[26] Besides, they are not stable and they are easily degraded, which means they must develop more until they become a reality in the photovoltaic market.[27]

To solve the toxicity problem of the lead, researches are experimenting with bismuth-based lead-free perovskite cells, but they are far from the efficiency levels reached with lead perovskite cells.[26]

3.1.5 Multi-junction solar cells

Multi-junction solar cells are composed by multiple pn junctions of different semiconductor materials. This configuration allows producing current from different wavelengths. The range of absorbing light is wider than conventional configurations.[10]

Laboratory examples of multi-junction cells have demonstrated performances around 42%.[9] Nevertheless, it has been achieved at the cost of increased complexity and manufacturing price.

Because of their high power-to-weight ratio they are very desirable in aerospace industry. In terrestrial applications, the multi-junction cell is used in concentrated photovoltaics. Also, tandem cells have been used to improve the efficiency of the thin-film solar designs.[8]

The GaInP/GaAs/Ge solar cell has special mention in this context. Its great radiation resistance, high convert ion efficiency and low cost manufacture has made it one of the better options to use in space solar arrays.[11]

3.1.6 Optic concentrator photovoltaics

The following types of photovoltaic panels incorporate new mechanisms to improve the efficiency, no matter which materials are used for the cells.

Concentrator solar panels (CPV) use curved mirrors and lenses (or a combination of both) to concentrate a large area of sunlight onto a small beam. CPV are capable of capture specific wavelength of the solar light spectrum.

The concentration factor reduces the amount of semiconductor material needed and opens up the potential to cost-effectively CPV multi-junction cells, which have already demonstrated solar cell efficiencies of about 40%.[14]

Costs are still too high to compete with fossil fuel–fired generation, or even the most direct renewable competitor (wing power). However, CPV is a promising technology which opens the way for creative optimal designs.[2]

CPV requires effective cooling to avoid overheating the photovoltaic cells. It makes easier to cogenerate heat and power with hybrid photvoltaic-thermal systems. The heat can be used for industrial processes or desalination.[1]

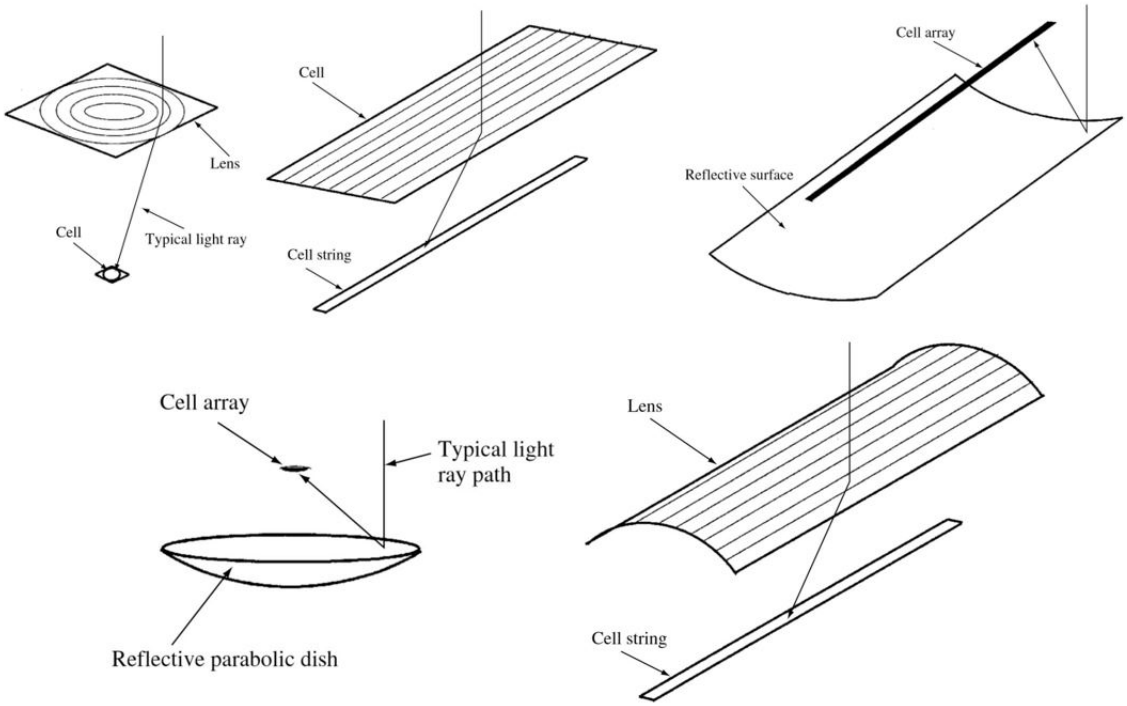

Figure 20: Different concentrator photovoltaic systems

Adapted from: Handbook of photovoltaics Science and Engineering, p453[2]

3.1.7 Sun-tracking solar panels

Concentrator photovoltaic systems often use solar trackers simultaneously to increase the amount of solar rays captured.[6] Many studies showed that using sun tracking systems increase significantly the electricity energy generation capacity of PV panels. Gain rates are approximately between 15%–45% throughout the year depending on the location and the panel area.[19]

Sun-trackers are used to ensure that the solar beams are pointing the cells perpendicularly.[3] This fact is key to leverage the sunlight and can be clearly explained with the cosine effect.

The cosine effect occurs with the static solar panels when the sun is lower. The energy is distributed over a larger area and therefore weaker per surface area. The radiation received on the surface is equal to the radiation on a surface perpendicular to the direction of the sun, multiplied by the cosine of

this angle.[1] Figure 21 illustrates this effect.

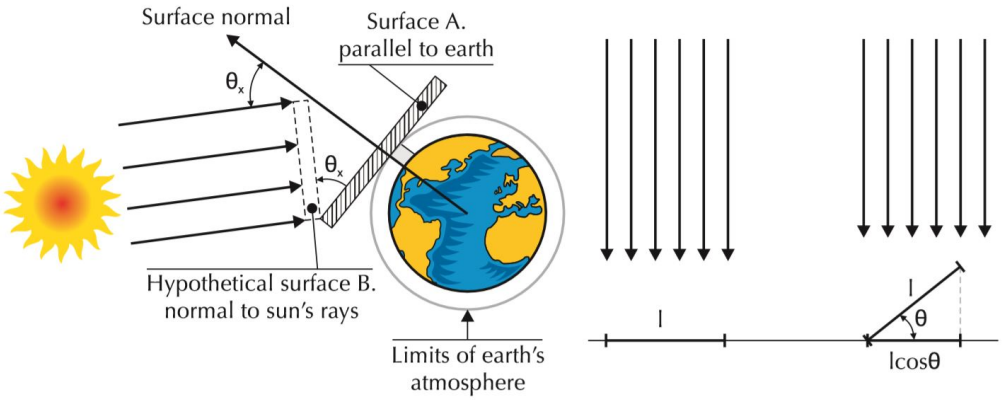

Figure 21: The cosine effect

Adapted from: Solar Energy Perspectives, p35[1]

Trackers can be classified depending on their system to detect the sun. Trackers based on optical sensors and microprocessor uses the change in the received light to relocate the panel perpendicularly to the rays of sunlight. Whereas trackers based on date and time use inputs (date, time and latitude) to achieve the desired position.[15]

Depending on their movement degrees of freedom, there are single axis solar tracking systems and dual axis solar tracking systems.[18]

One-axis tracker

They are expected to generate up to 15-20% more energy than fixed latitude panels. Although, one-axis trackers need more space to maneuver and requires more maintenance than the fixed panels, they are cost-effective.[17] The most common types of 1-DOF trackers are the horizontal single axis tracker (HSAT), the vertical single axis tracker (VSAT) and the polar single axis tracker (PSAT).[18]

- HSAP configuration rotates from east to west on a horizontal axis and it is oriented either north or south (depending on the hemisphere). HSAP is conceived to profit from the maximum energy moment of the day: the noon. HSAP is usually mounted in low latitude regions, where the elevation angle varies widely during the year.[16]

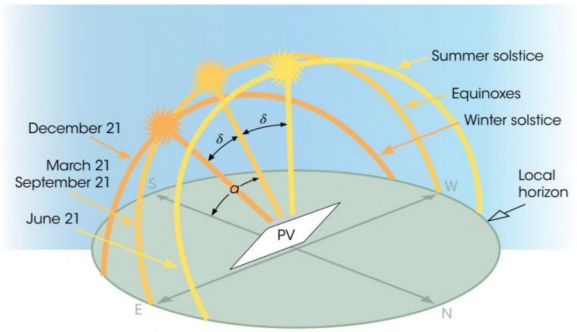

Figure 22: Solar trajectories over from a stationary observer

Adapted from: Electricity from Sunlight, p92[17]

With HSAP configuration, the solar panel only changes its elevation angle around the horizontal axis depending on the period of the year (see Figure 22).

- VSAT configuration, also known as azimuth tracker, has a fixed tilted angle of the panel and tracks the azimuth angle of the sun. It is more efficient in high latitudes.
- PSAT configuration is aligned with the polar axis (Earth rotation axis). It limits the suns offset angle to a maximum of 23,45° (the maximum declination of the sun) from the plane of illumination, giving more efficient overall energy collection than with a horizontal axis. Thus, as the Earth is close to the equinox the PSAT works better.

The simplicity of the horizontal-axis configuration and the scarce difference between PSAT and HSAT configuration in terms of efficiency makes the HSAP the more common choice over the polar-axis approach.[17] The latitude of the installation place plays an important role when choosing between HSAT and VSAT configuration.

Two-axis tracker

It consists in two degrees of freedom solar panel. Although they are mechanically more expensive and complex, two-axis trackers managed to boost efficiency by 15%-17% in comparison to single axis tracker systems[33] and gains of 30% when comparing with fixed tilted panels.[19]

Figure 23 illustrates the most common type of dual-axis tracker: a central

pedestal supporting a tracking mounting structure. Tracking is usually effected by a gearbox, which tracks the Sun along the vertical axis (azimuth rotation) and along the horizontal axis (elevation rotation).

The main problem of the pedestal configuration remains in the large torque caused by the wind loads translated to the central gear drive.

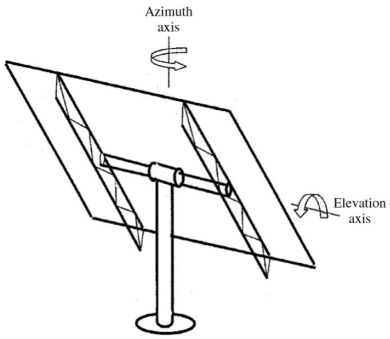

Figure 23: Back side of a dual-axis tracker array

Adapted from: Handbook of photovoltaics Science and Engineering, p457[2]

The roll-tilt structure (see Figure 24) reduces considerably the large torque problem but incorporate more rotating bearings. More linkages are required too.[2]

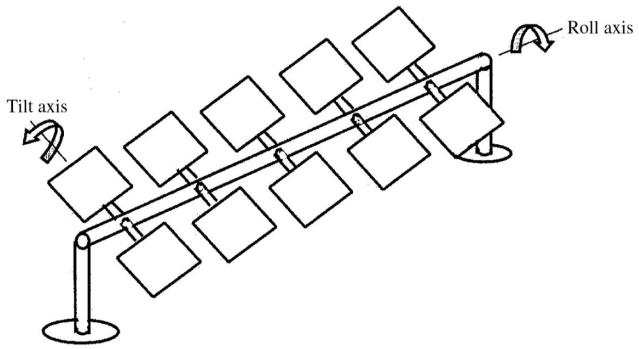

Figure 24: Roll-tilt dual-axis structure

Adapted from: Handbook of photovoltaics Science and Engineering, p458[2]

3.2 Effect of the temperature on the efficiency

The power output of a photovoltaic module depends on the operating temperature.[20] When choosing photovoltaic cells for a solar panel it is important to take into account the effect of the temperature on the efficiency, above all in those regions where the solar flux is higher.

Some experiments with polycrystalline cells expose that the maximum output power has a reduction of 18% when the temperature cell reaches values of 64 °C.[22] In addition, the module efficiency reduces with temperature as states Table 2.

Cell type	**Reduction rate [%/°C]**
c-Si	0.5
thin-film	0.02-0.41

Table 2: Effect of temperature on the efficiency

Data extracted from: On the temperature dependence of photovoltaic module electrical performance[23]

Figure 25 shows graphically the effect of the temperature on a silicon cell with a work temperature of 20°C.

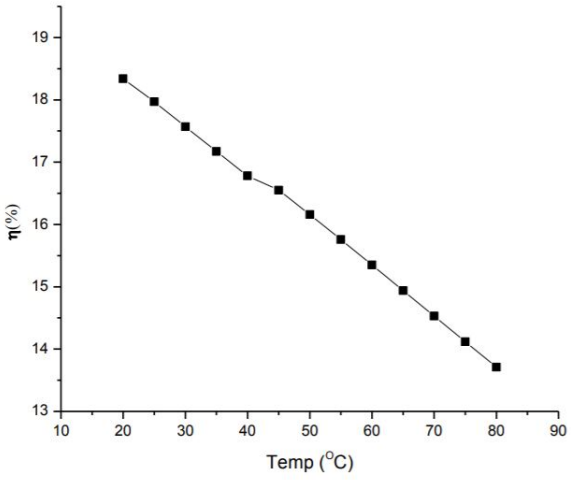

Figure 25: Variation of efficiency with temperature for a 100 μm Si cell

The effect of temperatures on the silicon cell[24]

In this context, it is important to calculate the cell temperature and compare it with the work temperature of a marketable module. Cell temperature (in celsius degrees) can be calculated with Equation 22.[47]

$$T_{cell} = T_{amb} + \overline{m} \cdot S \tag{22}$$

Where T_{amb} is the ambient temperature (in celsius degrees), $\overline{m}$ is a factor given at Equation 23[47] and S corresponds to the insolation in mW/cm^2.

$$\overline{m} = \frac{NOCT - 20}{80} \qquad \left[\frac{^{\circ}C \cdot cm^2}{mW}\right] \tag{23}$$

The nominal operating cell temperature (NOCT) is the temperature reached by open circuited cells in a module under the following conditions:

- Irradiance on cell surface: 800 W/m^2
- Air temperature: 20 degrees.
- Wind velocity: 1 m/s
- Mounting: open back side

Open back side configuration means the wind can circulate around the back side of a solar module.[47]

NOCT is usually given by the manufacturer. Typical NOCT values are:

- Worst case: 58 degrees
- Typical case: 48 degrees
- Best case: 33 degrees

Considering Burkina Faso has typical ambient temperatures between 30 and 40 degrees, work temperature cell will be an important criteria when deciding the module. If work temperature cell is exceeded, efficiency losses could be a reality.

In case of overheating and a pronounced lost in terms of efficiency, a cooling system with fins could be incorporated.[21] However, it must be outlined that commercial solar panels usually incorporate this kind of passive cooling systems and modules are bought to operate in customer desired scenarios.

(a) Manual (b) Automatic

Figure 26: SolarTurtle Hub

Adapted from: www.solarturtle.co.za

3.3 Solar energy in shipping containers

A shipping container is a container with enough strength and resistance to withstand shipment, storage and handling.

There are so many different companies that commercialise shipping containers using renewable solar energy. The current that solar panels produce can be widely used. From purifying water to supply electricity, they are useful for remote rural areas that are not electrified. These places tend to be located in third world countries with few resources.

The majority of solar container companies use foldable solar panels, either automatically or manually. They are packaged over the margins of the container size. Situated at the top, they are unfolded during the day to charge batteries, which can provide later current once the sun is not lighting up.

The *Solar Turtle* company manufactures this kind of solar containers in South Africa. Their SolarTurtle Hub product (see Figure 26) provides current for rural kiosk business such as a small tailoring, a bakery or even school classrooms. They have the automatic and the manual foldable version.[30] In addition, they commercialise a smaller version called SolarTurtle Mini (see Figure 27), which consists on a non-foldable horizontal flat solar panel. It must be mounted manually and it is transported independently.

Figure 27: SolarTurtle Mini

Adapted from: www.solarturtle.co.za

The Automatic SolarTurtle Hub uses a hydraulic system to raise two solar modules (arranged one over the other) no more than 45°. Once the modules package is in the mentioned position, the upper solar panel starts to slide using lanes on the extremes of the lower solar panel.

Although the automatic version permits the regulation of the zenith angle, it was developed for convenience. As some African places are unstable, it is a proper design to avoid damages in case of protests. Thus, the purpose is not the regulation of the angle.

The company *Africa GreenTec* presents another alternative. Its solar container is capable of unfold lots of solar modules forming inclined house roofs (see Figure 28). They are static but its design allow for unfold easily the high number of solar panels. GreenTec container was designed to ensure a fast assembly and dismantling due to the instability of some African countries. Solar panels can be rapidly saved if a conflict breaks out.[31]

Figure 28: Solar container from *Africa GreenTec* at Amaloul, Nigeria

Adapted from: www.africagreentec.com

The *MOVEit* auto-foldable solar container (see Figure 29c) is an innovative solution to easily transport solar farms without the need to assemble on site. The solar array is easy to prepare. It only takes 15 minutes of preparation to start the energy harvesting. One of the key functions of Mobile Solar is the ability to track the Sun on two axis. As a result, it is constantly aligning solar panels by sensors to ensure the highest energy yield possible. The *MOVEit* Mobile Solar uses a central pedestal, which provides horizontal and vertical movement to the solar array.

(a) Lifting (b) Unfolding (c) Tracking

Figure 29: MOVEit two-axis sun-tracking array

Adapted from: www.moveit.tech

While both *SolarTurtle* and *Africa GreenTec* containers requires labour to be mounted, *MOVEit* array is automatically ready in a few minutes. Nevertheless, *MOVEit* solar module has been entirely developed to produce energy and not to develop a task or a business inside a container. It provides more

freedom in terms of space designing because the container space is exclusively used for the Sun-tracking foldable array.

According to the International Energy Agency, more than 630 million people lack electricity in sub-Saharan Africa.[31] *SolarTurtle* or *Africa GreenTec* kind of shipping containers promote the commerce, increase the employment in rural areas and bring current in schools, which directly improves education.

In terms of water treatment in Africa, there are numerous companies that provides potable water using solar energy. *OffGrid Box*, *Elemental water Makers*, *Sustain Power* or *ERM Energies*, for example. However, they use static solar panels and they requires mounting labour. Semi-automatic or automatic unfolding solar panels are not provided.

OffGrid Box not only uses solar panels to provide energy. Wind turbines are used in some designs (see Figure 30).

Figure 30: *OffGrid Box* container with a wind turbine

Adapted from: www.offgridbox.com

Studying the market, it can be seen that does not exist Sun-tracking solar containers automatically unfolded whose internal space is used for developing a task. The current solar panels are manually mounted on site, which increases the labour and wastes the Sun irradiance. One of the main problems automatic solar containers face is the lack of space. It must be a compromise between the automatic mechanism and the space for what the container will be used. Also the transport plays an important roll. The safety and protection of the system have to be assured.

4 Design resolution

This section presents the selection process of the tracking design. The choice is based on a study of energy collection for different Sun-tracking systems and decision matrix. Different design ideas are evaluated in order to satisfy the requirements and the conclusions of the previous study.

4.1 Radiation study for different Sun-tracking PV

The purpose of the study is the comparison of the irradiance collected for different Sun-tracking panels. The different study cases are presented at Table 3. The angles β and α represent the elevation and the orientation of the panel, respectively (see Figure 15).

Sun-tracking system	β	α
Static	$3.7 + 0.69 \cdot \lvert\phi\rvert$	0
Horizontal 1-axis	θ_{zs}	0
Azimuth 1-axis	$3.7 + 0.69 \cdot \lvert\phi\rvert$	ψ_s
2-axis	θ_{zs}	ψ_s

Table 3: Energy collection study cases

There are different options to determine an annual optimal tilt angle (β_{opt}) for the static and the azimuth 1-axis cases. Although Luque and Hegedus propose $\beta_{opt} = 3.7 + 0.69 \cdot |\phi|$,[2] most researchers agree on to establish $\beta_{opt} = |\phi|$.[32] The angles θ_{zs} and ψ_s are the zenith and azimuth angles, respectively.

To calculate the solar irradiance on the panel, the method from Handbook of Photovoltaic Science and Engineering[2] is used, which finds the direct and diffuse irradiation (W/m^2), as a function of β and α (see Equations 24 and 25[2]), from the horizontal irradiation (see Figure 31).

$$B(\beta, \alpha) = B(0) \cdot \frac{max(0, \cos\theta_s)}{\cos\theta_{zs}} \tag{24}$$

$$D(\beta, \alpha) = D(0) \cdot (1 - k_1) \cdot \frac{1 + \cos\beta}{2} + D(0) \cdot k_1 \cdot \frac{max(0, \cos\theta_s)}{\cos\theta_{zs}} \tag{25}$$

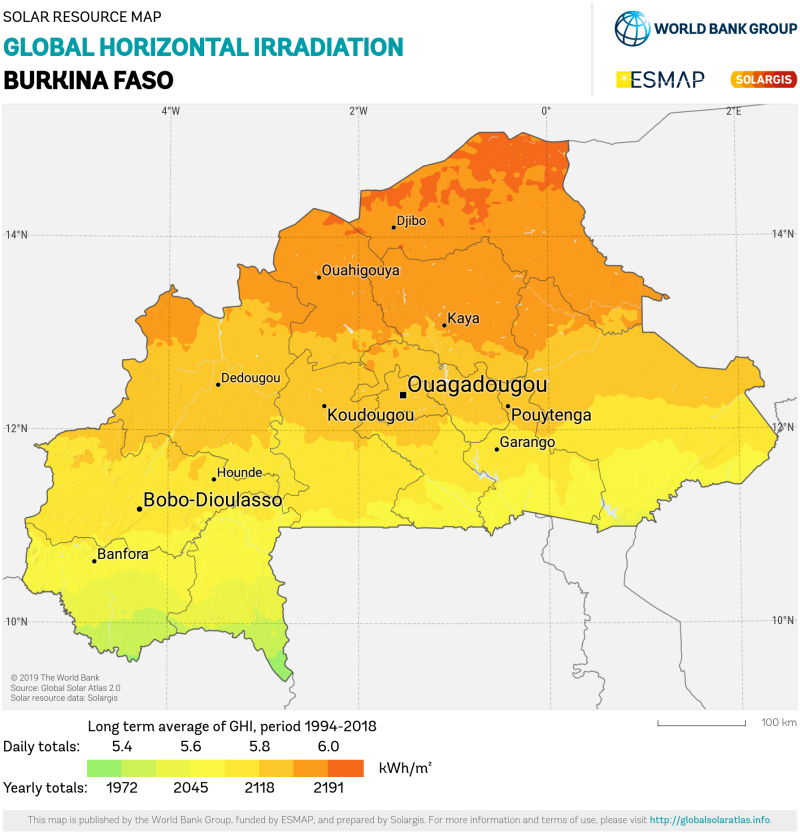

Figure 31: Global Horizontal Irradiation at Burkina Faso

Adapted from: Global Solar Atlas

The necessary irradiation data has been extracted from the European Comission's science and knowledge Service (EU Science Hub[50]).

The study has been performed at Ouagadougou ($\phi = 12.3$), capital of Burkina Faso. Figure 32 shows the yearly average global irradiance collected for static, azimuth 1-axis (VSAT), horizontal 1-axis (HSAT) and 2-axis solar panel systems during a day.

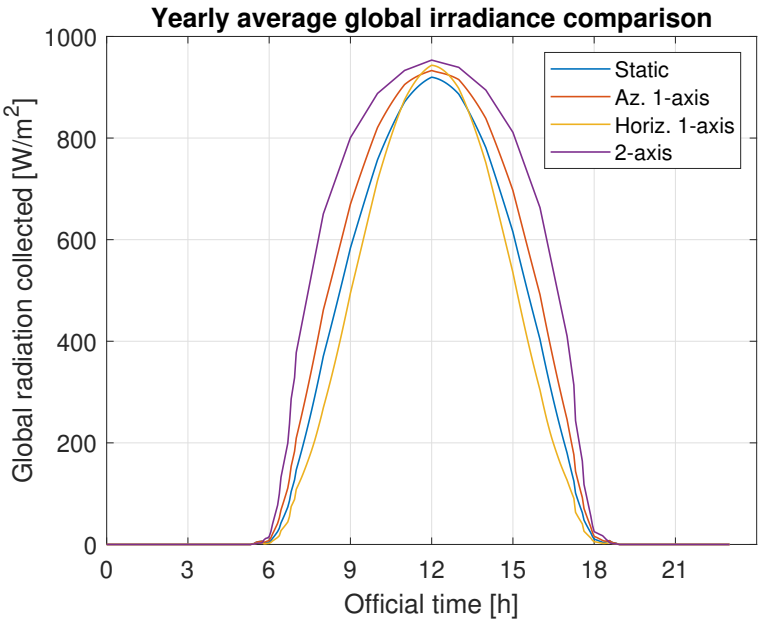

Figure 32: Yearly average global irradiance

Burkina Faso has a rainy season from April to October at South and from June to September at North. Differences during January, February, November and December gain in importance for exploitation reasons.

Figures 33 and 34 shows the December and February daily average global irradiance comparison between the different tracker systems. Plots state the high performance of dual axis Sun-tracking systems during both months. Similar results have been obtained for January and November (see Appendix B).

Differences are reduced at central months when the rainy season arrives. The radiation difference between trackers can be seen at Figures 35 and 36. Plots are a daily average of the difference of radiation between 2-axis and 1-axis for the rainy season and the dry season at North.

Differences between Sun-tracking systems are reduced when official time is near the noon. Larger differences are presented during dry season, which is a determining factor when deciding the tracking system. The MATLAB code used to plot the graphs is presented at Appendix A and the different monthly comparison plots generated are presented at Appendix B.

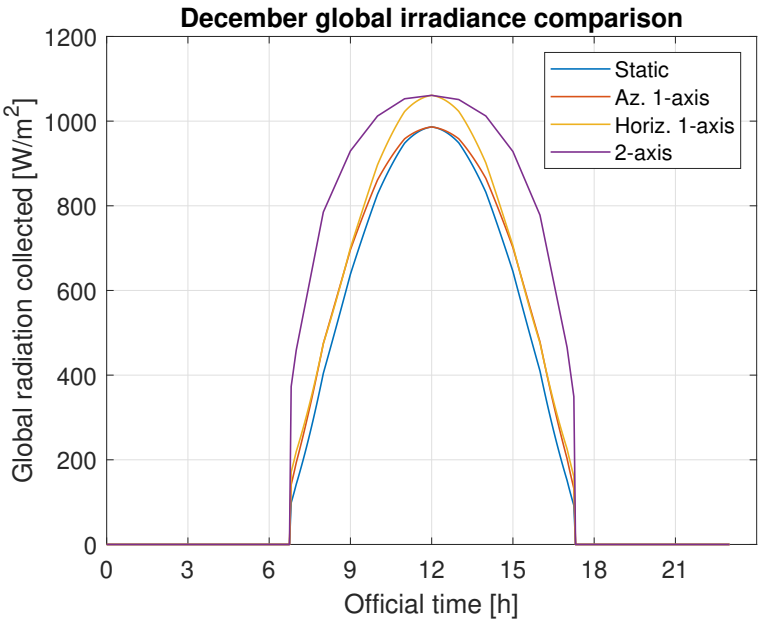

Figure 33: December daily average global irradiance

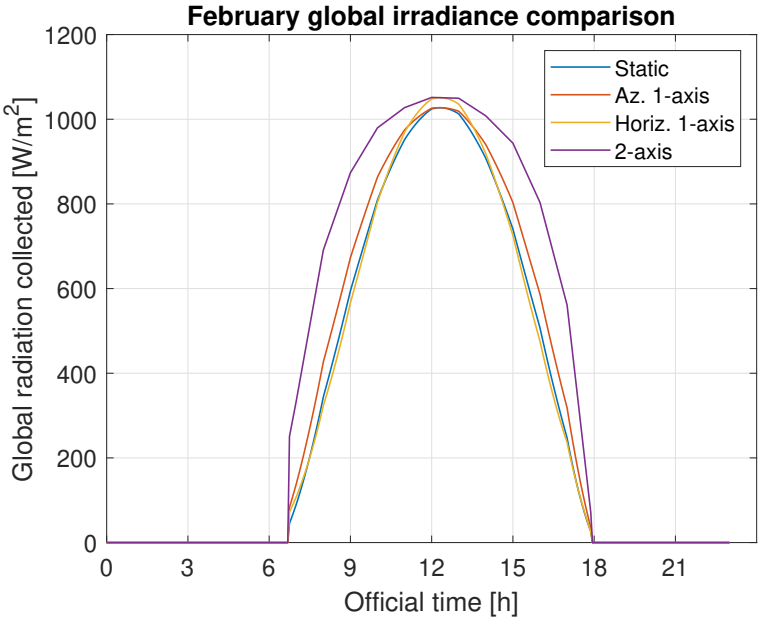

Figure 34: February daily average global irradiance

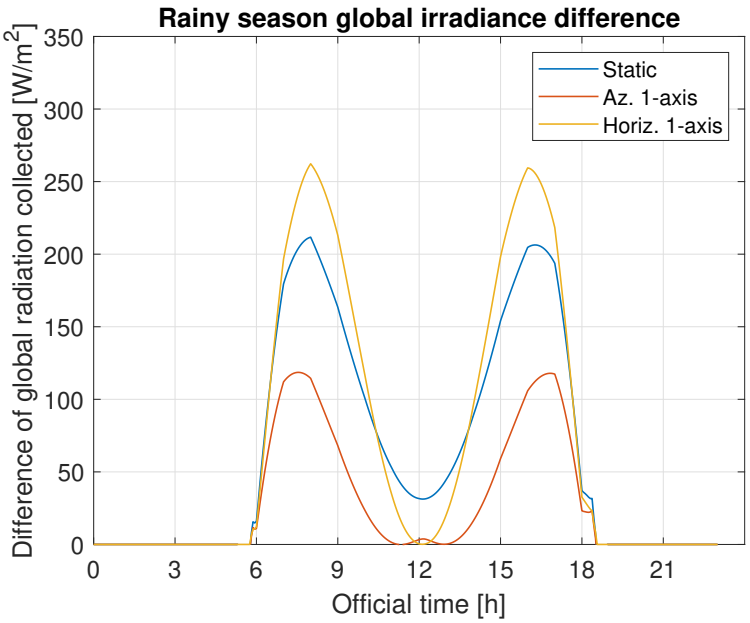

Figure 35: Rainy season daily average difference with 2-axis

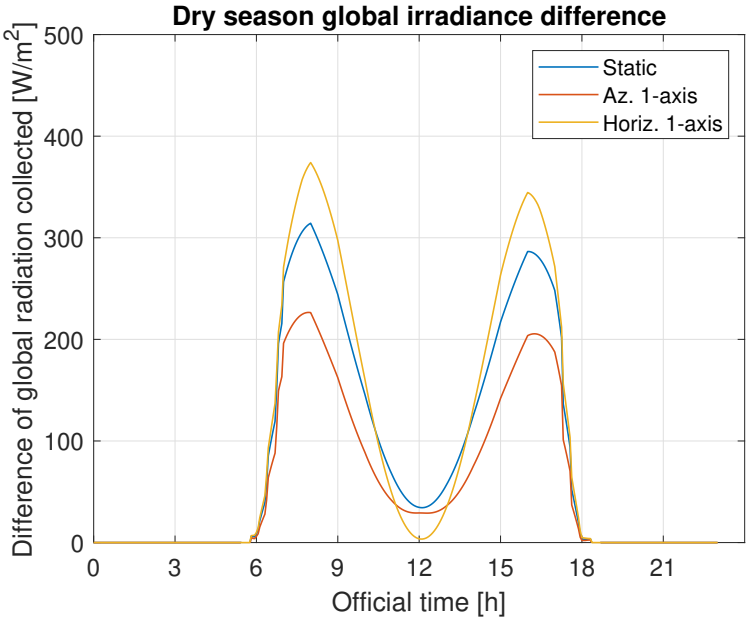

Figure 36: Dry season daily average difference with 2-axis

As a part of the study, it has been analysed the kWh/m^2 for all tracking systems. It has been studied an average power for the dry season (see Table 4) and the rainy season (see Table 5).

Tracking system	Static	Horizontal 1-axis	Azimuth 1-axis	2-axis
Power $[kWh/m^2]$	6.87	6.81	7.48	8.83

Table 4: Dry season power per m^2 for different Sun-tracking systems

Tracking system	Static	Horizontal 1-axis	Azimuth 1-axis	2-axis
Power $[kWh/m^2]$	5.74	5.56	6.56	7.22

Table 5: Rainy season power per m^2 for different Sun-tracking systems

The horizontal 1-axis tracker increases its performance if a static angle is imposed before 10 AM and after 2 PM. Only after imposing these conditions, its performance increases until 200 kWh/m^2 for the dry season and 500 kWh/m^2 for the rainy season.

4.2 Solar panel decision

The aim of this section is to present the features of diverse cell materials to make a final decision concerning the material used in the future design. The choice will be also defined using efficiency, manufacture cost, production energy, resistance and lifetime criteria. A decision matrix is developed to choose marketable models based on different criteria.

4.2.1 Cell material

Dye-sensitized solar cells are accepted as economical, efficient, and environmentally friendly photovoltaic device. Studies have shown that the performance of DSSC degrades over time, especially under high temperatures and UV irradiation conditions.[35]

As said in Section 3.1.4, perovskite cells are still in development. Although the manufacture costs are low, its lifetime is poor due to the instability of the cell so they are unmarketable. Improvements in decomposition under heat or sunlight are needed.[34]

Cell lifetime must be at least over 15 years with efficiencies of 15% to compete with thin film and silicon technology.[38]

There are lot of types of multi-junction cells because different junctions have been tested mixing a wide variety of materials. However, multi-junction cells are not commercially and the module cost would be only a speculation.

Although multi-junction cells can reach high efficiencies and they are used in space array application, they are still expensive to be marketable.

Cell type	**Efficiency**	**Module cost** $[\$/W]$	**EPBT**	**Lifetime**[34]
mono-Si	14-22 %	0.22-0.39 [40]	2.5 yrs[43]	25-30 yrs
poly-Si	14-22 %	0.17-0.3 [41]	2 yrs[43]	
HJT	18-23 %[39]	0.2 [39]	1.5 yrs[49]	
PERC	19-22 %[39]	0.2-0.39 [39]	1.4 yrs[44]	
a-Si	4-8 %	0.22-0.33 [41]	2.25 yrs[43]	17 yrs
CdTe	9-11 %		2.1 yrs[43]	37 yrs
CIGS	12-14 %		1.75 yrs[43]	15 yrs

Table 6: Features of the different cell materials

Table 6 gathers all the features of the different cell materials in order to make a decision which fulfill the requirements. Energy payback time (EPBT) shows the necessary years to generate the energy which was used to build the solar panel. EPBT is a good measure to evaluate the investment recovery.

Efficiency, costs, lifetime and energy payback depends on multiple factors such as the wafer thickness, the temperature conditions and the manufacture processes.[39] Furthermore, energy payback time depends on the place where the solar panel is located because the yearly solar irradiance has a great impact on the value. For that reason, lots of different values related to the EPBT have been found (different study conditions) and it has been concluded that the EPBT of silicon and thin-film solar cells oscillate between 1.4 and 2.5 years.

Although thin-film cells operate better under warm temperatures, they have been rejected for the final design due to silicon options are more mature and they cover the 85% of the market. Thus, silicon solar modules are cheaper and a wide variety of higher efficiency options are available. In addition, thin-film options are usually chosen for curve infrastructures, where flexibility is

necessary for the design. As our panel will sit in a flat structure, flexibility is not an essential feature.

The cell material election is between silicon crystalline options. From Table 6 it can be deducted that module cost is very similar between all the options. Mono-crystalline cells are the most expensive choice due to the silicon wafer must be purified.

Currently, HTJ and PERC are promising alternatives on account of high efficiency, reduced energy payback times and competitive costs. Poly-crystalline silicon cells do not perform as well as mono-crystalline cells in warm temperatures.

It has been decided to avoid being closed to any silicon market option due to the similarity between their properties. Some marketable silicon solar panel options will be considered and the one which better fits with the criteria exposed in Section 4.2.3 will be selected.

4.2.2 Installation calculations

This section presents the number of solar modules needed, the battery capacity and the selection of the regulator and the converter.[56]

The first step is to establish the energy consumed by the water treatment equipment. The requirements defined at section 1.3 indicates a daily energy use of 1 to 11 kWh.

$$C_{min} = 1\ kWh$$
$$C_{max} = 11\ kWh$$

It must be applied a 75% of installation performance. Thus, the total necessary energy remains in:

$$T = \frac{C}{0.75}$$

The second step is to identify the available solar radiation. The data generated during the radiation study at section 4.1 is used (European photovoltaic

application PVGIS). It must be chosen the worst case scenario, which is the most unfavourable moth.

$$H_d = 6.76 \, \frac{kW}{m^2}$$

H_d is the daily average global irradiance received by the solar modules and it has been calculated considering a dual-axis tracking system. The solar radiation is usually expressed in peak sun hours (HSP).

$$HSP = \frac{H_d}{1 \; kW/m^2} = 6.76 \; HSP$$

The third step is to calculate the number of solar modules from the peak power (W_p), the necessary energy (T) and the HSP. This calculation is found by iteration. As the module has not been already chosen (unknown W) and the number of modules is an unknown value (N), it would be calculated an estimation of modules keeping in mind the available space of the design. The tracker system frame will measure around 5.80 meters long and 2.10 meters wide. Marketable solar modules measure between 1.3 and 2 meters long and 1 meter wide. Thus, the system can contain 4 modules as minimum and 8-9 as maximum.

As usual, the most powerful solar modules have a huger area. It must be found a compromise between area occupied, power and cost.

Equation 26[56] relates the power peak of the module and the number of panels needed.

$$N = \frac{T}{HSP \cdot \eta \cdot W_p} \tag{26}$$

The therm η are the losses for deterioration and soiling. Usually, a work efficiency of 0.7-0.8 is considered.

Figure 37 represents the relation between the power peak of the module and the number of modules needed to accomplish the energy requirements (1-11 kWh).

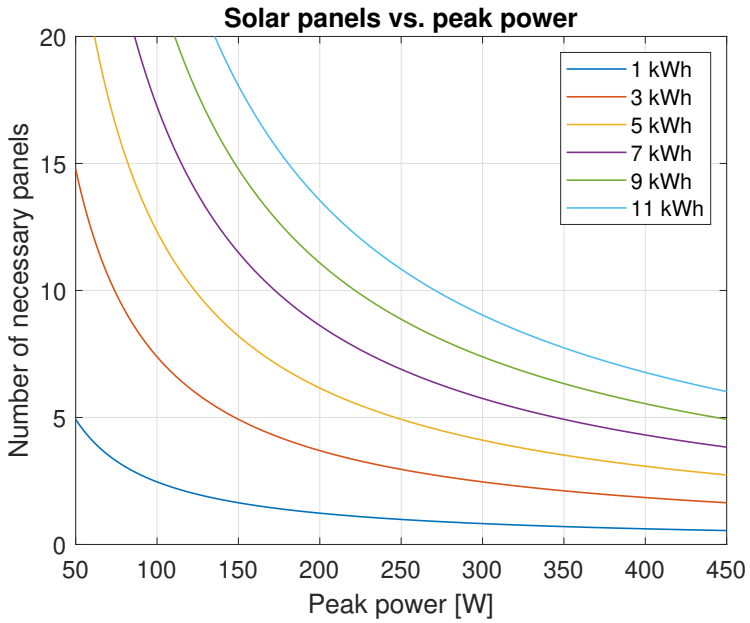

Figure 37: Number of solar panels needed to fulfill the requirements

The next step is to design the capacity of the battery (A). It is necessary to establish the autonomy desired in case of having unfavourable days without radiation for cloudiness. Equation 27[56] presents the relation between the capacity (A), the necessary energy (T), the autonomy (d), the voltage (V) and the depth of discharge (DoD).

$$A = \frac{T \cdot d}{V \cdot DOD} \quad [Ah] \tag{27}$$

Figures 38 and 39 show the relation between the depth of discharge, the energy output, the voltage of the battery and the battery capacity (in Ah). Through the plots it is possible to choose a battery that adjust with the needs of the design. The plots have been obtained for one and two days of autonomy.

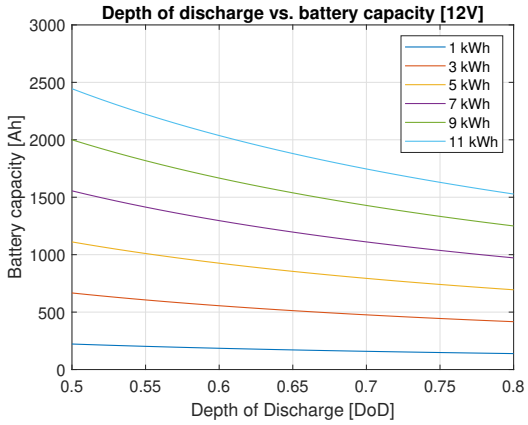

(a) One day autonomy

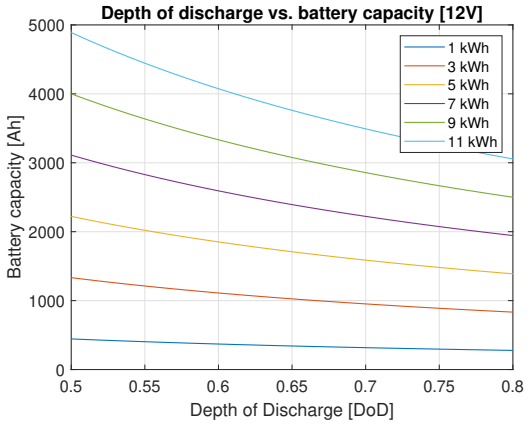

(b) Two days autonomy

Figure 38: Capacity of the battery for different DoD and energy [12V]

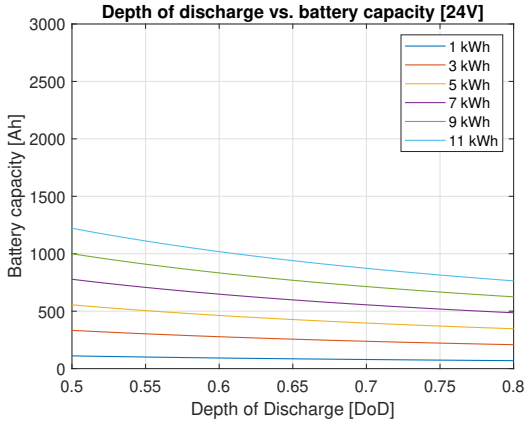

(a) One day autonomy

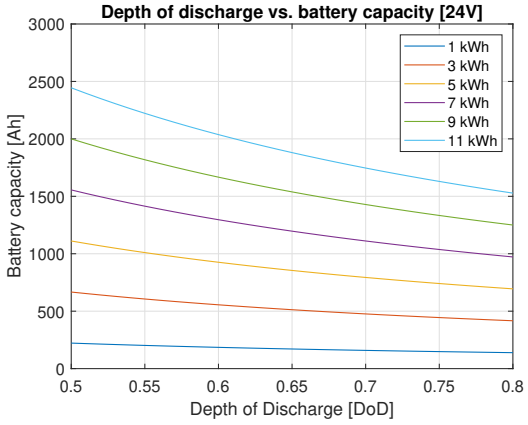

(b) Two days autonomy

Figure 39: Capacity of the battery for different DoD and energy [24V]

The last step is the selection of the charge regulator and the converter to have AC. The charge regulator is chosen in function of the maximum intensity and the voltage of the installation.

The power of the converter (see Equation 28[56]) must be selected depending on all the nominal power (P_n) of the equipment and the coefficient of

simultaneity (β) of them (normally between 0.5 and 0.7 in a home).

$$P_{converter} = P_n \cdot \beta \quad [W] \tag{28}$$

The MATLAB code used to plot the graphs is presented at Appendix A.

4.2.3 Marketable solar panels

This section presents different marketable solar panels. The options will be analysed according to the following criteria:

1. Distribution proximity: it will be positively considered because of the savings of transports and the improvement of the national economy.
2. Work temperature range: NOCT value and work temperatures must be evaluated considering Burkina Faso can reach 40 degrees of ambient temperature and 1,000 W/m^2 of radiation.
3. Module efficiency beyond 15% to assure a great performance.
4. High power
5. High corrosion resistance.
6. Lifetime beyond 15 years.
7. Reasonable price.
8. Low temperature coefficient.
9. Low weight.
10. High Power-area ratio.

Solar panel 1 (M1): ESPSA ERA 180

Distribution	Valencia
NOCT	45 ºC
Work temperature	-40ºC - 85ºC
Efficiency	18%
Power	180 W
Energy obtained	4.4 kWh
Number of panels	6
Price	133€
Lifetime	10 y. (90%), 25 y. (80%)
Weight	11.1 kg
Material	Monocrystalline Si
Temperature coefficient (Power)	-0.43%/ºC

Table 7: *ESPSA ERA 180* summary

Adapted from: AutoSolar

Solar panel 2 (M2): TALLMAX TSM-PE15H

Distribution	Valencia
NOCT	41 ºC
Work temperature	-40ºC - 85ºC
Efficiency	17.5%
Power	340 W
Voltage	24 V
Energy obtained	5.5 kWh
Number of panels	4
Price per module	149.3€
Lifetime	10 y. (90%), 25 y. (80%)
Weight	22.8 kg
Material	Multicrystalline Si
Temperature coefficient (Power)	-0.38%/ºC

Table 8: *TALLMAX TSM-PE15H* summary

Adapted from: AutoSolar

Solar panel 3 (M3): JA SOLAR JAM72S10 405 MR

Distribution	Valencia
NOCT	45 °C
Work temperature	-40°C - 85°C
Efficiency	20.2%
Power	405 W
Voltage	24 V
Energy obtained	6.6 kWh
Number of panels	4
Price per module	227.21€
Lifetime	12 y. (90%), 25 y. (80%)
Weight	22.7 kg
Material	Monocrystalline Si
Temperature coefficient (Power)	-0.35%/°C

Table 9: *JA SOLAR JAM72S10 405 MR* summary

Adapted from: AutoSolar

Solar panel 4 (M4): WAREE SERIE ARUNA 200

Distribution	Valencia
NOCT	46 °C
Work temperature	-40°C - 85°C
Efficiency	15.67%
Power	200 W
Voltage	24 V
Energy obtained	4.8 kWh
Number of panels	6
Price per module	180.65€
Lifetime	10 y. (90%), 25 y. (80%)
Weight	17 kg
Material	Monocrystalline Si
Temperature coefficient (Power)	-0.3845%/°C

Table 10: *WAREE SERIE ARUNA 200* summary

Adapted from: AutoSolar

Solar panel 5 (M5): ESCELCO PESC 340

Distribution	Santiago de Compostela
NOCT	45 °C
Work temperature	-40°C - 85°C
Efficiency	17.53%
Power	340 W
Voltage	24 V
Energy obtained	8.3 kWh
Number of panels	6
Price per module	149.6€
Lifetime	10 y. (90%), 25 y. (80%)
Weight	24 kg
Material	Policrystalline Si
Temperature coefficient (Power)	-0.42%/°C

Table 11: *ESCELCO PESC 340* summary

Adapted from: SunFields Europe

Solar panel 6 (M6): ESCELCO PESC 280

Distribution	Santiago de Compostela
NOCT	45 °C
Work temperature	-40°C - 85°C
Efficiency	17.28%
Power	280 W
Voltage	24 V
Energy obtained	6.8 kWh
Number of panels	6
Price per module	128.8€
Lifetime	10 y. (90%), 25 y. (80%)
Weight	20 kg
Material	Policrystalline Si
Temperature coefficient (Power)	-0.41%/°C

Table 12: *ESCELCO PESC 280* summary

Adapted from: SunFields Europe

Solar panel 7 (M7): AKCOME SK6610M

Distribution	Málaga
NOCT	45 °C
Work temperature	-40°C - 85°C
Efficiency	19.1%
Power	310 W
Voltage	24 V
Energy obtained	7.6 kWh
Number of panels	6
Price per module	130€
Lifetime	10 y. (90%), 25 y. (80%)
Weight	18.5 kg
Material	Monocrystalline Si
Temperature coefficient (Power)	-0.39%/°C

Table 13: *AKCOME SK6610M* summary

Adapted from: Suministros del Sol

Solar panel 8 (M8): ATERSA GS A-280P

Distribution	Valencia
NOCT	45 °C
Work temperature	-40°C - 85°C
Efficiency	17.21%
Power	280 W
Voltage	24 V
Energy obtained	6.8 kWh
Number of panels	6
Price per module	111.32€
Lifetime	10 y. (90%), 25 y. (80%)
Weight	17.75 kg
Material	Policrystalline Si
Temperature coefficient (Power)	-0.38%/°C

Table 14: *ATERSA GS A-280P* summary

Adapted from: Atersa

4.2.4 Decision matrix

The aim of this section is to decide the best suitable solar panel for the design with a decision matrix. A decision matrix is a list of values in rows and columns that allows identify, analyse and rate the performance based on certain decision criteria. The decision criteria are rated as Table 15 establish.

The different criteria used to choose the solar panel are:

- Criteria 1: Distribution proximity
- Criteria 2: Temperature (NOCT)
- Criteria 3: Energy
- Criteria 4: Corrosion resistance
- Criteria 5: Lifetime
- Criteria 6: Price
- Criteria 7: Efficiency temperature coefficient
- Criteria 8: Weight

Criteria	**1**	**2**	**3**	**4**	**5**
Criteria 1	Other continent	Europe	UE	National	Catalonia
Criteria 2	upper 45ºC	44-45ºC	42-43ºC	41-42ºC	under 41ºC
Criteria 3	under 3 kWh	3-4 kWh	4-5.5 kWh	5.5-7 kWh	above 7 kWh
Criteria 4	high	significant	medium	low	very low
Criteria 5	under 5 y.	5-10 y.	10-15 y.	15-20 y.	above 20 y.
Criteria 6	above 200€	150-200€	125-150€	100-125€	under 100€
Criteria 7	below -0.45	-0.42/-0.45	-0.4/-0.42	-0.38/-0.4	upper -0.38
Criteria 8	above 25 kg	22-24 kg	20-21 kg	18-19 kg	under 18 kg

Table 15: Rate criteria of solar panel decision

The features efficiency, power and power-area ratio have been translated into energy obtained (Criteria 3).

The final decision matrix is presented at Table 16.

Criteria	**Weight**	**M1**	**M2**	**M3**	**M4**	**M5**	**M6**	**M7**	**M8**
Criteria 1	10%	4	4	4	4	4	4	4	4
Criteria 2	10%	2	4	2	1	2	2	2	2
Criteria 3	25%	3	3	4	3	5	4	5	4
Criteria 4	10%	4	4	4	4	4	4	4	4
Criteria 5	10%	5	5	5	5	5	5	5	5
Criteria 6	25%	3	3	1	2	3	3	3	4
Criteria 7	10%	2	4	5	4	3	3	4	4
Criteria 8	10%	5	2	2	5	2	3	4	5
Total	100%	3.4	3.5	3.2	3.3	3.6	3.5	3.9	**4**

Table 16: Solar panel decision matrix

Regarding the distribution proximity, all the solar panels are nationally distributed. Work temperature neither is a concern: all the options work between -40-85 ºC. With NOCT values not exceeding 46ºC, the worst case scenario is a cell with a temperature of 73 ºC, which is inside the work temperature. Also, lifetime is not a problem: manufacturers assure a 10 years lifetime (with a 90% of the initial power) and a 25 years guarantee (with a 80% of the initial power).

The most decisive criteria are energy (criteria 3) and price (criteria 6). After analysing the decision matrix results, three options are feasible (Table 17).

Module	**Energy**	**Cost**
Solar panel 5 (ESCELCO PESC 340)	8.3 kWh	149.6 €
Solar panel 7 (AKCOME SK6610M)	7.6 kWh	130 €
Solar panel 8 (TERSA GS A-280P)	6.8 kWh	111 €

Table 17: Feasible solar panel options

The final decision depends on the user priority: minimum price or extra power. For the moment, all three options are possible and a deeper study will be performed when the global design converges.

ATERSA GS A-280P is used to perform the sizing of the preliminary design because it fulfill the energy requirements in the margins of a reasonable price.

4.3 Design decision

This section presents the different designs obtained after a brainstorming and the design selection after developing a decision matrix. The justification of the design selected is provided.

4.3.1 Brainstorming

Since the beginning of the project, different design ideas have been sketched with the purpose of selecting the most suitable alternative.

Design 1 (D1)

Design 1 (see Figure 40) is a dual axis Sun-tracking system. It consists in two perpendicular crossbars which provide zenith (red) and azimuth (blue) movement. Zenith axis is attached to two pillars (yellow) with linear movement. The pillars are hidden during transport and they provide vertical movement once in place. Solar panel frame (green) is attached to azimuth axis.

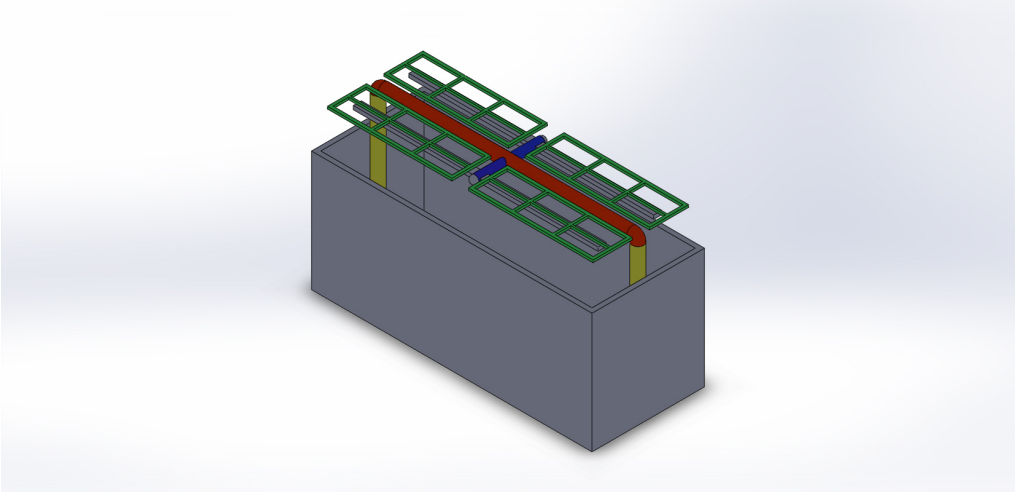

Figure 40: Design 1. Dual-axis Sun-tracking

Design 2 (D2)

Design 2 (see Figure 41) is a dual axis Sun-tracking system. It has three vertical pillars (red) which provide vertical movement. Thus, solar panels

frame (blue) can point the Sun by regulating the linear movement of the pillars.

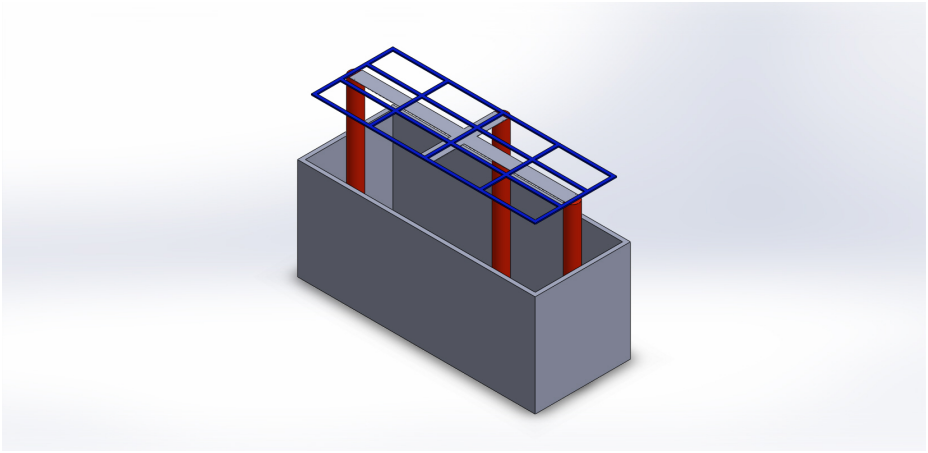

Figure 41: Design 2. Dual-axis Sun-tracking

Design 3 (D3)

Design 3 (see Figure 42) is made up of a horizontal crossbar (red) to track the elevation angle. Two supports transmit the movement to the solar panel frame (green). The vertical pillars allow vertical movement to deploy the system.

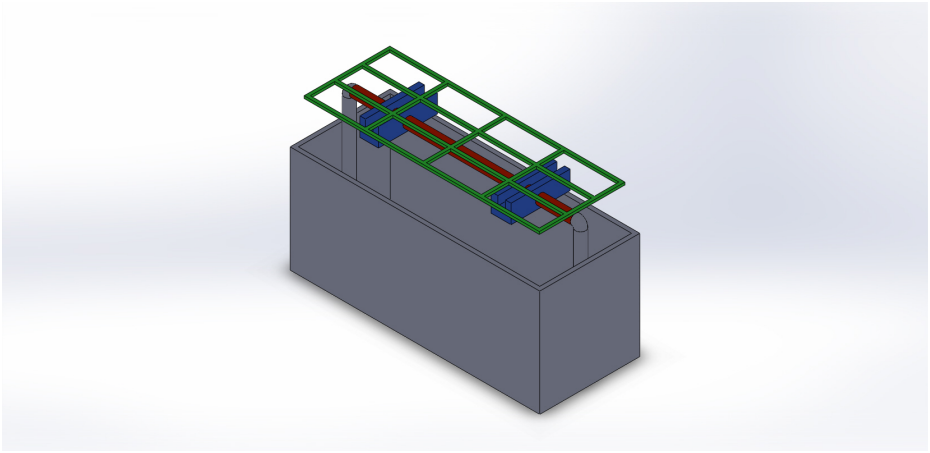

Figure 42: Design 4. Horizontal 1-axis Sun-tracking

Design 4 (D4)

Design 4 (see Figure 43) consists of a single vertical pillar that transmit the movement to the container roof. Only elevation angle can be modified with this system. It is devised to use thin-film solar panels over the roof because they are flexible and can be kept inside the shipping container during transportation.

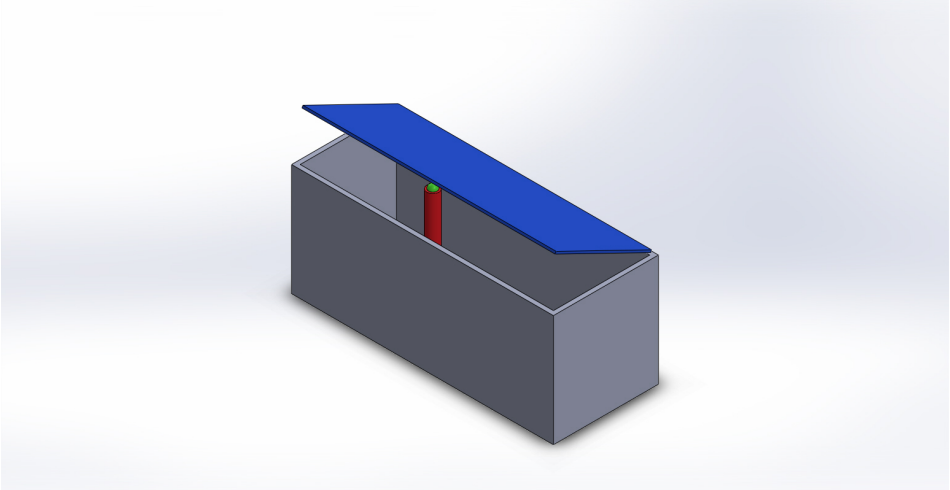

Figure 43: Design 4. Horizontal 1-axis Sun-tracking

Design 5 (D5)

Design 5 (see Figure 44) has a single crossbar (red) to track the azimuth angle. Two supports transmit the movement to the solar panel frame (green). The vertical pillars allow vertical movement to deploy the system.

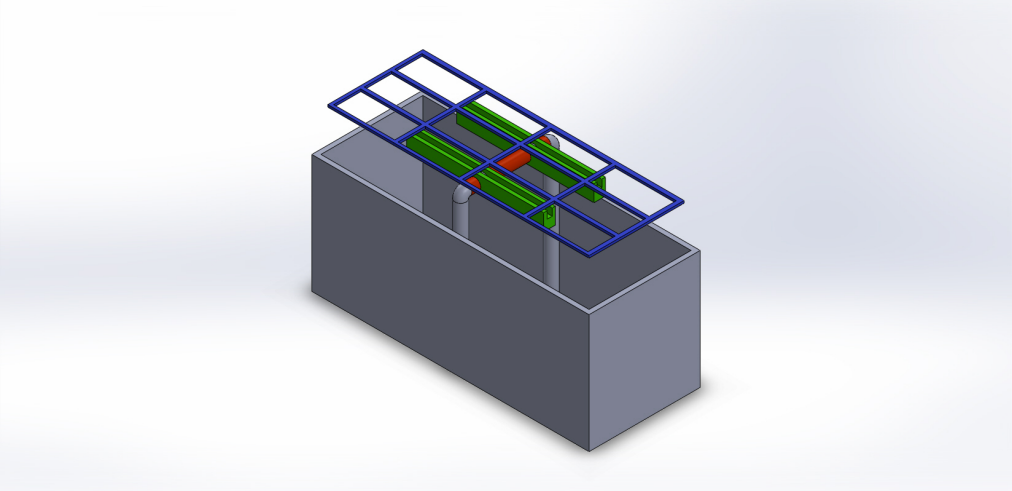

Figure 44: Design 5. Azimuth 1-axis Sun-tracking

Design 6 (D6)

Design 6 (see Figure 45) has a false ceiling (yellow) and a central pedestal (red and blue) that sits on it. The central pedestal can unfold itself vertically. Once the Sun-tracking system is deployed, the blue pillar can rotate to track the azimuth angle. The top of the blue pillar permits the elevation angle movement.

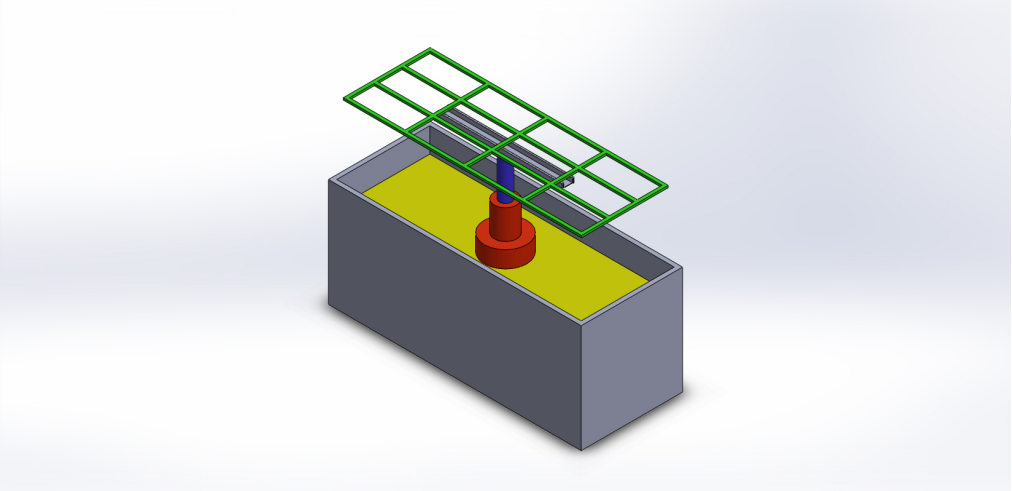

Figure 45: Design 6. Dual-axis Sun-tracking

Design 7 (D7)

Design 7 (see Figure 46) is based on a static track system that use all the available space inside the shipping container to increase the area. The system uses lateral lanes to deploy one or two solar panel frames (red). It also has casement modules at the extremes (green).

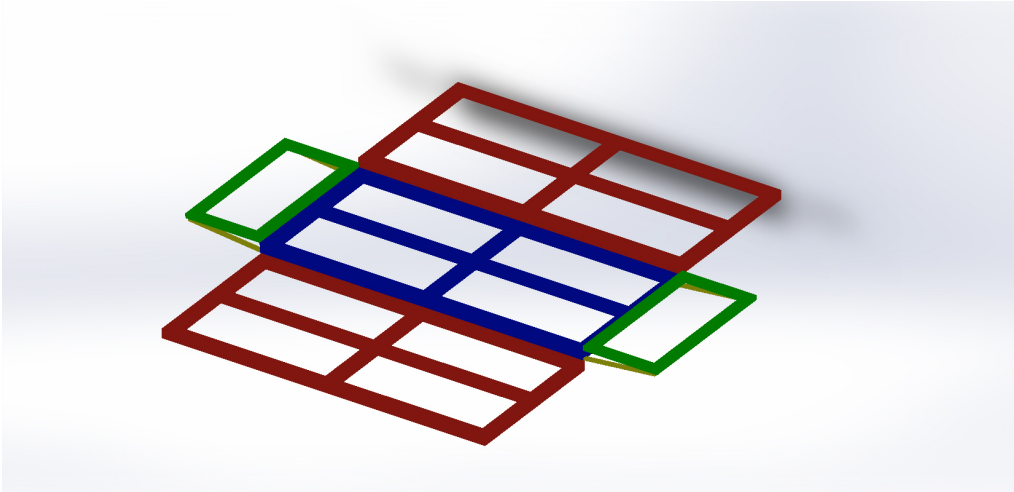

Figure 46: Design 7. Foldable static system

After analysing the results from Table 4 and Table 5, the area of the static panel must be increased a 30% with casement and sliding frames to obtain the same power as dual axis Sun-tracking system.

Extra area add-on

A foldable static system can be added to all the designs. Casement modules can be used not only to provide more photovoltaic area but to provide safety during transportation. It will be considered as future work.

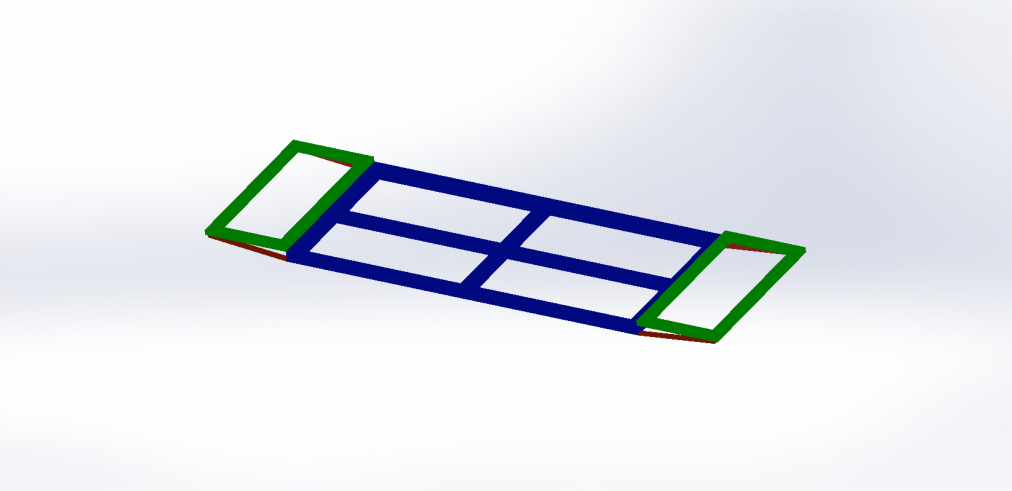

Figure 47: Extra area add-on

Design 8 (D8)

Design 8 (see Figures 48 and 49) is a dual axis tracker system that uses a circular platform (blue) for the azimuth angle and a linear actuator (yellow) for the zenith angle. There is a square platform (green) over the circular. Two joints permit the elevation movement of the solar panels (red) while the entire design is rotating. The design is over a false ceiling that can be lifted with screw jacks. The design remains inside the shipping container during transport; once in place it is deployed.

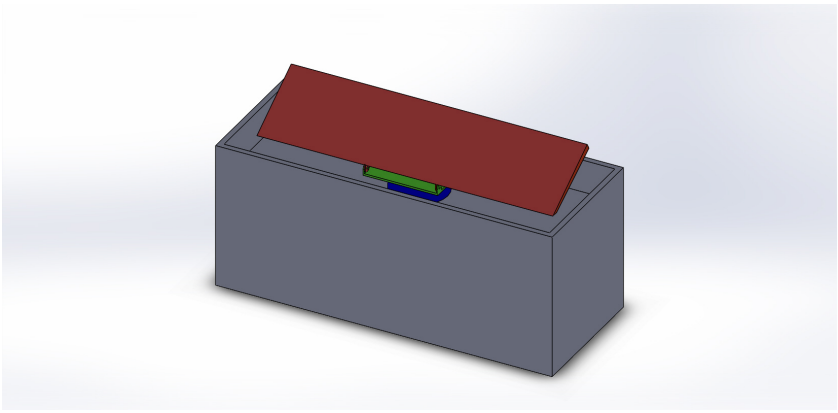

Figure 48: Design 8. Dual axis Sun-tracking

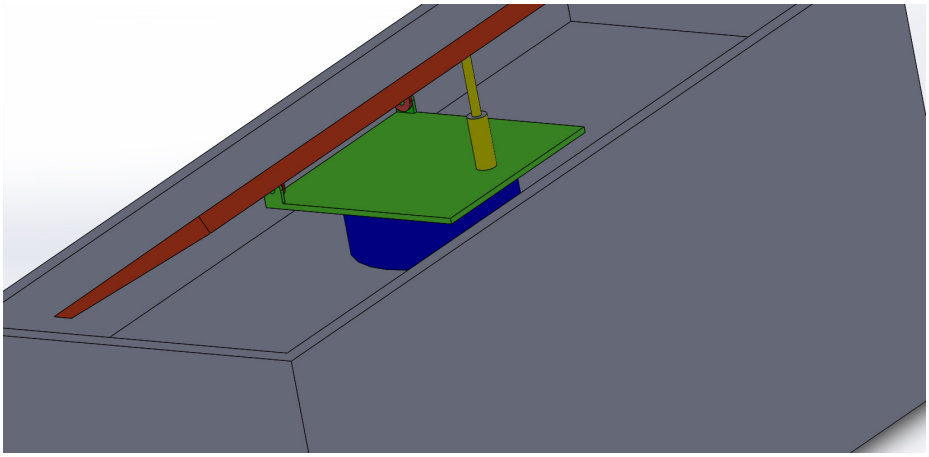

Figure 49: Design 8. Rear part

Design 9 (D9)

Design 9 (see Figures 50 and 51) is a dual axis tracker system that uses two linear actuators (yellow) to provide azimuth (green) and zenith movement (blue). The design uses joints. The shipping container has been removed in order to see the design. The main structure can be lifted with screw jacks once the shipping container is in place.

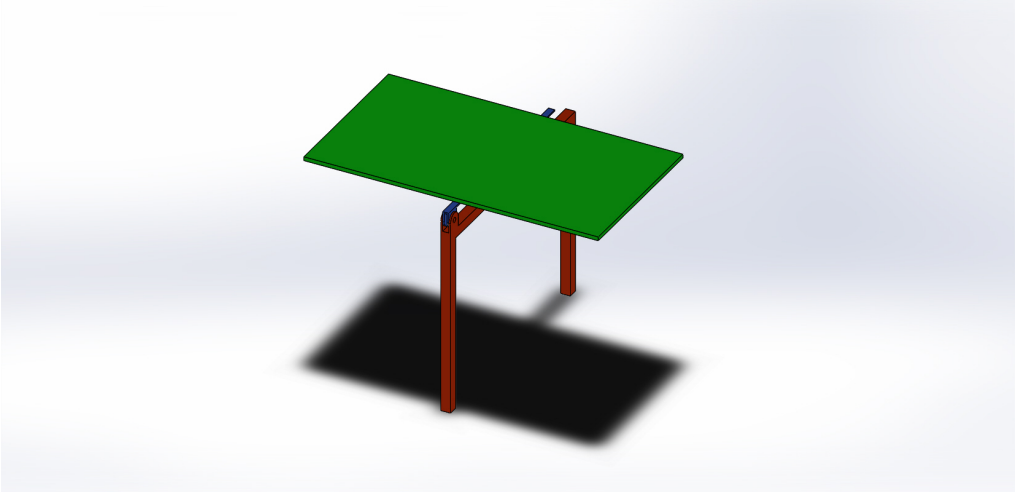

Figure 50: Design 9. Dual axis Sun-tracking

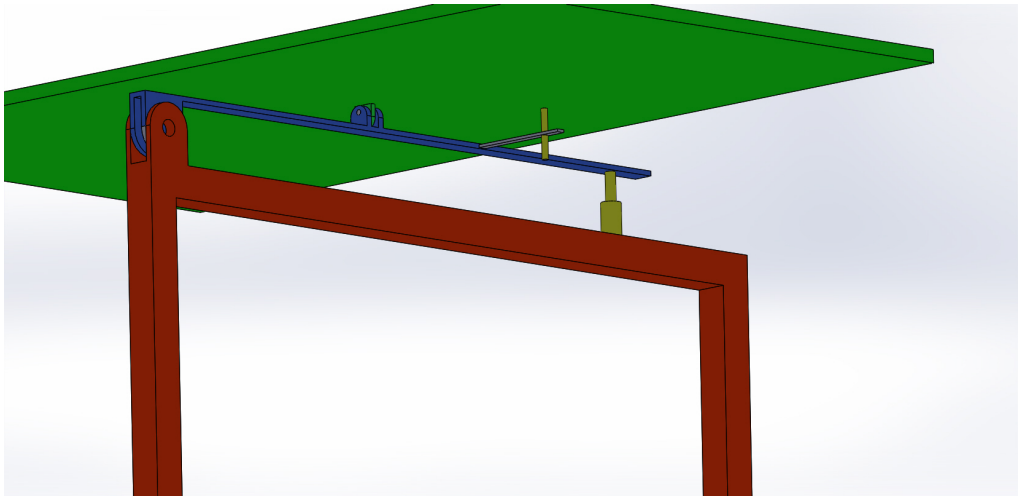

Figure 51: Design 9 detail

Design 10 (D10)

Design 10 (see Figures 52 and 53) is a dual axis tracker system that uses linear actuators (yellow). The main structure permits the azimuth movement with joints. Red structure also has joints and solar panels are moved with linear actuators to allow elevation movement.

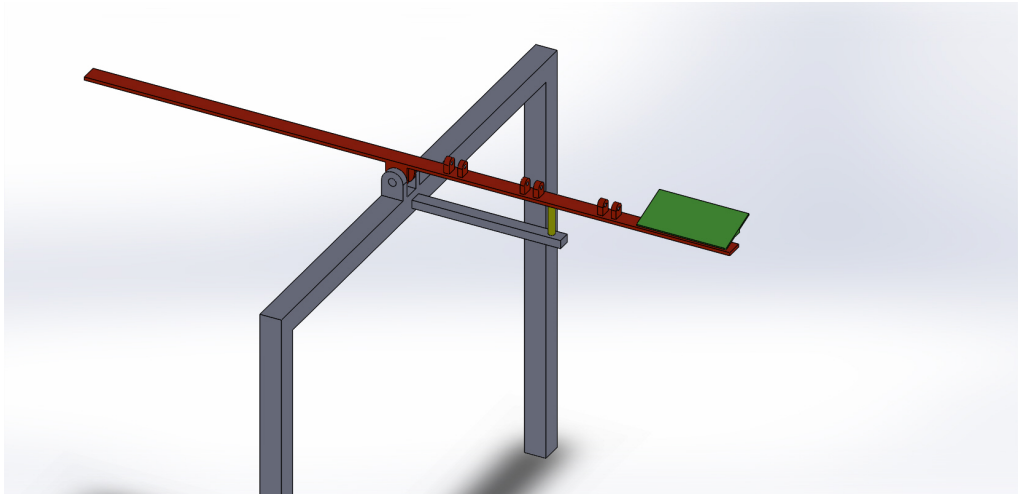

Figure 52: Design 10. Dual axis Sun-tracking

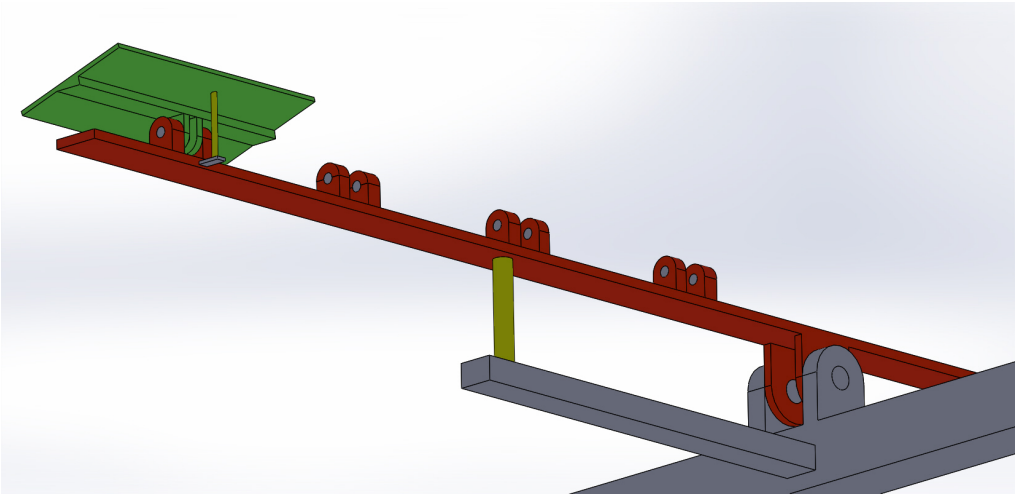

Figure 53: Design 10. Rear detail

4.3.2 Sun-tracking in Burkina Faso

A code has been developed to track the Sun during a whole year in Burkina Faso (see Appendix C), specifically in Ouagadougou ($\phi = 12.3^{o}N$, $\lambda = 1.3^{o}W$).

The results show that locations below the Tropic of Cancer (23° 16') have a distinctive feature: At noon the Sun points at south or at north depending on the day of the year. This means that during some days the Sun does not cross the East-West line. The dual axis tracker system must point at north the 32% of the year instead of the south. This feature work against static and 1-axis azimuth tracker options because they use a fixed zenith angle.

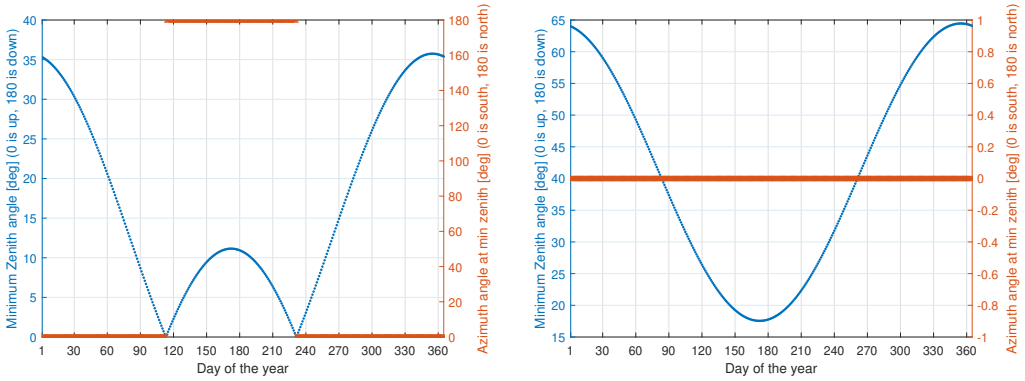

(a) ϕ=12.3º (b) ϕ=41º

Figure 54: Azimuth and zenith angles at noon during the year

Figure 54 shows that the azimuth angle is always at 0 degrees (South) at noon for a latitude above Tropic of Cancer. For latitudes below Tropic of Cancer, azimuth angle changes (0º=South/180º=North) at noon during the year. Thus, the dual-axis tracker gains importance due to it is flexible and can be prepared to face the north. If a whole year is divided in days from 1 to 365, this fact occurs from day 114 to 232 at $\phi = 12.3^{o}N$.

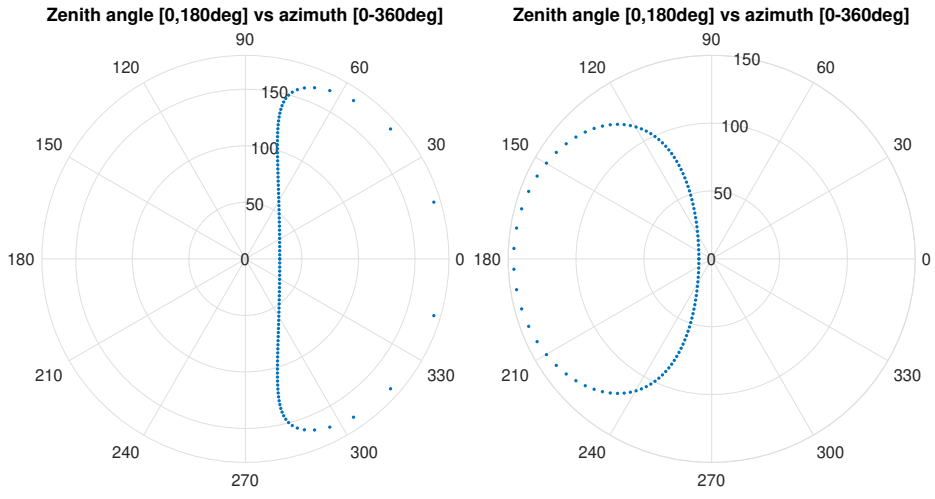

(a) Day 30 (b) Day 150

Figure 55: Azimuth and zenith angles during a day in Ouagadougou

Figure 55 also illustrates the change of azimuth angle at noon: 0º represents the South and 180º represents the North.

Designing a dual-axis tracker is the most expensive option, but the most effective solution for latitudes above Tropic of Cancer. Considering only laterals can be used because of space requirements, azimuth trackers and 2-axis trackers will need a structure of lateral pillars to hide the design during the transport of the shipping container.

Horizontal 1-axis trackers only excels when the sun is at noon, but it hardly exceed the performance of a static solar panel from a global point of view.

Design 2 was thought to be the most feasible option using hydraulic telescopic cylinders to lift the frame. Also, it is very stable because it has three pillars. However, technical difficulties were found during a deeper development. The linear actuator must have two ball joints (one with the solar panel structure and other with the shipping container) to permit the dual axis tracking. The structure can't be risen once in place due to it is hidden vertically during transportation.

Design 1 presents technical difficulties too. The union of the two axis could present structural difficulties due to overweight. In addition, the liftable pillars (yellow) should elevate more than two and a half meters to avoid shadowing. This is a problem that almost all the designs present and only can be resolved with expensive telescopic cylinders.

Design 6 uses a central pedestal over a table structure to track the Sun. Its main problem is the high vertical space it uses when the system is folded. Although the telescopic cylinder saves space, the half of the shipping container height would be used.

Designs 1, 2, 6 and 9 present the same limitation. All of them work if they are pointing towards the South. It means they can track the Sun a 33% of the year, when the system should point the North.

In the context of technical difficulty, designs 8 and 10 are the most feasible options. However, design 10 needs long telescopic cylinders to avoid shadowing.

Design 8 uses a lineal actuator to track the elevation angle and uses a rotational drive to track the azimuth. The system is mounted over a table structure that only needs to be lifted some centimeters to avoid shadowing.

Also, the shipping container can be positioned without orientation requirements due to the rotational drive can rotate 360 degrees. This feature is key when designing technology for African rural areas with lack of resources. Thus, placement and orientation will not be a concern.

The design decision is corroborated with a decision matrix at section 4.3.3.

4.3.3 Decision matrix

The aim of this section is to decide the best suitable design to track the Sun through a decision matrix. The decision criteria are rated as Table 18 establishes. The different options have been presented at section 4.3.1.

The different criteria used to choose the design are:

- Criteria 1: Power (depending on the axis tracked)
- Criteria 2: Reliability (1: Rotating axis; 5: No rotating axis)
- Criteria 3: Technical difficulty (1: design new pieces; 5: all off-the-shelf)
- Criteria 4: Cost (1: telescopic actuators; 5: any mechanism)
- Criteria 5: Labour on site (1: mount everything on site; 5: do nothing)

Criteria	**1**	**2**	**3**	**4**	**5**
Criteria 1	static	1-axis H	1-axis V	2-axis S	2-axis S-N
Criteria 2	low	regular	normal	high	excellent
Criteria 3	very high	high	moderate	low	very low
Criteria 4	very expensive	expensive	moderate	low	very low
Criteria 5	high	significant	normal	low	very low

Table 18: Rate criteria of the design decision

The decision matrix is presented at Table 19.

Criteria	**Weight**	**D1**	**D2**	**D3**	**D4**	**D5**	**D6**	**D7**	**D8**	**D9**	**D10**
Criteria 1	40%	4	4	2	2	3	4	1	5	4	5
Criteria 2	25%	3	3	4	4	4	3	5	3	3	3
Criteria 3	10%	2	2	3	3	3	2	4	3	3	3
Criteria 4	15%	1	1	3	3	3	1	1	3	2	2
Criteria 5	10%	3	4	3	3	3	4	3	3	3	3
Total	100%	3	3.1	2.85	2.85	3.25	3.1	2.5	**3.8**	3.25	3.65

Table 19: Design decision matrix

The decision matrix confirms the justification in section 4.3.2. Design 8 is proven to be the most feasible option.

5 Design development

This section presents the development of the preliminary design, with a preliminary structural analysis and a study of the wind effects in the solar panels.

The following methodology is adopted for developing the design:

- Step 1: Conceptual design and parts definition.
- Step 2: Sizing of the parts based on structural analysis
- Step 3: Design of linear actuator and rotational drive.
- Step 4: CAD development with SolidWorks.

5.1 Conceptual design

The conceptual design was manually sketched before developing the CAD design (see Figure 56). The tracker system have the following parts:

1. Bottom flat support (yellow)
2. Upper flat support (green)
3. Horizontal beams (blue)
4. Vertical beams (red)
5. Linear actuator (pink)
6. Rotational drive (slew drive)

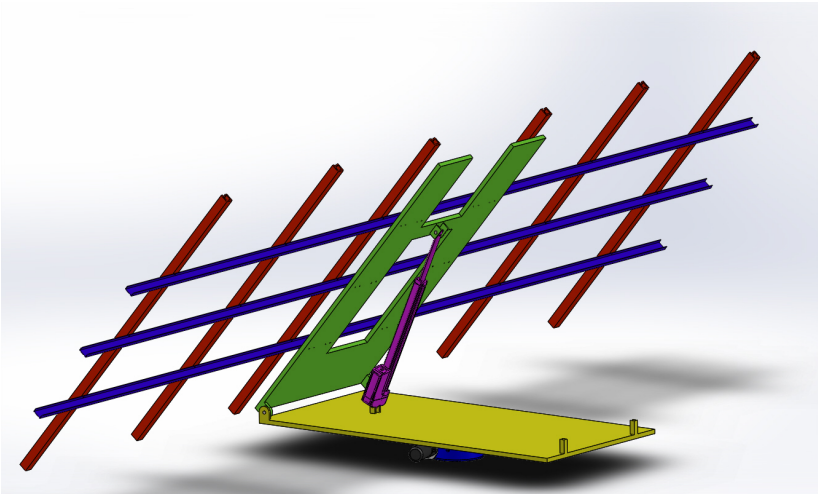

Figure 56: Conceptual design

The slew drive is mounted over a table structure (green color in Figure 57). The rotary actuator is screwed to the bottom flat support and allow rotation once the green table is out of the shipping container. The legs of the table structure are liftable through screw jacks, so the system is hidden inside the shipping container during transport.

Upper flat support is movable through joints. The linear actuator is united to the upper flat support and can rotate when force is applied. Thus, there is space for the linear actuator and it can lift the system when the stroke increases.

Three horizontal beams support six vertical beams and six solar panels.

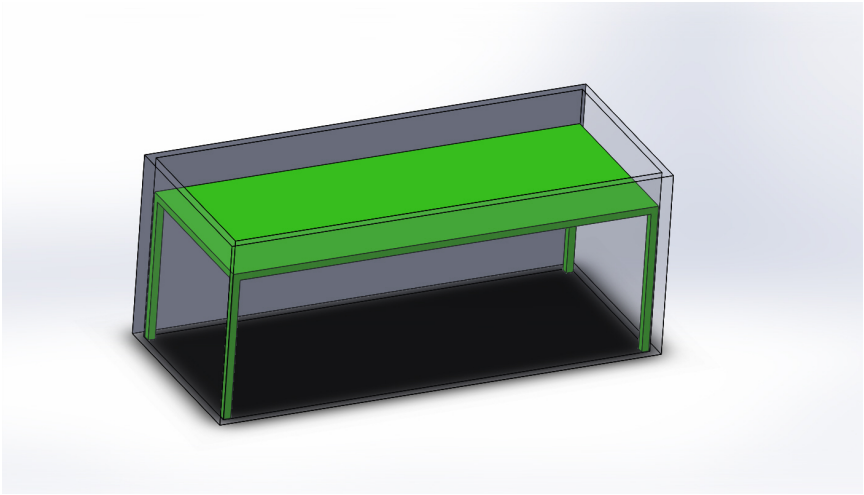

Figure 57: Liftable table structure

5.2 Materials

The material of the Sun-tracking system is an important step because it affects the weight of the system, the resistance of the structure and the corrosion.

Keeping in mind that there is a rainy season in Burkina Faso, the material used can't oxidise with water.

All the components have been designed using galvanized steel. However, there is room for improvement in the material selection. A deeper study has to be performed to analyse the resistance of the material.

Density	7,850 kg/m^3
Ultimate tensile strength (UTS)	357 MPa
Yield strength (f_k)	204 MPa
Young's Modulus	210 GPa
Poison's ratio	0.29

Table 20: Properties of galvanized steel

5.3 Vertical beams

Solar panels are attached at vertical beams with end clamps (Figure 58).

Figure 58: End clamp

Adapted from: Sone PV

After analysing different options, the C type cross section (Figure 59) is the best option due to the material optimization. Also, end clamps can be easily fixed to C type cross sections.

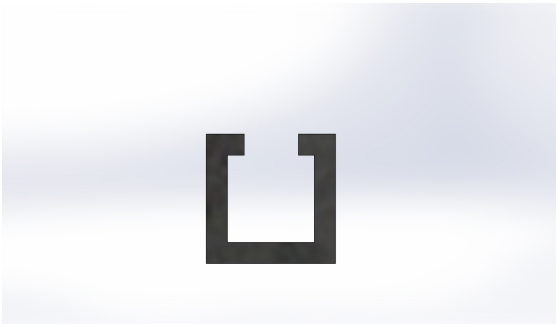

Figure 59: C type cross section

Only six solar panels can be used due to space requirements (see Figure 60). Solar panels have been simplified to point loads (blue) in order to size the vertical beams (see Figure 61). The length of vertical beams shall exceed 1,988 mm, which is the width of two solar panels, plus the space occupied by the end clamps. Structural calculations have been performed with a vertical beam of $L_v = 2,010\ mm$.

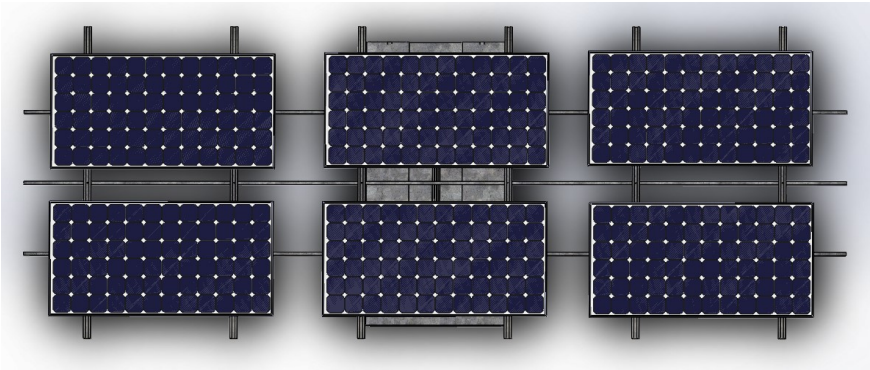

Figure 60: Solar panels disposition

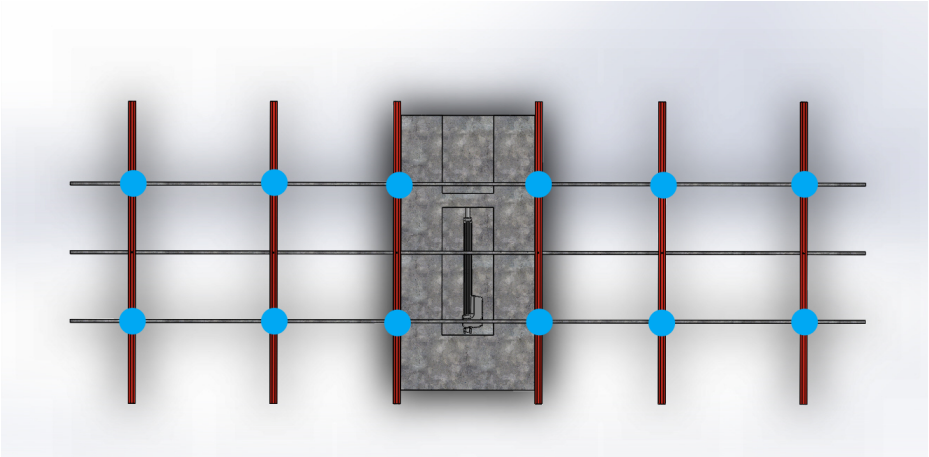

Figure 61: Point loads location

Every point load (Q) has a value of 88N. The result is obtained from Equation 29.

$$Q = \frac{W_p \cdot g}{n} \tag{29}$$

Where W_p is the panel weight (17.85 kg), g is the gravity and n is the number of beams in which the solar panel is attached.

To compute the shear, the bending moment and the deflection, *Deflection Blue Ketchep* has been used, which is a structural beam calculator.

The structural conditions of the vertical beam have been replicated using point loads and simple supports. The diagrams obtained from the beam calculator show a low shear stress and a low bending stress (see Table 21).

Maximum shear stress (τ_{max})	0.0932 MPa
Maximum bending stress (σ_{max})	2.33 MPa
Maximum deflection (δ_{max})	0.079 mm

Table 21: Vertical beam: analytical results

Complete results: Deflection Blue Ketchep

The cross section used is shown at Figure 62.

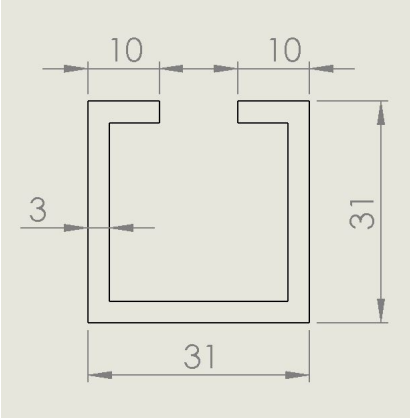

Figure 62: Cross section of vertical beam [mm]

Although maximum stress results are low, some structural verification have to be made (Equations 30, 31 and 32[62]).

$$f_d = \frac{f_k}{\gamma_s} \geq \sigma_{max} \tag{30}$$

$$f_{vk} = \frac{f_d}{\sqrt{3}} \geq \tau_{max} \tag{31}$$

$$\delta_l = \frac{L}{500} \geq \delta_{max} \tag{32}$$

Where f_k is the yield strength of the galvanized steel, γ_s is the factor of safety (1,05 for steel), δ_l is the vertical limit deflection and L is the length of the beam.[62]

The value of δ_l depends on the type of beam and its use. One of the most restrictive deflection limits has been considered.[63]

The vertical beam designed is structurally secure and satisfy all the structural requirements. Observing the stress profiles, it can be seen that central support can be removed without compromise the structural security. Only after analysing the horizontal beams conceptual design could be modified.

5.4 Horizontal beams

Vertical beams are attached at horizontal beams with threaded bolts. Horizontal beams have a length of 5,800 mm and they are fixed to the upper flat support.

An U type cross section has been selected to design the horizontal beams. As C type does, the material can be optimized as well as it has good structural results.

Horizontal beams must support the weight of the solar panels and the vertical beams. Being a beam so long, maximum deflection will be found at the extremes. The length of the horizontal beams shall exceeds 4,920 mm, which is the length of three solar panels. Thus, structural calculations have been performed with a vertical beam of $L_h = 4,950mm$.

Two central simple supports and six point loads have been considered to analyse the beam performance.

Point loads have been calculated considering there is a central horizontal beam (Equation 33) and without it (Equation 34). Both ways have been analysed using the structural beam calculator *Deflection Blue Ketchep*.

$$Q = \left(\frac{1}{2}W_p + \frac{1}{3}W_c\right) \cdot g = 105N \tag{33}$$

$$Q = \left(\frac{1}{2}W_p + \frac{1}{2}W_c\right) = 114N \tag{34}$$

Where W_p is the weight of a solar panel and $W_c = 5.3\ kg$ is the weight of a vertical beam.

The analytical results for case 1 ($Q = 105N$) and case 2 ($Q = 114N$) are presented at Table 22.

	Case 1	**Case 2**
Maximum shear stress (τ_{max})	2.5 MPa	2.66 MPa
Maximum bending stress (σ_{max})	29.3 MPa	31.1 MPa
Maximum deflection (δ_{max})	9.18 mm	9.78 mm

Table 22: Horizontal beam: analytical results

Complete results (1): Deflection Blue Ketchep

Complete results (2): Deflection Blue Ketchep

The cross section of the horizontal beam is shown at Figure 63.

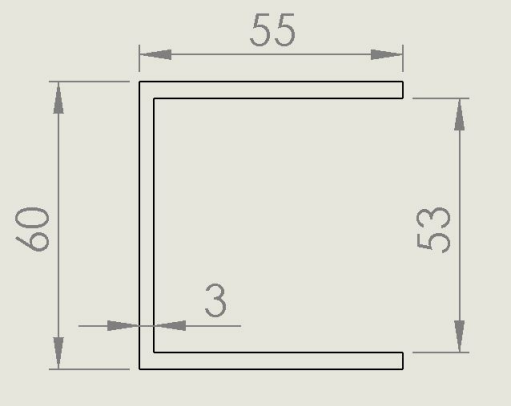

Figure 63: Cross section of horizontal beam [mm]

Structural verification have to be made to confirm the structural security of the sizing (Equations 30, 31 and 32).

After assuring both cases satisfy the structural requirements, the central horizontal beam can be removed from the design.

5.5 Bolt connections

Bolt connections are used to connect vertical with horizontal beams and horizontal beams with the upper flat support.

The quality of the steel used in the bolt manufacture determine the type of bolt. Table 23 shows the tensile strength and the ultimate tensile strength (UTS) of the bolts.

Type of bolt	4.6	4.8	5.6	5.8	6.8	8.8	10.9
Yield strength [MPa] (f_{yb})	240	320	300	400	480	640	900
UTS [MPa] (f_{ub})	400	400	500	500	600	800	1000

Table 23: Types of bolts

Data extracted from: Uniones atornilladas[64]

The factor of safety for bolts is $\gamma_{Mb} = 1.25$.

The connections of the design can fail by shear stress or tensile stress (see Figure 64). The worst case scenarios will be produced when the elevation angle is 0 degrees (maximum tensile) and when the elevation angle is 90 degrees (maximum shear stress). Both stresses are caused by the weight of the panels and the beams. Preloaded[14] bolts are rejected due to they do not benefit a quicker dismantling in case of repair in rural areas of Burkina Faso.

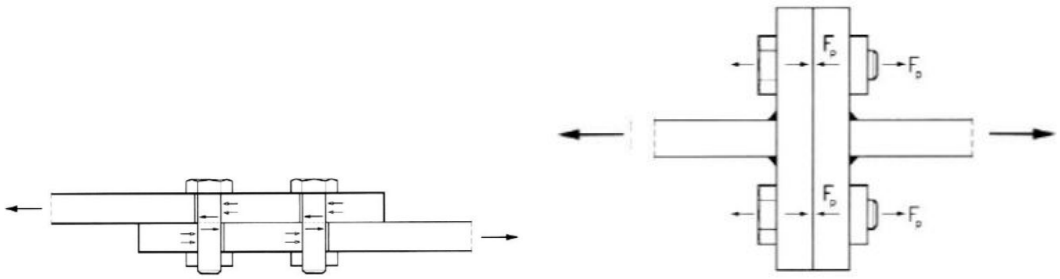

(a) Shear stress (b) Tensile stress

Figure 64: Failure stresses

Adapted from: Uniones[65]

[14]Preloading is a technique that consists in compress a system in the opposite direction of the loads.

The bolts used must satisfy the structural requirements presented at Equations 35, 36, 37 and 38.[64]

$$F_{\nu,Sd} \leq F_{\nu,Rd} \tag{35}$$

$$F_{\nu,Sd} \leq F_{b,Rd} \tag{36}$$

$$F_{t,Sd} \leq F_{t,Rd} \tag{37}$$

$$\frac{F_{\nu,Sd}}{F_{\nu,Rd}} + \frac{F_{t,Sd}}{1.4 \cdot F_{t,Rd}} \leq 1 \tag{38}$$

Where $F_{\nu,Rd}$ is the shear resistance of the bolt, $F_{b,Rd}$ is the crushing resistance at the adjacent zone of the bolt and $F_{t,Rd}$ is the tensile resistance of the bolt. Equation 38 is a requirement to test the combination of the shear and the tensile stresses. It will be maximum when the elevation angle is at 45 degrees.

$F_{\nu,Rd}$ is calculated as states Equation 39.[64] It is given in Newtons (N).

$$F_{\nu,Rd} = \frac{0.6 \cdot f_{ub} \cdot A_s}{\gamma_{Mb}} \tag{39}$$

Where f_{ub} is the ultimate tensile strength of the bolt, A_s is the resistance area (threaded part) and γ_{Mb} is the factor of safety for bolts.

$F_{b,Rd}$ is calculated as states Equation 40.[64] It is given in Newtons (N).

$$F_{b,Rd} = \frac{2.5 \cdot \alpha \cdot f_u \cdot d \cdot t}{\gamma_{Mb}} \tag{40}$$

Where f_u is the ultimate tensile strength of the element that connects the bolt (beams and upper flat support), d is the diameter of the bolt, t is the thickness of the beam/support and γ_{Mb} is the factor of safety for bolts.

The α value[64] is calculated as:

$$\alpha = min \left\{ \frac{e_1}{3 \cdot d_0} ; \frac{p_1}{3 \cdot d_0} - \frac{1}{4} ; \frac{f_{ub}}{f_u} ; 1 \right\}$$

Where d_0 is the diameter of the hole, e_1 is the distance to the frontal extreme and p_1 is the separation between bolts.

$F_{t,Rd}$ is calculated as states Equation 41.[64] It is given in Newtons (N).

$$F_{t,Rd} = \frac{0.9 \cdot f_{ub} \cdot A_s}{\gamma_{Mb}} \tag{41}$$

The geometry of a bold is presented in Figure 65. In order to speed up the calculations, bolt geometry tables are shown at Appendix D.

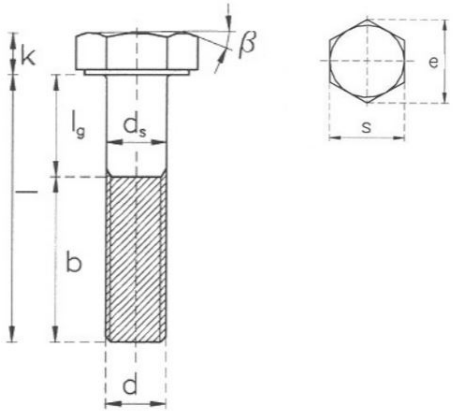

Figure 65: Bolt geometry

Adapted from: Uniones[65]

5.5.1 Sizing of the holes

The holes of the bolts have to be done ideally by drilling.

The standard hole diameter (D) shall satisfy Equation 42.[64]

$$D = d + d' \tag{42}$$

Where d is the body diameter and d' takes different values depending on the bolt diameter.

$$d' = \begin{cases} 1\ mm & \text{if } 12mm \leq d \leq 14mm \\ 1-2\ mm & \text{if } 16mm \leq d \leq 24mm \\ 2-3\ mm & \text{if } 27\ mm \leq d \end{cases}$$

Positioning requirements for holes have to be considered, too. Figures 66 and 67 presents all the distances to consider.

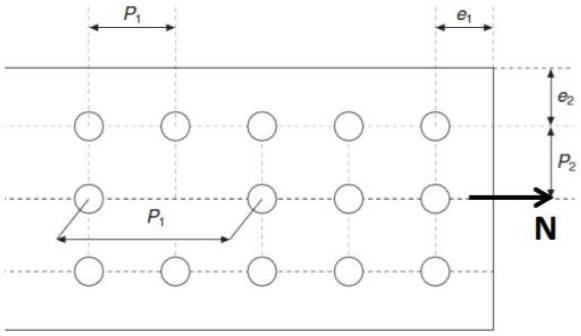

Figure 66: Holes distances

Adapted from: Uniones[65]

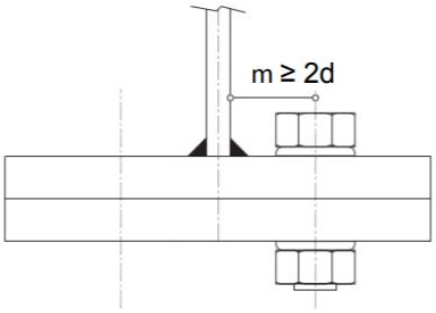

Figure 67: Hole distance to an element

Adapted from: Uniones[65]

Table 24 states the minimum and maximum values for e_1, e_2, p_1, p_2 and m.

The abbreviation M corresponds to mandatory, R to recommended, N to normal environment and C to corrosive environment or outdoors application.

Distance	Min. M	Min. R	Max. N	Max. C
e_1	1.2·d_0	2·d_0	125 mm or 8t	40 mm + 4t
e_2	1.2·d_0	1.5·d_0	125 mm or 8t	40 mm + 4t
p_1	2.2·d_0	3·d_0	28t or 400 mm	28t or 400 mm
p_2	2.4·d_0	3·d_0	14t or 200 mm	14t or 200 mm
m	-	3·d	-	-

Table 24: Constructive holes layout

Data extracted from: Uniones[65]

Where d_0 is the diameter of the hole, d is the diameter of the bolt and t is the thickness of the thinnest part to connect.

5.5.2 Vertical beam - Horizontal beam connection

Every vertical beam is connected to the horizontal beams by two points. Thus, there are twelve bolts to support the weight of the solar panels and the vertical beams. The central horizontal beam has been removed from the calculations.

As said in Section 5.5, maximum shear stress occurs when elevation angle is 90 degrees and maximum tensile stress when elevation angle is 0 degrees. Both values are the same because the only force considered is the weight of the structure and it can be calculated as states Equation 43.

$$F_{\nu,Sd} = F_{t,Sd} = \left(\frac{1}{2}W_p + \frac{1}{2}W_c\right) \cdot g = 114N \tag{43}$$

$F_{\nu,Sd}$ and $F_{t,Sd}$ are the shear stress and the tensile stress that one bolt has to support.

The vertical-horizontal beam connection (Figure 68) has 6.5 mm of thickness (3.5 mm from vertical and 3 mm from horizontal beam).

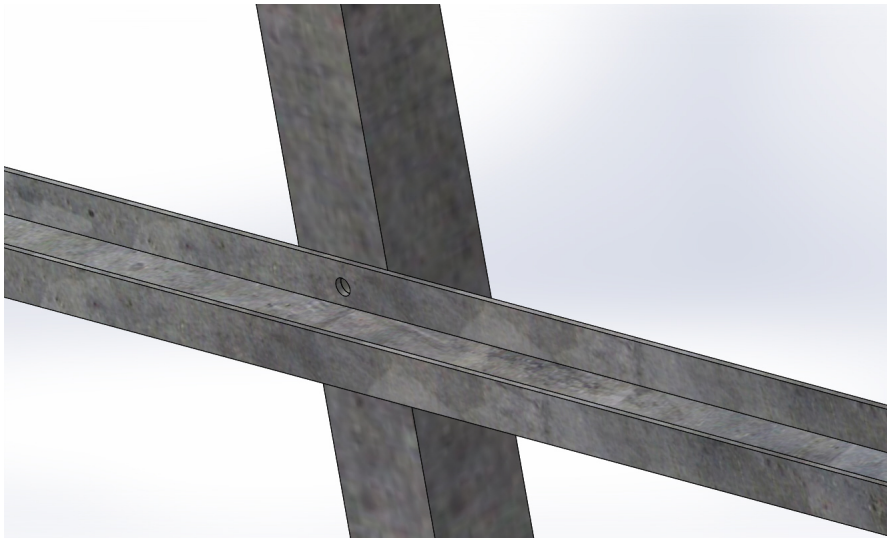

Figure 68: Vertical-horizontal beam connection

The features of the bolt selected are presented at Table 25.

Type	Diameter	Hole	Length	Threaded length	A_s
4.6	M10	11 mm	30 mm	20 mm	0.58 cm^2

Table 25: Bolt selected for vertical-horizontal beam connection

It has been defined a separation between holes of $p_1 = 45\ mm$, which exceed the minimum recommended.

The results obtained fulfill the structural requirements and the hole distance requirements:

$$F_{\nu,Rd} = 11.13\ kN \geq F_{\nu,Sd}$$

$$F_{b,Rd} = 32.7\ kN \geq F_{\nu,Sd}$$

$$F_{t,Rd} = 16.7\ kN \geq F_{t,Sd}$$

$$\frac{F_{\nu,Sd}}{F_{\nu,Rd}} + \frac{F_{t,Sd}}{1.4 \cdot F_{t,Rd}} = 0.0038 \leq 1$$

$$e_1 = 15.5\ mm \geq 1.2 \cdot d_0$$

5.5.3 Horizontal beam - Upper support connection

The approach is the same as developed in section 5.5.2, but the weight that produce shear and tensile stresses has changed.

The preliminary design considered eight bolts for each horizontal beam (see Figure 69). However, the number of bolts used has been reduced after analysing the high resistance of the bolts. Finally, only four bolts are used per beam. Thus, $F_{\nu,Sd}$ and $F_{t,Sd}$ are calculated as Equation 44 states. The equation represents the stress supported by one bolt.

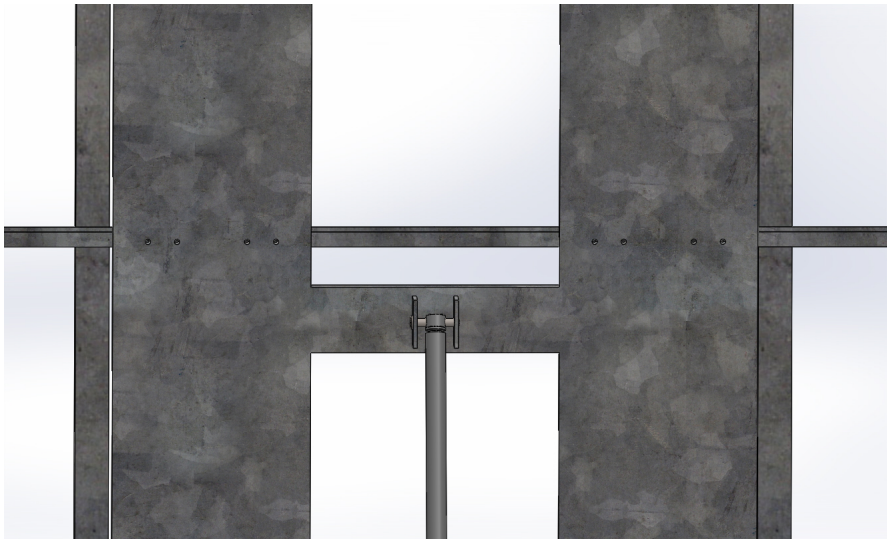

Figure 69: Horizontal beam - Upper support connection

$$F_{\nu,Sd} = F_{t,Sd} = \left(\frac{3}{4}W_p + \frac{3}{4}W_c + \frac{1}{4}W_h\right) \cdot g = 223N \tag{44}$$

Where $W_h = 21.3\ kg$ is the weight of a horizontal bar.

The bolts used shall fulfill the structural requirements established at Equations 35, 36, 37 and 38.[64]

The horizontal beam - upper support connection has 28 mm of thickness (3 mm from the horizontal beam and 25 mm from upper flat support).

The features of the bolt selected are presented at Table 26.

Type	Diameter	Hole	Length	Threaded length	A_s
4.6	M12	13 mm	40 mm	22 mm	0.843 cm^2

Table 26: Bolt selected for horizontal beam - upper support connection

The results obtained satisfy the structural requirements and the hole distance requirements:

$$F_{\nu,Rd} = 16.18\ kN \geq F_{\nu,Sd}$$

$$F_{b,Rd} = 216\ kN \geq F_{\nu,Sd}$$

$$F_{t,Rd} = 24.27\ kN \geq F_{t,Sd}$$

$$\frac{F_{\nu,Sd}}{F_{\nu,Rd}} + \frac{F_{t,Sd}}{1.4 \cdot F_{t,Rd}} = 0.0026 \leq 1$$

$$e_1 = 27.5\ mm \geq 2 \cdot d_0$$

5.6 Cotter pin connections

Cotter pin connections allow relative movement between elements. Cotter pins have special interest in:

- Connection between upper and bottom flat supports
- Connection between bottom support and linear actuator
- Connection between the linear actuator and the upper flat support

Figures 70 and 74 show the location of the cotter pins in the preliminary design.

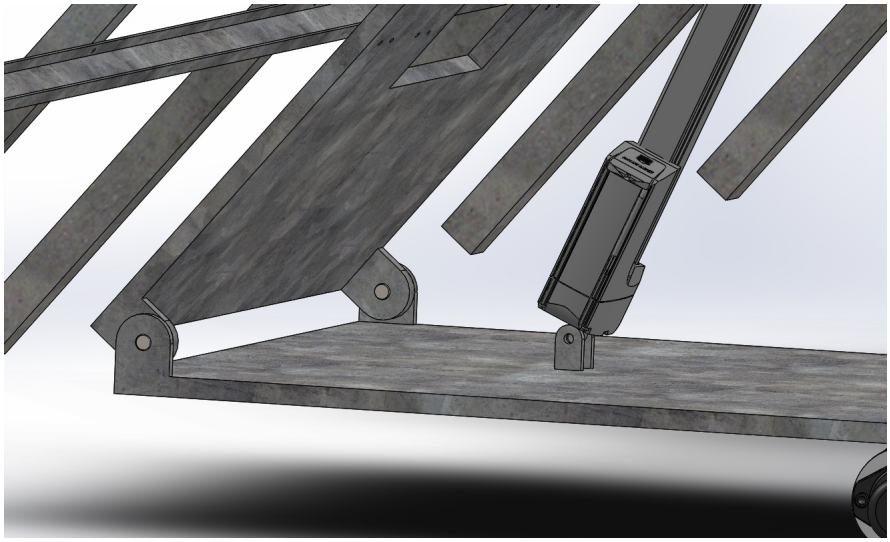

Figure 70: Cotter pins in the design

Cotter pin connections shall fulfill structural requirements, which are presented at Equations 45, 46, 48 and 49.[65]

$$F_{\nu,Ed} \leq F_{\nu,Rd} = \frac{0.6 \cdot A \cdot f_{ub}}{\gamma_{Mp}} \cdot n \tag{45}$$

Where $F_{\nu,Ed}$ (N) is the shear stress applied, $F_{\nu,Rd}$ (N) is the shear stress that the cotter pin can support, A is the circular area of the cotter pin, f_{ub} is the ultimate tensile strength of the cotter pin, γ_{Mp} is the factor of safety for cotter pins (1.25) and n is the number of pieces the pin go through.

$$M_{Ed} \leq M_{Rd} = \frac{0.8 \cdot \pi \cdot d^3 \cdot f_{yb}}{32 \cdot \gamma_{Mp}} \tag{46}$$

Where M_{Ed} is the maximum bending moment and it is calculated as Equation 47[65] states, M_{Rd} is the bending moment the pin can support, d is the diameter, f_{yb} is the yield strength and γ_{Mp} is the factor of safety for cotter pins.

$$M_{Ed} = \frac{F_{Ed}\,(b + 4c + 2a)}{8} \tag{47}$$

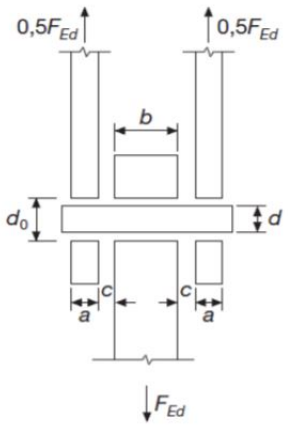

Figure 71: Bending moment in the cotter pin

Adapted from: Uniones[65]

$$\left(\frac{M_{Ed}}{M_{Rd}}\right)^2 + \left(\frac{F_{\nu,Ed}}{F_{\nu,Rd}}\right)^2 \leq 1 \tag{48}$$

This requirement has something to do with the interaction between the effect of the bending moment and the shear stress.

$$F_{b,Ed} \leq F_{b,Rd} = \frac{1.5 \cdot t \cdot d \cdot f_{yb}}{\gamma_{Mp}} \tag{49}$$

Where $F_{b,Ed}$ (N) is the crushing force received, $F_{b,Rd}$ (N) is the crushing force resistance of the pin and t is the thickness of the element connected by the pin.

Table 72 is used to determine the yield strength and the ultimate tensile strength of the cotter pin.

Estado	Temple y revenido						Normalizado			
	d ≤ 16 mm		16 mm < d ≤ 40 mm		40 mm < d ≤ 100 mm		d ≤ 16 mm		16 mm < d ≤ 100 mm	
Designación	f_{yb}	f_{ub}	f_{yb}	f_{ub}	f_{yb}	f_{ub}	f_{yb}	f_{ub}	f_{yb}	f_{ub}
C 22	340	500 a 650	290	470 a 620	—	—	240	430	210	410
C 25	370	550 a 700	320	500 a 650	—	—	260	470	230	440
C 30	400	600 a 750	350	550 a 700	300 (*)	500 a 550 (*)	280	510	250	480
C 35	430	630 a 780	380	600 a 750	320	550 a 700	300	550	270	520
C 40	460	650 a 800	400	630 a 780	350	600 a 750	320	580	290	550
C 45	490	700 a 850	430	650 a 800	370	630 a 780	340	620	305	580
C 50	520	750 a 900	460	700 a 850	400	650 a 800	355	650	320	610
C 55	550	800 a 950	490	750 a 900	420	700 a 850	370	680	330	640
C 60	580	852 a 1.000	520	800 a 950	450	750 a 900	380	710	340	670

Figure 72: Yield strength (MPa) for different pin diameters

5.6.1 Geometry

The sizing of the cotter pin connections has to satisfy the requirements presented in Figure 73.

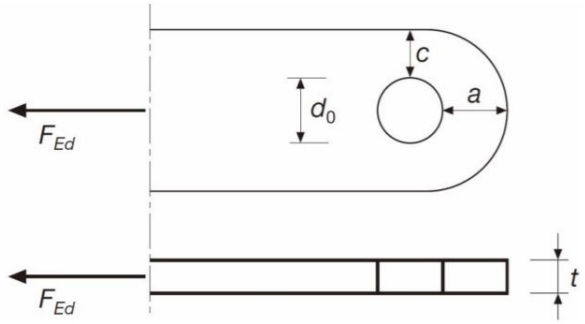

$$a \geq \frac{F_{Ed} \cdot \gamma_{M0}}{2 \cdot t \cdot f_y} + \frac{2 \cdot d_0}{3}$$

$$c \geq \frac{F_{Ed} \cdot \gamma_{M0}}{2 \cdot t \cdot f_y} + \frac{d_0}{3}$$

Figure 73: Geometric conditions for pin connections

Data extracted from: Uniones[65]

Where γ_{M0} is the factor of safety for cotter pins and f_y is the yield strength.

5.6.2 Upper support - Linear actuator connection

Linear actuator is connected to the upper flat support to transmit movement and track the zenith angle (see Figure 74). The connection shall support the force of the actuator (Equation 50).

$$F_a = 12.5\ kN \tag{50}$$

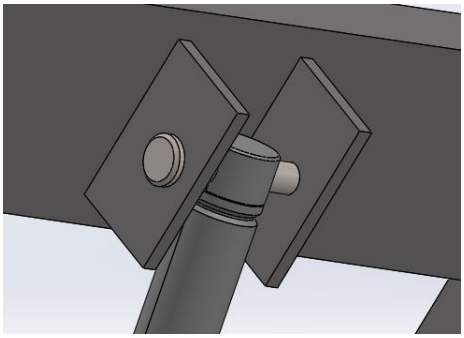

Figure 74: Linear actuator - Upper support connection

Table 27 presents the features of the pin selected.

Type	**Diameter**	**Tensile strength**	**UTS**
C25	16 mm	260 MPa	470 MPa

Table 27: Actuator-upper support connection pin

Parameters from Figure 71 are also defined:

$$a = thickness\ of\ the\ piece = 5\ mm$$

$$b = diameter\ of\ the\ actuator = 30\ mm$$

$$c = space\ between\ symmetric\ pieces\ and\ actuator = 0.5\ mm$$

The results obtained fulfill the structural requirements:

$$F_{\nu,Rd} = 90.7\ kN \geq F_{\nu,Sd} = 12.5\ kN$$

$$M_{Rd} = 66.9\ kN \cdot mm \geq M_{Ed} = 65.6\ kN \cdot mm$$
$$\left(\frac{M_{Ed}}{M_{Rd}}\right)^2 + \left(\frac{F_{\nu,Ed}}{F_{\nu,Rd}}\right)^2 = 0.98 \leq 1$$
$$F_{b,Rd} = 25\ kN \geq F_{b,Ed} = 12.5\ kN$$

The symmetric pieces shall fulfill the following geometry requirements:

$$a \geq 16.7\ mm$$
$$c \geq 11.35\ mm$$
$$t = 5\ mm$$
$$d_0 = 16\ mm$$

5.6.3 Bottom support - Upper support connection

There is relative movement between the bottom flat support and the upper flat support (Figure 75). The weight of the structure stands in two cotter pins . Thus,

$$F_{\nu,Ed} = \frac{(6 \cdot W_p + 6 \cdot W_c + 2 \cdot W_h + W_u) \cdot g}{2} = 1.5\ kN$$

Where W_p is the weight of one panel, W_c is the weight of one vertical bar, W_h is the weight of one horizontal bar and W_u is the weight of the upper flat support.

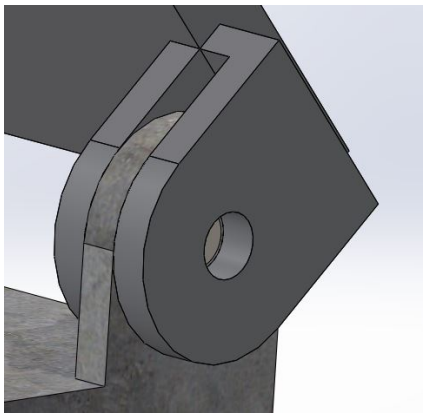

Figure 75: Bottom support- Upper support connection

Table 28 presents the features of the pin selected.

Type	**Diameter**	**Tensile strength**	**UTS**
C22	12 mm	240 MPa	430 MPa

Table 28: Bottom support - Upper support connection pin

Geometric parameters from Figure 71 are also defined:

$$a = thickness\ of\ the\ symmetric\ pieces = 12\ mm$$

$$b = thickness\ of\ the\ central\ base = 12\ mm$$

$$c = space\ between\ symmetric\ pieces\ and\ central\ base = 0.05\ mm$$

The results obtained fulfill the structural requirements:

$$F_{\nu,Rd} = 46.68\ kN \geq F_{\nu,Sd} = 1.5\ kN$$

$$M_{Rd} = 26\ kN \cdot mm \geq M_{Ed} = 6.9\ kN \cdot mm$$

$$\left(\frac{M_{Ed}}{M_{Rd}}\right)^2 + \left(\frac{F_{\nu,Ed}}{F_{\nu,Rd}}\right)^2 = 0.07 \leq 1$$

$$F_{b,Rd} = 41.47\ kN \geq F_{b,Ed} = 1.5\ kN$$

The symmetric pieces shall fulfill the following geometry requirements:

$$a \geq 8.33\ mm$$

$$c \geq 4.33\ mm$$

$$t = 12\ mm$$

$$d = 12\ mm$$

5.6.4 Bottom support - Linear Actuator connection

The relative moment between the bottom flat support and the end of the linear actuator permits the tracker system to be foldable (Figure 76).

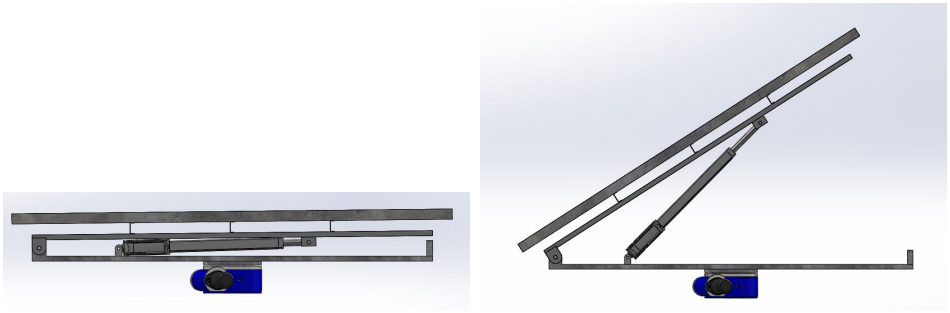

(a) 0 degrees (b) 45 degrees

Figure 76: Foldable tacker system

The cotter pin have to stand the weight of the structure plus the weight of the linear actuator. To size the connection it has been used an actuator weight of 15 kg. Thus,

$$F_{\nu,Ed} = 3.25\ kN$$

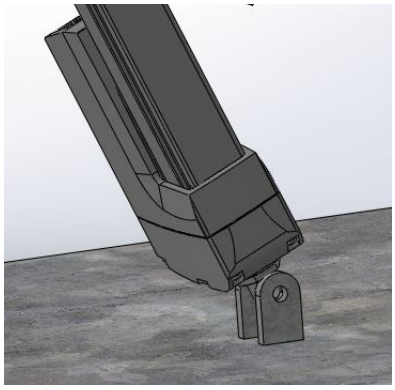

Figure 77: Bottom support - Linear actuator connection

Table 29 presents the features of the pin selected.

Type	Diameter	Tensile strength	UTS
C22	12 mm	240 MPa	430 MPa

Table 29: Bottom support - Linear actuator connection pin

Geometric parameters from Figure 71 are also defined:

$$a = thickness\ of\ the\ symmetric\ pieces = 10\ mm$$

$$b = diameter\ of\ the\ actuator = 25.4\ mm$$

$$c = space\ between\ symmetric\ pieces\ and\ actuator = 2.4\ mm$$

The results obtained fulfill the structural requirements:

$$F_{\nu,Rd} = 46.68\ kN \geq F_{\nu,Sd} = 3.25\ kN$$

$$M_{Rd} = 26\ kN \cdot mm \geq M_{Ed} = 22.3\ kN \cdot mm$$

$$\left(\frac{M_{Ed}}{M_{Rd}}\right)^2 + \left(\frac{F_{\nu,Ed}}{F_{\nu,Rd}}\right)^2 = 0.74 \leq 1$$

$$F_{b,Rd} = 34.56\ kN \geq F_{b,Ed} = 3.25\ kN$$

The symmetric pieces shall fulfill the following geometry requirements:

$$8.9\ mm \leq a \leq 11\ mm$$

$$4.9\ mm \leq c \leq 11\ mm$$

$$t = 10\ mm$$

$$d = 12\ mm$$

The parameters a and c are delimited to avoid interference between the electrical motor and the connection.

5.7 Linear actuator

The design incorporates a linear actuator to track the elevation angle of the Sun. Linear drives usually integrate a motor drive with a screw, gearbox, control board, position sensor and limit switches. Linear actuators is the cheapest option to track the Sun.[57]

When designing a linear actuator, some specifications must be considered: stroke, weight, voltage tolerance, IP rating [15], work temperature, static and dynamic maximum load.

An Electrak *Thomson Linear* actuator (see Figure 78) has been used to perform the CAD. They are light, with a high stroke ranges (from 350 mm to 1,000 mm) and a wide variety of load capacities (1.7-16 kN). They also have an integrated motor which provides a compact design and a better use of the space.

Figure 78: Thomson linear Electrak actuator

Adapted from: Thomson Linear

Linear actuators are incorporated assiduously to Sun-tracking systems due to they are the cheapest and the most marketable option.[57]

The linear actuator must be selected depending on the necessary force to maintain the system static in the desired position. It has to support the pressure of the wind and the weight of the structure including the solar panels.

To calculate the force of the wind it has been considered the solar panels as a flat plate with a $C_D = 1.28$[59] and a surface of $S = 10\ m^2$.

[15] Actuators are used in severe external conditions, and will be exposed to direct sunlight and rain. The industry specification should at least consider IP65 or better

Using wing data of Burkina Faso from PVGIS,[50] the maximum wind speed is $v = 10\ m/s$.

Drag equation (see Equation 51[59]) is used to calculate the wind force (D) against the solar panels with a zenith angle of 90 degrees. It is given in Newtons (N).

$$D = \frac{1}{2}\rho u^2 C_D S \tag{51}$$

Where u is the flow speed (m/s) relative to the object (shipping container is static), S is the solar panel surface (m^2), ρ is the density of the air (kg/m^3) and C_D is the drag coefficient of a flat plate.

The resulting drag ($D = 784\ N$) corresponds to solar panels inclined at 90º. The inclination of the panel during the operational application can vary from 0º to 90º, thus the average drag force will be lower. Nevertheless, overengineering the design for the worst case also accounts for any imprecision in the calculations due to the simplifications of the model, and it also serves as an implicit safety factor in this specific case. In case wind speed is not perpendicular to the panel, the linear actuator selected and the hinge have to support transverse forces. The case has not been studied in detail, but it remains as future work.

In case an extra area is added in a future with foldable solar panels (two more panels), the actuator shall overcome a maximum drag of $D = 1,020\ N$.

Besides the wind effect, the linear actuator must lift the weight of the structure. To calculate the necessary force (F_a) the sum of moments is evaluated at point A of the developed CAD (Figure 79), where reactions are unknown.

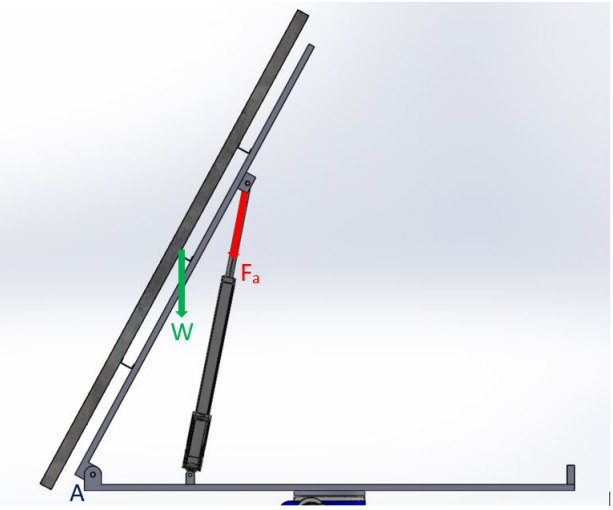

Figure 79: Forces diagram

To assure the equilibrium of the system:

$$\sum M_A = 0 \tag{52}$$

$$-W \cdot d_W - F_{a_y} \cdot d_{a_x} + F_{a_x} \cdot d_{a_y} = 0 \tag{53}$$

Where d_W is the horizontal distance from W to A, $F_{a_{x,y}}$ are the forces of the actuator decomposed and $d_{a_{x,y}}$ are the horizontal and vertical distances from F_a to A, respectively.

Analysing the data, it was found that the system needed lot of force to elevate the system. Thus, it was redesign the elevation system. The problem with the preliminary design was that the linear actuator had a small initial angle ($\alpha = 1.5^o$), so it needed a high force to compensate the weight.

To solve the problem, the linear actuator is installed at the modification of the bottom flat support, with an initial angle of $\alpha = 36^o$. The structural analysis performed at section 5.6.4 has still validity.

Figure 80 shows the new layout of the design. There is a modification in the bottom support. Now, it is not a rectangular solid plate. There is more space to locate the linear actuator. There is no interference between the bottom support and the table structure. This is key to assure the azimuth movement. It also saves material and, as a result, weight.

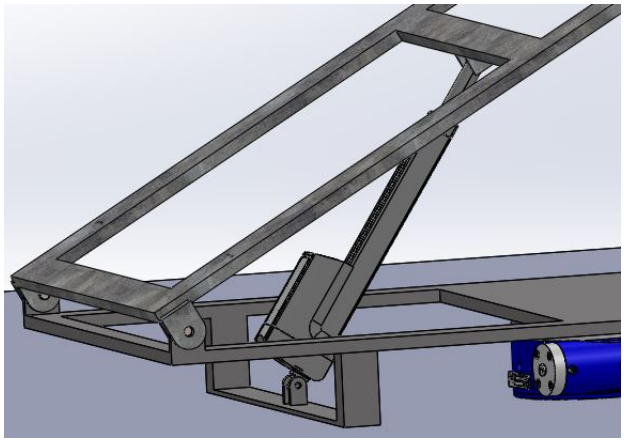

Figure 80: Actuator redesign

The new calculations have been done for all the possible elevation angles and different connections between the linear actuator and the upper support.

Figure 81 shows the relation between AF, SF_{min}, SF_{max} and the necessary actuator force. AF is the distance between the applied force of the actuator and the hinge (point A), SF_{min} is the length of the actuator when elevation angle is 0^{o} and SF_{max} is the length of the actuator when elevation angle is 90^{o}. The plot is a tool to determine the necessary stroke and the maximum force of the actuator.

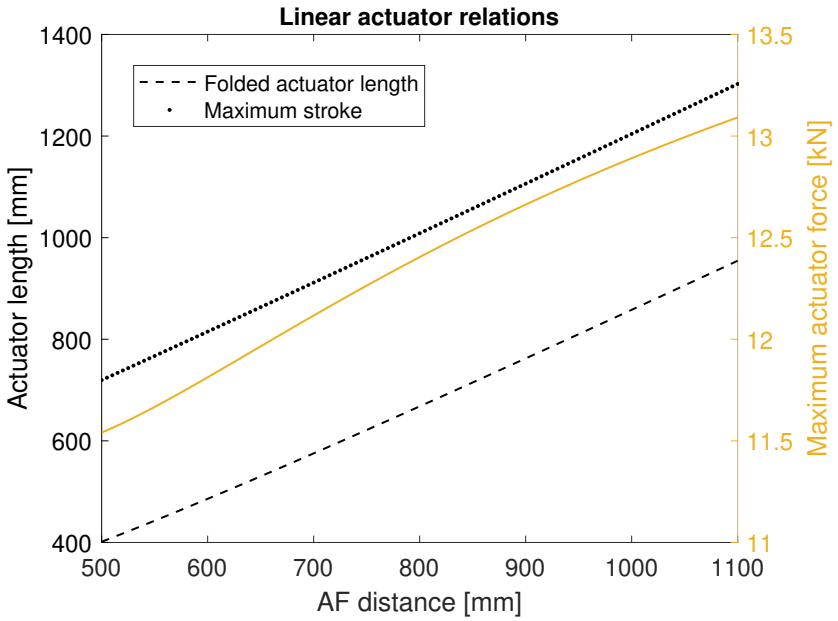

Figure 81: Actuator distance relations

Table 30 presents the features of the Electrak *Thomson Linear* actuator selected to develop the CAD design.

Folded length (mm)	**Max. stroke (mm)**	**Max. dynamic load (kN)**
653.5	1053.5	16

Table 30: Linear actuator specifications

Data extracted from: Thomson Linear

The maximum dynamic load needed is 12.5 kN, so the actuator fits the length requirements and the load requirements.

As galvanized steel is used to size the parts of the design, the force needed is high. It has to be developed a detailed material study to reduce the actuator force.

5.8 Rotary actuator

The average angular movement rate of the Sun is 0.25°/min. This results in a minimum rotational speed motion of 0.000694 rpm. Electrical motors usually move at 1750-200 rpm, so a gear drive or transmission system is required to gear-down the speed while providing sufficient torque.

To achieve an optimum design, the motor/gearbox combination must be able to deliver an acceptable tracking speed such that the electrical motor operates as close as possible to its point of maximum torque or maximum efficiency. In this context, the motor performance curve is a key source during the design.[58]

The slew drive selected shall support the axial loads and the tilting torque. A better dynamic structural analysis must be performed to size the slew drive.

For solar tracking applications is recommendable to use a DC motor with a planetary gear box combined with the slew drive. It can be driven at a very low speed.[58]

Slew drives have a low maintenance and although they aren't a cheap option, its market is mature so a wide range of different options could be considered.[57]

5.9 Table structure

The table structure has two main goals:

1. Support the weight of the entire system
2. Lift the system once in Burkina Faso

The table structure has two critical points: the four table legs and the thickness of the horizontal board. to size the four legs, the buckling is analysed through Euler's critical load (see Equation 54[66]). It is given in Newtons (N).

$$P_{cr} = \frac{\pi^2 EI}{(KL)^2} \tag{54}$$

Where E is the Young's modulus of the material, I is the cross section, L is the length of the legs and K is a factor that determines the effective length.

The legs have to satisfy Equation 55.[66]

$$\sigma_{cr} = \frac{P_{cr}}{A} \leq \frac{\sigma_y}{\gamma_s} \tag{55}$$

Where P_{cr} is the Euler's critial load, A is the cross section area and σ_y is the yield strength of the material.

The horizontal board can be analysed as a rectangular plate resting on four corner points with all edges free.[67] As the calculations requires Fourier series, it has been used Xcalcs, an online plate calculator which is able to provide the maximum bending and shear stresses.

The simulation has been developed with a point load of $P_{load} = 6\ kN$ applied at the center of a board (6060mm length, 2043mm width). At Table 31 are presented the results obtained.

Thickness	**Material**	σ_{max}	τ_{max}	w_{max}
70 mm	Aluminium	5 MPa	1.4 MPa	15.3
40 mm	Galvanized steel	13.7 MPa	4.1 MPa	10.7

Table 31: Rectangular plate results

Bending and shear stresses for both materials are below yield strength. The maximum plate deflection should be smaller than one half of its thickness.[68] Thus, the proposed sizing fulfill the structural requirements.

To size the four legs, the reactions on the corners are also calculated. This is the force the legs have to support.

$$R_y = 1.5\ kN$$

Using Equation 54, the minimum inertia value applying a factor of safety of $\gamma_s = 2$ is given.

$$I_{min} \geq \frac{R_y \gamma_s \cdot (KL^2)}{\pi^2 E}$$

Where E is the Young's modulus of the legs ($E = 210\ GPa$ for galvanized steel). The value of K is 0.5 for both ends fixed.[66] However, it is recom-

mended to use a value of 0.65. The parameter L corresponds to the maximum length of the legs ($L_{max} = 2.59\ m$)[16].

$$I_{min} \geq 4.1023 \cdot 10^3\ mm^4$$

The minimum area is given by Equation 56 and it assures that the legs satisfy the structural requirements.

$$A_{min} \geq \frac{P_{cr} \cdot \gamma_s}{\sigma_y} \tag{56}$$

5.10 CAD assembly

This section presents the assembly of the preliminary design. Although it is a preliminary design, the CAD is presented to visualise the final result of the study. All the parts have been designed keeping in mind the structural requirements and the calculations previously performed. Neither the screw jacks and the rotary drive nor its merging have been designed. They remain as a future work to develop.

Figures 82, 83 and 84 show the preliminary CAD. The design is presented without solar panels to see the vertical and horizontal beams.

[16]The system incorporates screw jacks to lift the tracking system until 2.59 m. The legs are hidden during transport

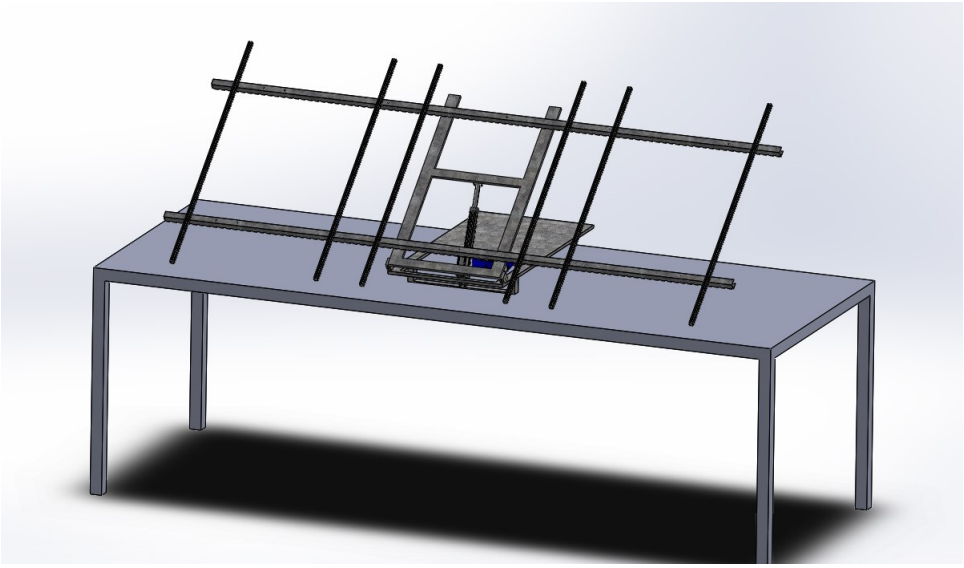

Figure 82: CAD assembly. Overview

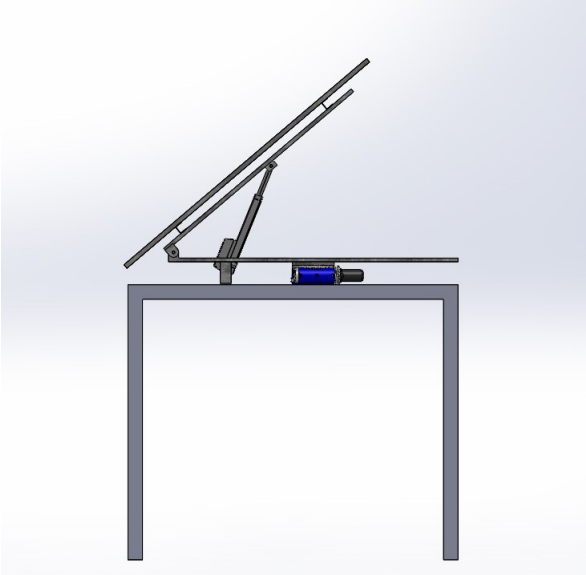

Figure 83: CAD assembly. Profile view

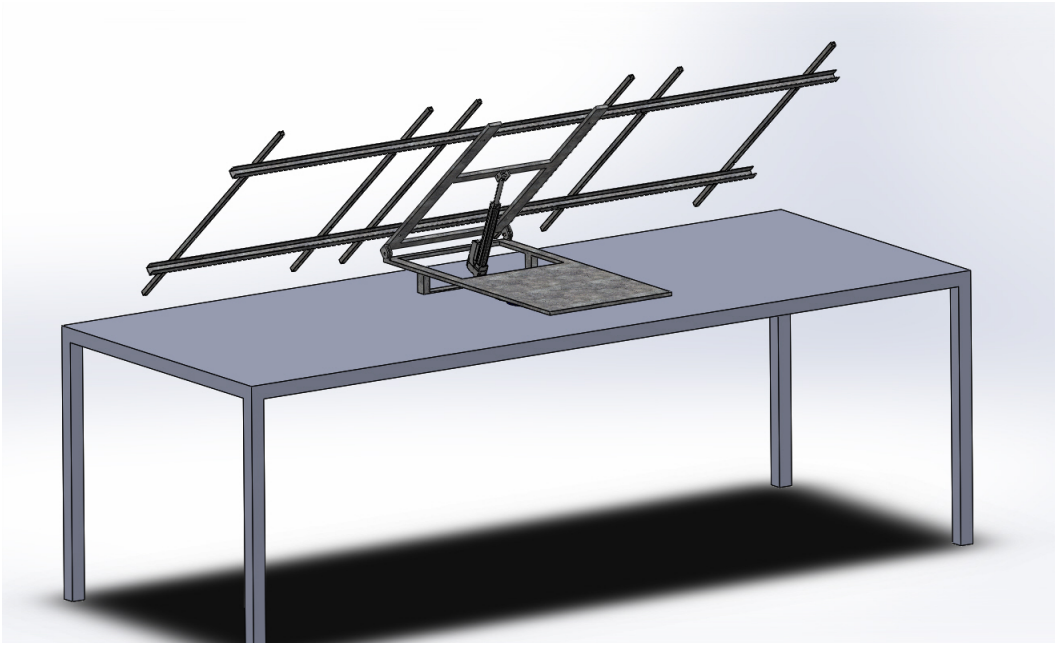

Figure 84: CAD assembly. Rear view

The system folded only needs 420 mm of height inside the shipping container.

5.11 Software control system

The software control system used to track the Sun is not developed in this project. However, Professor David de la Torre developed an in-house toy prototype with Arduino capable of tracking the azimuth and the zenith angles. The code has been completely developed using the *C* programming language. Thus, the code only has to be scaled to the Sun-tracking system size. As the toy model works with two stepper motors, the code has to be adapted to the linear actuator and the rotary actuator.

The hardware assembly of the toy prototype is presented at Figure 85.

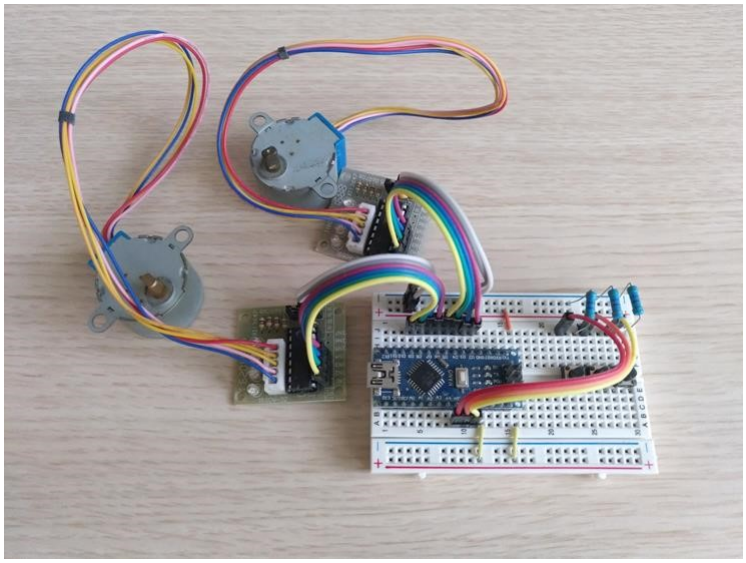

Figure 85: Toy prototype

Adaptem from: Professor David de la Torre

6 Economical feasibility

The lack of electrical energy cause social and economical underdevelopment in Africa. Two thirds of the population in Africa live without electricity. Thus, it is not strange that around the 75% of the consumption comes from renewable energies. Africa contains the hottest places of the world and high rates of radiation. Solar energy is a feasible way to carry electricity all over the continent.

Powerful institutions promote this kind of projects in rural zones of Africa, so receiving funding to develop the design is not difficult.

Besides the opportunity to get a grant, the Sun-tracking system has been designed considering performance-cost criteria. Cells are made of silicon, the most mature and cheap marketable option. Structural analysis has been key in order to save material and consequently to save costs. In addition, linear actuators are the most economic option to track the Sun among actuators. Although slew drives are not as viable as linear actuator they need low maintenance, which will save costs long term.

Furthermore, the market prices have been drastically reduced during the last years on account of the high number of organisations searching for solar solutions. Nowadays solar panels, batteries and converters are even affordable for the base of the social pyramid.

The design has been developed as simple as possible to avoid long repairs and ease the maintenance. This is key considering the Sun-tracking system will be used in rural areas of Burkina Faso.

Although all the points previously mentioned have been considered, there is no specific details in global costs of the design presented.

7 Environmental feasibility

In this project of designing an azimuth/elevation mount for Sun-tracking used to purify water in Burkina Faso, an in-depth environmental analysis is not inside the scope. However, a reflection about the topic has been developed.

Despite the fact that the design is not green building, the use of solar energy has a huge direct impact in Burkina Faso. Solar energy brings purified water and electricity closer to rural African areas, which implies business and social improvements. The use of solar panels is an alternative for kerosene, which is the most light source used in Africa and a serious danger for health.

Table 32 presents a comparison between different ways to obtain electricity. As can be seen, solar energy generates 13 times less CO_2 than combined cycle power plants of gas and 6 times less than coal power stations.

Type	**CO2 emissions [gr/kWh]**
Solar energy	25-32
Combined cycle	400
Coal plant	200
Nuclear energy	25
Wind energy	11

Table 32: Emissions comparison

As a part of a global project, this Sun-tracking design will purify water and produce electricity in a greener way than conventional thermal power stations.

From an environmental point of view, wind energy is the most feasible option, followed by the solar energy. Nevertheless, solar energy is the best option due to the lack of wind speed in the southern area of the country. Furthermore, although solar energy is less efficient than wind energy, it is the most sustainable in the long term.

8 Conclusions

The main goal of this project was develop a preliminary design of a Sun-tracking solar panel system keeping in mind some requirements.

This project has been focused in the design selection from a brainstorming (ten different designs were proposed), the solar panel selection and the sizing of the parts based on structural analysis. As stated in the scope of the project, the software control system has not been developed.

Dealing with the space and transportation requirements was the main problem of the design. Common dual-axis solar panels can use a central pedestal to support the solar panels. In our context, solar panels are the energy source of a water treatment plant so central space of the shipping container was not available. The other issue was to use the minimum possible vertical space. Only 420 mm of vertical space is needed to place the Sun-tracking system designed inside the shipping container. In addition, the legs of the table structure only have to lift up the system 20 cm in comparison with the 2.5 m that some of the others designs demand.

The design present an upgrade that was not contemplated at the beginning of the project. The slew drive that track the azimuth angle allows a rotation of 360 degrees. It means that positioning requirements of the shipping container are not needed.

Despite the fact that no blueprint nor specifications are provided in this project, a solid preliminary design based on space, power, operation and structural requirements has been developed. Thus, this project that belong to a global project goes towards a deeper development and its later implementation.

Operational requirements regarding to the control system implementation are not fulfilled due to lack of time. Concluding an entire design takes a long time and, as a part of a global project, the pending tasks and improvements remain as future work.

The software CAD SolidWorks has been key to develop the design due to the wide variety of tools it incorporates. As an iterative process, SolidWorks facilitate the redesign and the assembly of the improvements.

To conclude, developing this design has been gratifying because I have had

the opportunity to participate in a real engineering project applying all the knowledge acquired along the engineering degree.

9 Future work

The main goal of this final degree has been developing a preliminary solar panel design capable of tracking the Sun. However, there are some improvement ideas that are of special interest for future work.

1. Structural analysis with a software simulator: develop the mesh and confirm the analytical results. Adapt the design to new structural requirements encountered.
2. Study of the wind speed: study the possible transverse forces due to the wind influence and analyse the impact on the hinge and the linear actuator.
3. Select a slew drive: depending on the torque generated, the axial and the radial loads found after the structural simulation.
4. Motor and planetary gear selection: study of the precision needed to track the azimuth angle and choose the components that fulfill it.
5. Sizing of the connection table structure - slew drive - bottom flat plate.
6. Software control system implementation: adapt the existing control system to the final design.
7. Design of the electrical installation: although this project presents some calculations and features regarding to the electrical components, a deeper study is needed to select a marketable battery, a charge regulator, the converter and the wiring.
8. Folding side solar panels to increase the effective area.
9. Material improvement: study different material options to construct the Sun-tracking design. Analyse the climatology and select the best material which satisfies structural requirements and reduces the cost.
10. Screw jacks design: screw jacks are needed to lift up the whole system out of the shipping container.

References

[1] PHILIBERT, C. (2011). *Solar Energy Perspectives*. Paris: Solar Energy Agency. Available from: www.iea.org [31-09-2019]

[2] LUQUE, A., & HEGEDUS, S. (2012). *Handbook of photovoltaic science and engineering*. Chichester, West Sussex, U.K.: Wiley and Sons Ltd.

[3] HANDOYO, E., ICHSANI, D., & PRABOWO. (2013). The optimal tilt angle of a solar collector. *Energy Procedia* 32, 166-175. Available from: www.sciencedirect.com [08-10-2019]

[4] SPROUL, A. (2003). Understanding the pn Junction. *Solar Cells: Resource for the Secondary Science Teacher*.

[5] GE, W. (1990). Survey of semiconductor physics: Electron and other particles in bulk semiconductors (Karl W. Böer, Van Nostrand Reinhold, New York, 1990). *Journal of Luminescence, 47*, 193-194.

[6] MOHAMMAD BAGHER, A. (2015). Types of solar cells and application. *American Journal of Optics and Photonics*, 3(5), 94. www.sciencepublishinggroup.com [24-01-2020]

[7] MARKVART, T., & CASTAÑER, L. (2012). *Solar cells: Materials, Manufacture and Operation*, Elsevier.

[8] U.S DEPARTMENT OF ENERGY. (2013). Photovoltaics. Washington, DC: *Energy efficiency and renewable energy*. Available from: www.energy.gov [20-01-2020]

[9] JESTIN, Y. (2012). Down-Shifting of the incident light for photovoltaic applications. In *Comprehensive Renewable Energy*. (Vol. 1, pp. 563–585). Elsevier Ltd. Available from: www.sciencedirect.com [06-02-2020]

[10] GREEN, M. (2006). *Third generation photovoltaics: Advanced solar energy conversion*. Berlin, Springer.

[11] XU, W., CHENG, Z., & XU, X. (2018). The model of performance change of GaInP/GaAs/Ge triple-junction solar cells in pico-satellite. *Solar Energy, 169*, 105–110. Available from: www.sciencedirect.com [06-02-2020]

[12] RAMANUJAM, J., BISHOP, D. M., & TODOROV, T. K. (2019). Flexible CIGS, CdTe and a-Si:H based thin film solar cells: A review. *Progress in*

Materials Science. Elsevier Ltd. Available from: www.sciencedirect.com [22-01-2020]

[13] IQBAL, M., ALI, S., & KHAN, S. (2019). Progress in dye sensitized solar cell by incorporating natural photosensitizers. *Solar energy*. Elsevier Ltd. Available from: www.sciencedirect.com [07-02-2020]

[14] CHONG, K., LAU, S., YEW, T., & TAN, P. (2013). Design and development in optics of concentrator photovoltaic system. *Renewable and Sustainable Energy Reviews*. Elsevier Ltd. Available from: www.sciencedirect.com [08-02-2020]

[15] HOFFMAN, F., MOLZ, R., KOTHE, J., NARA, E., & TEDESCO, L. (2018). Monthly profile analysis based on a two-axis solar tracker proposal for photovoltaic panels. *Renewable Energy, 115*, 750–759. Available from: www.sciencedirect.com [08-02-2020]

[16] AL GARNI, H., AWASTHI, A., & WRIGHT, D. (2019). Optimal orientation angles for maximizing energy yield for solar PV in Saudi Arabia. *Renewable Energy, 133*, 538-550. Available from: www.sciencedirect.com [08-02-2020]

[17] FTHENAKIS, V., & LYNN, P. (2018). *Electricity from sunlight: Photovoltaic-Systems Integration and Sustainability*. 2nd ed. Wiley and Sons Ltd.

[18] HAFEZ, A., YOUSEF, A., & HARANG, N. (2018). Solar tracking systems: Technologies and trackers drive types – A review. *Renewable and Sustainable Energy Reviews*. Elsevier Ltd. Available from: www.sciencedirect.com [08-02-2020]

[19] THORAT, P., EDALABADKAR, A., CHADGE, R., & INGLE, A. (2017). Effect of sun tracking and cooling system on Photovoltaic Panel: A Review. In *Materials Today: Proceedings* (Vol. 4, pp. 12630-12634). Elsevier Ltd. Available from: www.sciencedirect.com [08-02-2020]

[20] DUBEY, S., SARVAIYA, J., & SESHADRI, B. (2013). Temperature dependent photovoltaic (PV) efficiency and its effect on PV production in the world - A review. In *Energy Procedia* (Vol. 33, pp. 311-321). Elsevier Ltd. Available from: www.sciencedirect.com [09-02-2020]

[21] WONGWUTTANASATIAN, T., SARIKARIN, T., & SUKSRI, A. (2020). Performance enhancement of a photovoltaic module by passive cooling using phase change material in a finned container heat sink. *Solar Energy, 195*, 47-53. Elsevier Ltd. Available from: www.sciencedirect.com [09-02-2020]

[22] AGROUI, K. (2012). Indoor and outdoor characterizations of photovoltaic module based on mulicrystalline solar cells. In *Energy Procedia* (Vol. 18, pp. 857-866). Elsevier BV. Available from: www.sciencedirect.com [09-02-2020]

[23] SKOPLAKI, E., & PALYVOS, J. (2009). On the temperature dependence of photovoltaic module electrical performance: A review of efficiency/power correlations. *Solar Energy, 83(5)*, 614-624. Available from: www.sciencedirect.com [09-02-2020]

[24] JAVED, A. (2014). The effect of temperatures on the silicon cell. *International Journal of Emerging Technologies in Computational and Applied Sciences, 9(3)*, June-August, pp. 305-308. Available from: www.iasir.net [09-02-2020]

[25] PARK, N. (2015). Perovskite solar cells: An emerging photovoltaic technology. *Materials Today*. Elsevier. Available from: www.sciencedirect.com [09-02-2020]

[26] HU, W., HE, X., FANG, Z., LIAN, W., SHANG, Y., LI, X., & YANG, S. (2020). Bulk heterojunction gifts bismuth-based lead-free perovskite solar cells with record efficiency. *Nano Energy, 68*. Available from: www.sciencedirect.com [09-02-2020]

[27] WANG, D., WRIGHT, M., ELUMALAI, N., & UDDIN, A. (2016). Stability of perovskite solar cells. *Solar Energy Materials and Solar Cells*. Elsevier. Available from: www.sciencedirect.com [09-02-2020]

[28] PERPIÑÁN O. (2012). *Energía solar fotovoltaica*. Creative commons. www.procomun.wordpress.com [12-02-2020]

[29] ROY, G., RODRIGO, M. & KING, W. (1989). A Note on Solar Declination and the Equation of Time. *Architectural Science Review, 32*, 43-51.

[30] SOLAR TURTLE. (March, 2020). Products & Services. Johannesburg: *Solar Turtle*. Available from: www.solarturtle.co.za [14-02-2020]

[31] BOYD, O. (26 Sept, 2016). Africa's portable solar revolution is thwarting thieves. *The Guardian*. Available from: www.theguardian.com [14-02-2020]

[32] HERRERA-ROMERO, J., COLORADO-GARRIDO, D., ESCALANTE SCOBERANIS, M., & FLOTA-BAÑUELOS, M. (2020). Estimation of the optimum tilt angle of solar collectors in Coatzacoalcos, Veracruz. *Renewable Energy*. Available from: www.sciencedirect.com [27-02-2020]

[33] AWASTHI, A., KUMAR, A., MANOHAR, M., & DONDARIYA, C. (2020). Review on sun tracking technology in solar PV system. *Energy Reports, 6*, 392-405. Available from: www.sciencedirect.com [28-02-2020]

[34] HE, S., QIU, L., ONO, L., & QI, Y. (2020). How far are we from attaining 10-year lifetime for metal halide perovskite solar cells? *Materials Science and Engineering R: Reports*. Elsevier Ltd. Available from: www.sciencedirect.com [29-02-2020]

[35] LIU, W., LIU, Y., AI, Y., & DUAN, J. (2018). Lifetime multiplier of dye-sensitized solar cell: Origin of performance degradation and the core photoelectric conversion interface reconstruction. *Electrochimica Acta, 280*, 216-220. Available from: www.sciencedirect.com [29-02-2020]

[36] GONG, J., SUMATHY, K., QIAO, Q., & ZHOU, Z. (2017). Review on dye-sensitized solar cells (DSSCs): Advanced techniques and research trends. *Renewable and Sustainable Energy Reviews*. Elsevier Ltd. Available from: www.sciencedirect.com [29-02-2020]

[37] ASGHAR, M., MIETTUNEN, K., HALME, J., VAHERMAA, P., TOIVOLA, M., AITOLA, K., & LUND, P. (2010). Review of stability for advanced dye solar cells. *Energy and Environmental Science*. Available from: www.researchgate.net [29-02-2020]

[38] FU, K., WING, A., KUMAR, H., & THU, P. (2019). Perovskite Solar Cells: Technology and Practices, *Apple Academic Press*.

[39] LIU, Z., SOFIA, S., LAINE, H., WOODHOUSE, M., WIEGHOLD, S., PETERS, I., & BUONASSISI, T. (2020). Revisiting thin silicon for photovoltaics: A technoeconomic perspective. *Energy and Environmental Science, 13(1)*, 12-23. Available from: www.pubs.rsc.org [01-03-2020]

[40] HSU, E. (February, 2020). Price Trend. Tokyo: *Energy Trend*. Available from: www.energytrend.com [01-03-2020]

[41] PVINSIGHTS. (March, 2020). Solar PV Module Weekly Spot Price. Taipei: *PVinsights*. Available from: www.pvinsights.com [02-03-2020]

[42] HUANG, D., & YU, T. (2017). Study on Energy Payback Time of Building Integrated Photovoltaic System. In *Procedia Engineering* (Vol. 205, pp. 1087-1092). Elsevier Ltd. Available from: www.sciencedirect.com [03-03-2020]

[43] GHOSH, B., SAAD, I., TEO, K., & GHOSH, S. (2020). mcSi and CdTe solar photovoltaic challenges: Pathways to progress. *Optik*. Elsevier GmbH. Available from: www.sciencedirect.com [03-03-2020]

[44] LUNARDI, M., ALVAREZ-GAITAN, J., CHANG, N., & CORKISH, R. (2018). Life cycle assessment on PERC solar modules. *Solar Energy Materials and Solar Cells, 187*, 154-159. Available from: www.sciencedirect.com [04-03-2020]

[45] GREEN, M. (2015). The Passivated Emitter and Rear Cell (PERC): From conception to mass production. *Solar Energy Materials and Solar Cells, 143*, 190-197. Available from: www.sciencedirect.com [06-03-2020]

[46] MÜLLER, M., FISCHER, G., BITNAR, B., STECKEMETZ, S., SCHIEPE, R., MÜHLBAUER, M., ... NEUHAUS, D. (2017). Loss analysis of 22% efficient industrial PERC solar cells. In *Energy Procedia* (Vol. 124, pp. 131-137). Elsevier Ltd. Available from: www.sciencedirect.com [06-03-2020]

[47] CUDDIHY, E., COULBERT, C., GUPTA, A., & LIANG, R. (1986). Flatplate Solar Array Project Final Report. *JPL Publication 86-31*, 1–74. Available from: www.jpl.nasa.gov [16-03-2020]

[48] WU, P., MA, X., JI, J., & MA, Y. (2017). Review on Life Cycle Assessment of Energy Payback of Solar Photovoltaic Systems and a Case Study. In *Energy Procedia* (Vol. 105, pp. 68-74). Elsevier Ltd. Available from: www.sciencedirect.com [16-03-2020]

[49] LOUWEN, A., VAN SARK, W., SCHROPP, R., TURKENBURG, W., & FAAIJ, A. (2015). Life-cycle greenhouse gas emissions and energy payback time of current and prospective silicon heterojunction solar cell de-

signs. *Progress in Photovoltaics: Research and Applications*. John Wiley and Sons Ltd. Available from: www.onelibrary.wiley.com [16-03-2020]

[50] EU Science Hub (February, 2020). Photovoltaic Geographical Information System (PVGIS). Luxembourg: *European Union Website*. Available from: www.ec.europa.eu [20-03-2020]

[51] amante-garcía, B., grimau, V. L., & casals, L. C. (2017). LCA of different energy sources for a water purification plant in Burkina Fasso. *Desalination and Water Treatment, 76*, 375–381. Available from: www.deswater.com [30-03-2020]

[52] thomson, D., mullins, M., stager, C., & zante, A. (2012). *US 8,273,978 B2*. Alexandria, Virgina: U.S Patent and Trademark Office. Available from: www.patents.google.com [31-03-2020]

[53] boyk, B. (2010). *US 2010/0051083 A1*. Alexandria, Virgina: U.S Patent and Trademark Office. Available from: www.patents.google.com [31-03-2020]

[54] fraas, L. & minkin, L. (2013). *US 8,487,180 B1*. Alexandria, Virgina: U.S Patent and Trademark Office. Available from: www.patents.google.com [31-03-2020]

[55] strahm, M. (2013). *US 8,492,645 B1*. Alexandria, Virgina: U.S Patent and Trademark Office. Available from: www.patents.google.com [31-03-2020]

[56] clickrenovables. (2015). Cómo calcular una instalación solar fotovoltaica en 5 pasos. Available from: www.clickrenovables.com [16-05-2020]

[57] ruelas ruiz, J. (2019). PV Tracking Design Methodology Based on an Orientation Efficiency Chart. *Applied Sciences. 9. 894*. Available from: www.researchgate.com [04-06-2020]

[58] prinsloo, G.J., dobson, R.T. (2015). *Solar Tracking*. Stellenbosch: SolarBooks. ISBN 978-0-620-61576-1, p 1-542. Available from: www.researchgate.com [04-06-2020]

[59] benson, T. (2014). Shape effects on drag. Glenn Research Center: *NASA*. Available from: www.nasa.gov [04-06-2020]

[60] KAMAL, W., SAAD, N., AB GHANI, A., ABDULLAH, N., & JAZAM, K. (2013). Modelling and Simulation of a Single Deck Bus Subjected to Rollover Crash Loading. *Applied Mechanics and Materials, 393*, 453-459. Available from: www.scientific.net [08-06-2020]

[61] HELLIER, A., CHAPHALKAR, P. & PRUSTY, G. (2017). Fracture Toughness Measurement for Aluminium 6061-T6 using Notched Round Bars. *9th Australasian Congress on Applied Mechanics (ACAM9)*. Conference at UNSW, Sydney, Australia. Available from: www.researchgate.net [08-06-2020]

[62] DELGADO, A., DE JUSTO, E. & ALARCON, P. *La seguridad en las estructuras* [PDF]. Departamento de Mecánica de Medios Continuos y Teoría de Estructuras, Universidad de Sevilla. Available from: www.personal.us.es [08-06-2020]

[63] UPPFELDT, B. (2006). ICNC: Límites de flechas verticales y horizontales para edificios de varias plantas. *ASCEM*. Available from: www.ascem.org [09-06-2020]

[64] SERRANO, M., LÓPEZ-COLINA, C. & HERNANDO, R. *Uniones atornilladas* [PDF]. Mecánica de Medios Continuos y Teoría de Estructuras, Escuela Politécnica de Ingeniería de Gijón Available from: www.ocw.uniovi.es [09-06-2020]

[65] BALDOMIR, A. & ROMERA, L. *Uniones* [PDF]. Área de Mecánica de Medios Continuos e Teoría de Estruturas, Universidade da Coruña. Available from: www.caminos.udc.es [09-06-2020]

[66] YOO, C. & LEE, S. (2011). *Stability of Structures: Principles and Applications*. Elsevier Inc. Available from: www.sciencedirect.com [15-06-2020]

[67] TIMOSHENKO, S., & WOINOWSKY-KRIEGER, S. (1959). *Theory of Plates and Shells*. Univerity of Mishigan: Mcgraw-Hill.

[68] PETELE. M. (2019). Plate deflection and stress. Decin, Czech Republic: *MITCalc*. Available from: www.mitcalc.com [15-06-2020]